Ulm University Hospital

Institute of Virology

Director: Prof. Dr. med. Thomas Mertens

Characterization of the Human Cytomegalovirus Protein pUL71 and its Impact on viral Morphogenesis in Fibroblasts, Endothelial Cells and Macrophages

Dissertation

to obtain the Doctoral Degree of Human Biology (Dr. biol. hum.) at the Faculty of Medicine, University of Ulm

presented by

Martin Schauflinger

from Laichingen

2012

Dean of the Faculty: Prof. Dr. Thomas Wirth

1. Reviewer: Prof. Dr. Thomas Mertens

2. Reviewer: Prof. Dr. Paul Walther

Day doctorate awarded: 22.06.2012

Table of Contents

Abbreviations III

1 Introduction 1

1.1 Herpesviridae 1

1.2 The human cytomegalovirus 1

1.3 Tegument proteins 5

1.4 The protein pUL71 6

1.5 Aim of this study 7

2 Materials and Methods 8

2.1 Viruses 8

2.2 Cells 9

2.3 Mediums and solutions 10

2.4 Antibodies 12

2.5 Chemicals and reagents 13

2.6 Other materials 14

2.7 Molecular biological standard methods 15

2.8 DNA sequencing 15

2.9 Immuno blotting 15

2.10 BAC-mutagenesis 16

2.11 Cultivation of cells 18

2.12 Production of cell free virus stocks and titration 19

2.13 Production of monocyte derived macrophages 19

2.14 Fluorescence microscopy 21

2.15 Electron microscopy 22

3 Results 25

3.1 Cytomegalovirus morphogenesis in fibroblasts, endothelial cells and macrophages 25

3.2 Subcellular localization of pUL71 33

3.3 Cytomegalovirus morphogenesis in absence of pUL71 35

3.4 Investigation of potential N-terminal pUL71 palmitoylation sites 51

3.5 Investigation of a pUL71 leucine zipper like motif 60

3.6 Analysis of the pUL71 C-terminus 65

3.7 Generation and investigation of a pUL71 C-terminal deletion virus 71

3.8 Identification of a pUL71 tetra-lysine motif 75
3.9 Investigation of a pUL103 deficient cytomegalovirus 76
4 Discussion 78
4.1 Cytomegalovirus morphogenesis in fibroblasts, endothelial cells and macrophages 78
4.2 Membrane association of pUL71 80
4.3 Cytomegalovirus morphogenesis in absence of pUL71 81
4.4 The pUL71 palmitoylation site 85
4.5 The pUL71 leucine zipper like motif 87
4.6 The pUL71 tetra-lysine motif 88
4.7 Model of the impact of pUL71 functional domains on virus growth 88
5 Summary 91
6 Literature 93
Acknowledgements 104
Curriculum Vitae 105

Abbreviations

AC	viral assembly compartment
bp	base pairs
dpi	days post infection
E. coli	*Escherichia coli*
e.g.	for example (exempli gratia)
EM	electron microscopy / microscope
ESCRT	endosomal sorting complex required for transport
FIG.	figure
HA	hemaglutinin epitope tag from influenza virus
HCMV	human cytomegalovirus, betaherpesvirinae
HFF	human foreskin fibroblast cells
HUVEC	human umbilical vein endothelial cells
i.e.	that is (id est)
MDM	monocyte derived macrophages
MOI	multiplicity of infection, [PFU/cell]
MVB	multivesicular body
NLS	nuclear localization signal
ORF	open reading frame
PAGE	polyacrylamide gel electrophoresis
PCR	polymerase chain reaction
PFU	plaque forming unit, infectious unit in plaque titration assays
ppUL…	phosphoprotein encoded by the UL… ORF
pUL…	protein encoded by the UL… ORF
SD	standard deviation
SDS	sodium dodecyl sulfate
TEM	transmission electron microscopy / microscope
TGN	*trans*-Golgi network
WT	wild-type HCMV

1 Introduction

1.1 Herpesviridae

The herpesvirus family contains viruses of humans and animals. All herpesviruses are able to establish a lifelong latent persistence in their hosts (Roizman 1996). By biological criteria such as replication time, latency, cell tropism and host range they are classified in three subfamilies, the α-, β- and γ-herpesviruses (Roizman et al. 1981; Modrow et al. 2003).

The α-herpesviruses are characterized by a broad host range, a fast replication cycle, a rapid spread of infection in cell culture and by the establishment of latent infections in sensory ganglia. Three members of this subfamily exploit humans as natural hosts: herpes simplex virus type 1 and 2 (HSV-1, HSV-2), as well as varicella zoster virus (VZV). The β-herpesviruses are characterized by their pronounced host specificity, a slow replication cycle and a slow spread of infection in cell culture. Infection often leads to an enlargement of the host cell, i.e. cytomegaly. Three β-herpesviruses are pathogenic to humans: the human cytomegalovirus (HCMV), also referred to as human herpesvirus 5 (HHV-5), as well as human herpesviruses 6 and 7 (HHV-6, HHV-7). Similar to β-herpesviruses, the γ-herpesviruses are characterized by a narrow host range. This subfamily includes Epstein-Barr virus (EBV, HHV-4) and human herpesvirus 8 (HHV-8).

1.2 The human cytomegalovirus

As a member of the *β-Herpesvirinae*, the human cytomegalovirus (HCMV) exhibits a long replication cycle of about 72 hours and a narrow host range (Modrow et al. 2003). The virus is able to replicate in different cell types such as monocytes, macrophages, endothelial cells and fibroblasts (Sinzger et al. 2000). The virus is a ubiquitous pathogen and 40 to 100 % of people around the world are HCMV seropositive (Modrow et al. 2003). HCMV is transmitted via body fluids, such as saliva, blood, urine, breast milk, cervical secretion or semen (Reynolds et al. 1973; Stagno et al. 1980), and transmission is common during childhood (via saliva) and youth (via sexual contacts) (Modrow et al. 2003).

Postnatal HCMV infection of healthy individuals is asymptotic in most cases. Few patients suffer from symptoms of EBV-negative mononucleosis such as fever, headache and fatigue. In very few cases pharyngitis, splenomegaly or lymphadenopathy have been diagnosed. After primary infection the virus latently persists in the host organism. During

the latent phase the viral genome persists in an episomal circular form and is not replicated (although minimal gene expression does occur); however, the virus may be reactivated eventually (Britt and Alford 1996). In immunocompromised hosts (e.g. transplant recipients, tumor- or AIDS patients), HCMV infection may cause serious or even fatal diseases, like pneumonitis, gastrointestinal ulceration, hepatitis, encephalitis or retinitis. Primary infection of the mother during pregnancy is dangerous for the embryo and may cause serious neurologic damage, e.g. hearing loss after infection of the central nervous system. Five to ten percent of symptomatic CMV-infected newborns die (Pass 2001). The role of HCMV as a major human pathogen made this virus a target of intensive research since many years.

The double stranded DNA genome of HCMV encodes for about 200 genes and exhibits a size of about 230 kbp (Murphy et al. 2003). The linear genome is located within an icosahedral capsid, which is surrounded by viral and cellular proteins that form the tegument layer (Varnum et al. 2004) (FIG. 1). The virus is enveloped by a lipid membrane which contains virally encoded glycoproteins. Glycoproteins mediate membrane fusion processes at the plasma membrane of the host cell, therefore facilitating virus entry and contributing to cell tropism (Jiang et al. 2008). A single virus particle consists of more than 70 virus encoded proteins, 50 % of which are tegument proteins, 30 % are capsid proteins and 13 % are associated to the viral envelope (Varnum et al. 2004). The diameter of an enveloped virus particle is approximately 150 nm.

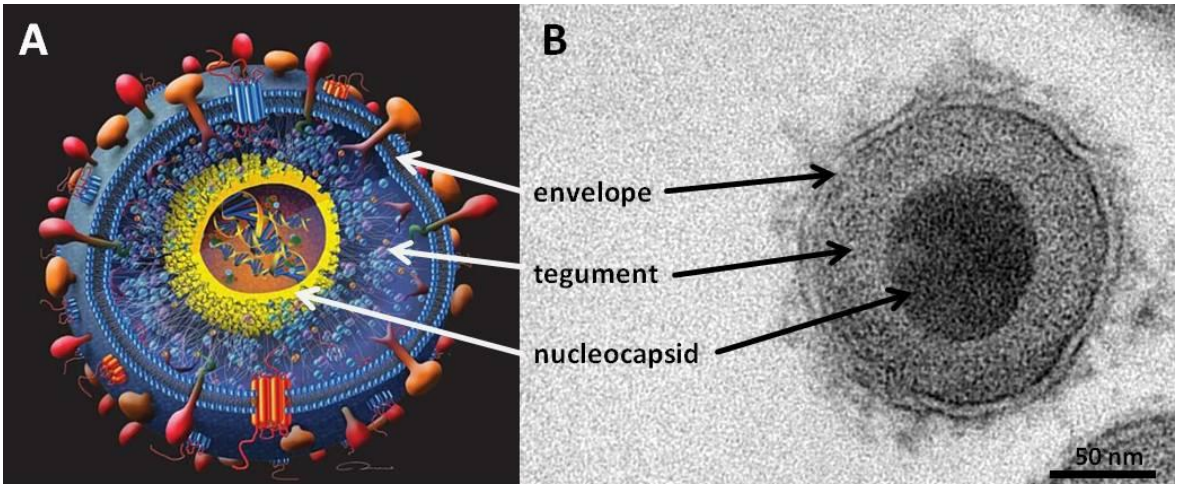


FIG. 1. A cytomegalovirus particle is composed of three major layers. The nucleocapsid contains the double-stranded DNA genome. Tegument proteins form a proteinaceous tegument layer. A host derived lipid bilayer which contains viral glycoproteins forms the viral envelope. **(A)** A schematic drawing (Streblow et al. 2006) and **(B)** a transmission electron microscopic micrograph of a HCMV particle are shown.

The mechanism of virus entry into the host cell is dependent on the cell type (Scrivano et al. 2011). The infection of fibroblasts is supposed to start by receptor mediated fusion of the viral envelope with the plasma membrane (Compton et al. 1992; Compton et al. 1993; Kinzler and Compton 2005), while the virus entry into various endothelial cell lines is facilitated through receptor mediated endocytosis (Bodaghi et al. 1999; Ryckman et al. 2006).

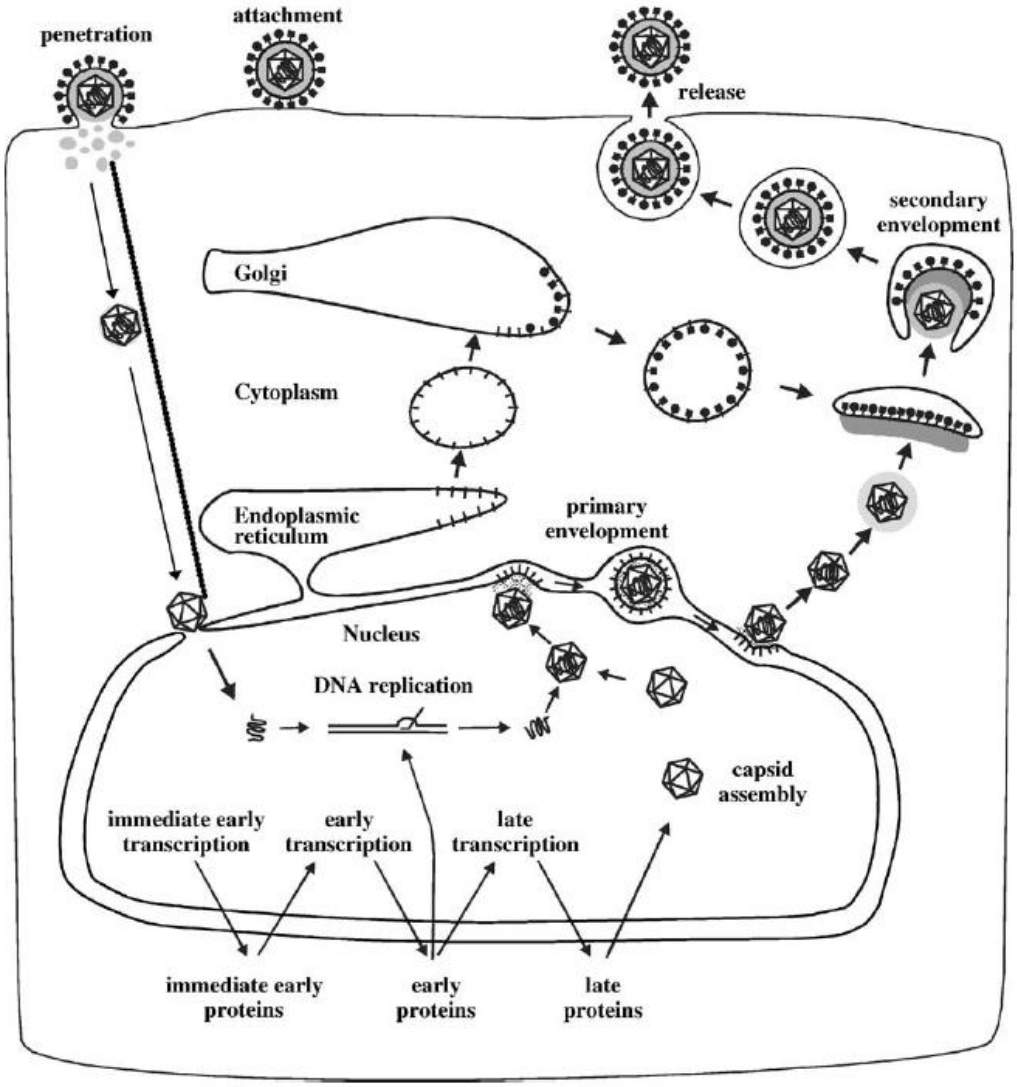


FIG. 2. A schematic representation of the herpesvirus replication cycle is shown (Mettenleiter 2004). It starts with the entry of the virion into the host cell. After penetration the incoming capsid is transported to the nuclear pore. Once the viral genome is released into the nucleus, DNA transcription and replication ensues. Capsid assembly and DNA packaging in the nucleus are followed by the exit of the capsid into the cytoplasm by budding and membrane fusion events at the nuclear membranes. Tegumentation and secondary envelopment of the virus particle is followed by its release into the extracellular space.

The capsid is then transported towards the nuclear pores (FIG. 2), supposedly exploiting the cellular transport system along microtubules, as proposed for HSV-1 (Sodeik et al. 1997). The viral genome is released into the nucleus through the nuclear pore complex, where the linear HCMV genome is circularized and gene expression starts. Three phases are generally distinguished during viral gene expression: i*mmediate-early* (IE), *early* (E), and *late* (L) (Becker et al. 1993). Since the expression of IE gene products does not depend on the expression of any viral genes, they are expressed immediately after infection and induce the second phase, namely expression of E genes. IE and E gene products mediate the expression of L genes. The L-phase is characterized by the replication of viral DNA and the synthesis of structural proteins (Johnson et al. 2001). Viral capsomeres are self-assembled in the nucleus to form the capsids. First, a B-capsid is formed, which contains scaffold proteins. Degradation of the scaffold ring and integration of the viral DNA into the particle leads to the formation of a mature C-capsid. Empty A-capsids occur if the packaging of the viral genome into the capsid fails (Schmolke et al. 1995). The following steps of HCMV morphogenesis are assumed to occur very similar to the generally accepted model of α-herpesvirus morphogenesis (Mettenleiter 2002; Mettenleiter 2004) (FIG. 2). After attachment of nuclear tegument proteins to the capsid (primary tegumentation) the nuclear capsid acquires a primary envelope from the inner nuclear membrane (Buser et al. 2007). The primary envelope then fuses with the outer nuclear leaflet. In the cytoplasm, further tegument proteins attach to the capsid (secondary tegumentation), thereby forming the tegument layer which facilitates the attachment of the particle to membranes of Golgi- (Homman-Loudiyi et al. 2003) or endosome-derived (Tooze et al. 1993) vesicles. These membranes wrap around the tegumented capsid, and by a subsequent fusion process the capsid becomes enveloped and is contained within a vesicle (FIG. 2). This process of secondary envelopment takes place in a defined area of the cell, the so called *assembly compartment* (AC) (Das et al. 2007; Das and Pellett 2011). The viral particles assemble in this area after their exit from the nucleus. This virally induced compartment is a highly organized structure which contains early endosomes within its centre and is bordered by *cis*- and *trans*-Golgi structures (FIG. 3). Eventually, a fusion process at the plasma membrane initiates the release of the enveloped virus particles into the extracellular space, which completes the replication cycle of the virus (FIG. 2).

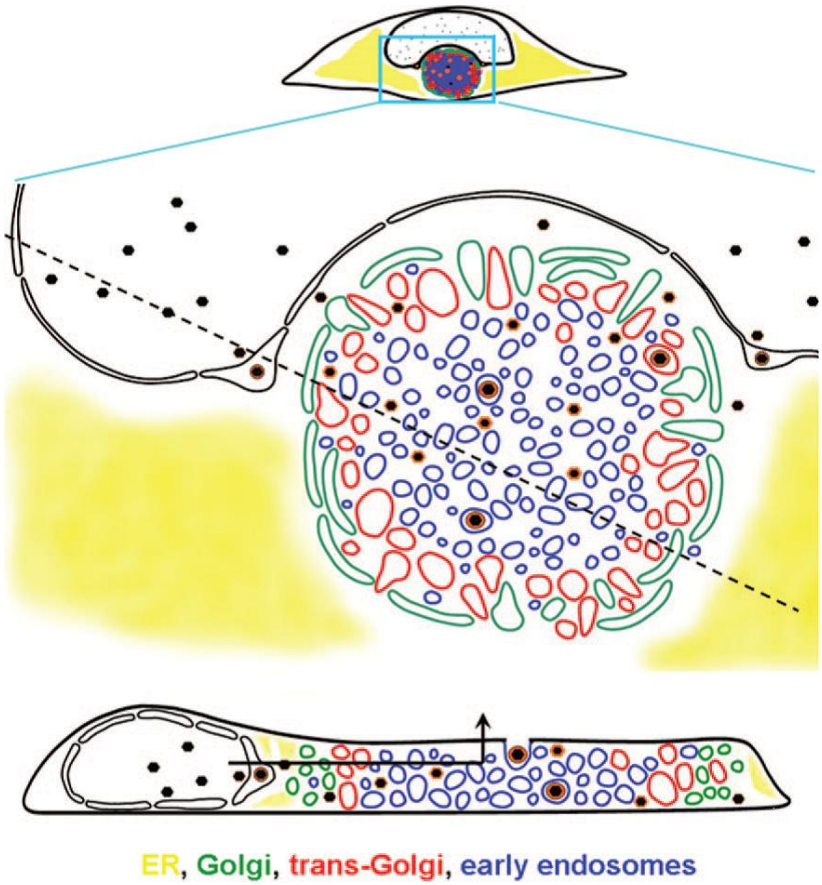


FIG. 3. A schematic picture of the viral assembly compartment (AC) shows its circular structure (Das et al. 2007). Golgi, *trans*-Golgi (TGN) and early endosomal vesicles are arranged in a concentric manner. Viral particles acquire their envelope from vesicles within this compartment. ER Endoplasmic Reticulum.

1.3 Tegument proteins

The HCMV tegument proteins are primarily virus encoded, although the tegument also contains cellular proteins (Varnum et al. 2004). From the 59 viral proteins which have been found in the tegument, only 39 proteins seem to be incorporated at significant levels into virus particles (Baldick and Shenk 1996; Varnum et al. 2004). In addition to their structural role, tegument proteins contribute to immune defense, virus transport, activation of viral and cellular promoters, and regulation of cellular processes (Bechtel and Shenk 2002; Schierling et al. 2004; Kalejta 2008). Some HCMV tegument proteins play an important role during morphogenesis. For example, essential functions have been shown for pp150 and pUL48 (Mocarski et al. 2001; Yu et al. 2003; Dunn et al. 2003); the tegument protein pp28 is required for secondary envelopment (Seo and Britt 2007). Yet, the functions of most HCMV tegument proteins are scarcely characterized or unknown. Many of these proteins, as well as their functions, seem to be conserved among herpesviruses. Data from

α-herpesvirus research propose an importance of tegument proteins for budding and secondary envelopment (Mettenleiter 2004).

1.4 The protein pUL71

The viral protein pUL71 is encoded by the HCMV gene UL71 and was the major subject of this study. Sequence analyses of pUL71 show that this protein is conserved within the family of herpesviruses (Mettenleiter 2004). pUL71 homologous can be found within all herpesvirus subfamilies, e.g. pUL51 of HSV-1, pUL51 of pseudorabies virus, and BSRF1 of EBV (Johannsen et al. 2004; Klupp et al. 2004; Nozawa et al. 2005). These proteins contribute to secondary envelopment and have been classified as membrane associated tegument proteins. Recent data suggest a similar role for HCMV pUL71 (Schauflinger 2008; Fischer 2008). HCMV pUL71 is a protein comprising 361 amino acids (FIG. 4) and 48kD in size, which exhibits an *Early* expression kinetic (Fischer 2008). The investigation of a pUL71 deficient HCMV showed that pUL71 is not essential for the replication of HCMV in fibroblasts (Schauflinger 2008). However, depletion of UL71 leads to a dramatic growth defect, reflected by an up to 16 fold reduction of released viral progeny, and a significant reduction of plaque size (Fischer 2008). HCMV morphogenesis in absence of pUL71 is characterized by an impairment of secondary particle envelopment, as well as the occurrence of enlarged cytoplasmic vesicles in infected fibroblasts (Schauflinger 2008).

```
  1    MQLAQRLCEL LMCRRKAAPV ADYVLLQPSE DVELRELQAF LDENFKQLEI
 51    TPADLRTFSR DTDVVNHLLK LLPLYRQCQS KCAFLKGYLS EGCLPHTRPA
101    AEVECKKSQR ILEALDILIL KLVVGEFAMS EADSLEMLLD KFSTDQASLV
151    EVQRVMGLVD MDCEKSAYML EAGAAATVAP PTPPAVVQGE SGVREDGETV
201    AAVSAFACPS VSDSLIPEET GVTRPMMSLA HINTVSCPTV MRFDQRLLEE
251    GDEEDEVTVM SPSPEPVQQQ PPVEPVQQQP QGRGSHRRRY KESAPQETLP
301    TNHEREILDL MRHSPDVPRE AVMSPTMVTI PPPQIPFVGS ARELRGVKKK
351    KPTAAALLSS A
```

FIG. 4. The amino acid sequence of HCMV pUL71 is represented in one letter code. Cysteines at position 8 and 13 are labeled yellow, leucines at position 34, 41, 48 and 51 are labeled blue, and the sequence $_{315}$PDVPRE$_{320}$ is labeled grey.

1.5 Aim of this study

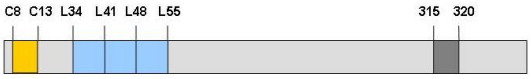
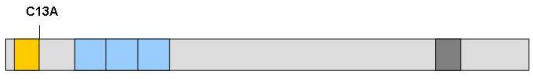
Due to the clinical relevance of HCMV infection especially in immunocompromised persons and during pregnancy, the development of new and better antiviral strategies is crucial. This requires a detailed knowledge about the mechanisms of HCMV morphogenesis. The aim of this thesis was to analyze and compare HCMV morphogenesis in different cell types that contribute to the spread of HCMV *in vivo*, such as fibroblasts, endothelial cells and monocyte derived macrophages. This included to determine and to compare the ultrastructural phenotypes of selected mutant viruses in these cell types. Furthermore, the role of the HCMV tegument protein pUL71 during HCMV morphogenesis had to be specified, including the identification and characterization of functional domains of pUL71. To achieve this, various recombinant viruses had to be generated and investigated by light and electron microscopy.

2 Materials and Methods

2.1 Viruses

All recombinant viruses used in this study have been generated in the Institute of Virology, Ulm University Hospital (Table 1). The BACs used to reconstitute the respective viruses are derived from the TB40-BAC4 (Sinzger et al. 2008b) and have been specifically designed and generated by markerless BAC-mutagenesis as described by Tischer et al. (2006).

Table 1. Recombinant viruses used during this study. In some cases a schematic representation of the respective recombinant protein pUL71 is given.

virus	properties
wild-type	reconstituted from the fully sequenced TB40-BAC4, which is derived from the endothelial cell adopted TB40/E strain (Sinzger et al. 2008b) 
TB71stop	wild-type virus with a point mutation that introduces a stop codon and a following frameshift at amino acid position 12 in pUL71, abrogating UL71 expression (Schauflinger 2008) 
TB71C8/13A	wild-type virus with a double point mutation in UL71, leading to amino acid changes C8A and C13A (Böck 2010) 
TB71C8A	wild-type virus with a point mutation in UL71, leading to an amino acid change C8A (Suffner 2011) 
TB71C13A	wild-type virus with a point mutation in UL71, leading to an amino acid change C13A (Suffner 2011) 
TB71del34–41	wild-type virus with a deletion of amino acids 34 to 41 in UL71 

TB71L34/41A	wild-type virus with a double point mutation in UL71, leading to amino acid changes L34A and L41A 
TB71del315-361	wild-type virus with a deletion of amino acids 315 to 361 in UL71 
TB71P315/318A	wild-type virus with a double point mutation in UL71, leading to amino acid changes P315A and P318A (Böck 2010) 
TB71del315–326	wild-type virus with a deletion of amino acids 315 to 326 in UL71 
TB71del327-361	wild-type virus with a deletion of amino acids 327 to 361 in UL71 
TB71del348-361	wild-type virus with a deletion of amino acids 348 to 361 in UL71 (Schauflinger, this study) 
TB71K348-351A	wild-type virus with a point mutation in UL71, leading to an exchange of the tetra-lysine region $_{348}$KKKK$_{351}$ to $_{348}$AAAA$_{351}$ 
TB71L357-358A	wild-type virus with a point mutation in UL71, leading to an exchange of the leucines L357 and L358 to alanine 
TB71HA	wild-type virus with the HA tag fused to the C-terminus of pUL71
TB103stop	wild-type virus with a point mutation that introduces a stop codon within the UL103 gene, abrogating UL103 expression

2.2 Cells

- HFF: human foreskin fibroblasts (Chang et al. 2002).
- HUVEC: endothelial cells, isolated from human umbilical cord veins.

- MDM (monocyte derived macrophages): primary macrophages derived from human monocytes of HCMV-seronegative blood donors through differentiation with M-CSF (Young et al. 1990).
- MRC-5: embryonic human lung fibroblasts (Jacobs et al. 1970).
- DH10B (Invitrogen) *E. coli* strain.
- XL1-Blue (Stratagene) *E. coli* strain.

2.3 Mediums and solutions

Mediums

- **HFF medium:** MEM (Invitrogen), 10 % (v/v) FCS, 1 % (v/v) streptomycin/penicillin, 1 % (v/v) glutamine, 1 % (v/v) non essential amino acids
- **MRC-5 medium:** DMEM (Gibco BRL), 10 % (v/v) FCS, 1 % (v/v) non essential amino acids, 1 % (v/v) glutamine, 1 % (v/v) streptomycin/penicillin
- **HUVEC medium:** EBM (Lonza, USA), final concentration of FBS 2 %
- **MDM medium:** RPMI 1640 (PAA Laboratories GmbH), 2 mM L-glutamine, 100 U/ml penicillin, 10 µg/ml streptomycin
- **LB-medium:** 10 g Bactotrypton, 5 g yeast extract, 10 g NaCl, adjusted to pH 7.5 with NaOH, ad 1 l aqua bidest

Standard solutions

- **0,01 M PBS:** 150 mM NaCl, 1 mM KH_2 PO_4, adjusted to pH 7.8 with NaOH, ad 1 l aqua bidest
- **10% SDS solution:** 100g SDS, ad 1 l aqua bidest, heat to 68 °C, adjust pH 7.2 with HCl
- **10x PBS:** 80 g NaCl, 2 g KCl, 14.2 g Na_2HPO_4, 2.4 g KH_2 PO_4, adjusted to pH 7.4 with HCl, ad 1 l aqua bidest
- **50x TAE**: 484 g tris (40 mM), 41 g sodium acetate (5 mM), 37 g EDTA (1 mM), adjusted to pH 7.4 with glacial acetic acid, ad 2 l aqua bidest
- **Miltenyi buffer:** 500 ml Dulbecco's PBS (PAA Laboratories GmbH), 10 ml 1 % EDTA in PBS w/o Ca^{2+}/Mg^{2+} (Biochrom AG), 8.3 ml 30 % BSA (Sigma Aldrich)
- **0.01 M PBS/EDTA:** 0.01 M PBS, 1 % EDTA-stock solution
- **Ripa buffer:** 6.84 ml 0.1M Na_2HPO_4, 3.16 ml 0.1 M NaH_2PO_4, 1 ml TritonX100, 1 ml 10 % SDS, 2 ml 0.5 M EDTA, 0.17 g NaF, 1 g sodium deoxycholate, ad 100 ml aqua bidest

Solutions for virus yield assay

- **50 mM sodium acetate buffer:** 2.05 g sodium acetate, adjusted to pH 5 with acetic acid, ad 500 ml aqua bidest
- **AEC stock solution:** 1 tablet AEC (3-amino-9-ethyl-carbazol) (Sigma-Aldrich GmbH), 4 ml N-N dimethylformamid
- **AEC working solution:** 200 µl AEC stock solution, 800 µl 50 mM sodium acetate buffer (50 mM), 1 µl H_2O_2

Solutions for SDS-PAGE and Western blotting

- **10 % APS solution:** 1 g ammonium persulfate, ad 10ml aqua bidest
- **10 % separation gel:** 2.5 ml 1.5 M tris pH 8.8, 100 µl 10 % SDS solution, 3333 µl 30 % acrylamide-bis solution, 50 µl 10 % APS solution, 5 µl TEMED (N, N, N‘, N‘-tetramethylethylen-diamin), ad 10 ml aqua bidest
- **3.9 % stacking gel:** 625 µl 0.5 M tris pH 6.8, 25 µl 10 % SDS solution, 325 µl 30 % acrylamide-bis solution, 12.5 µl 10 % APS solution, 2.5 µl TEMED, ad 2.5 ml aqua bidest
- **10x Lämmli buffer:** 30g tris, 144 g glycine, 10 g SDS, ad 1 l aqua bidest
- **4x protein loading buffer:** 2 ml 0.5 M tris-HCl pH 6.8, 1.6 ml glycerine, 3.2 ml 10 % SDS, 800µl 2-mercaptoethanol, 400µl 2 % bromphenol blue, ad 8ml aqua bidest
- **Blocking solution:** 200 ml 1x PBS pH 7.4, 10 g skim milk powder (5 %), 600 µl Tween-20 (0.3 %)
- **Blotting buffer:** 5.8 g 48 mM tris (48 mM), 2.9 g 39 mM glycine (39 mM), 0.37 g SDS (1.3 mM), 250 ml methanol, ad 1 l aqua bidest, adjusted to pH 9.2
- **Tris-HCl:** 6.06 g tris (50 mM), adjusted to pH 7.5 with HCl, ad 1 l aqua bidest

Solutions for electron microscopy

- **Standard freeze substitution solution:** 0.2 % (w/v) OsO_4, 0.1 % (w/v) uranyl acetate, 5 % (v/v) aqua bidest, in acetone
- **Freeze substitution solution for immuno labeling:** 0.05 % (w/v) uranyl acetate, 5 % (v/v) aqua bidest, in acetone
- **Epon stock solution I:** 155 g EPON 812, 250 g dodecenylsuccinic anhydride
- **Epon stock solution II:** 200 g EPON 812, 178 g methyl nadic anhydride
- **Epon working solution:** 60 ml stock solution I, 40 ml stock solution II, 1,5 ml tris(dimethyl aminomethyl)phenol

Solutions for DNA preparation

- **Buffer I:** 1.98 g glucose (50 mM), 0.61 g tris (25 mM), 0.74 g EDTA (10 mM), ad 200 ml aqua bidest
- **Buffer II:** 1 % (w/v) SDS, 0.2 M NaOH, ad 200 ml aqua bidest
- **Buffer III:** 58.8 g KaAC (3 M), 15.4 ml HCOOH (1.8 M), ad 200 ml aqua bidest

2.4 Antibodies

Table 2. Primary monoclonal antibodies (MAb) and polyclonal antibodies (PAb) applied in this study for immunofluorescence analyses (IF), Western blotting (WB) and electron microscopy (EM).

Primary Antibody	**Manufacturer**	**Dilution**
PAb rabbit anti-UL71	Institute of Virology, Ulm University	IF 1:250 WB 1:500
MAb mouse anti-pp28 IgG_{2B}	Santa Cruz	IF 1:500
MAb mouse anti-pp150 (XP-1)	Jahn et al. 1990	IF 1:600
MAb mouse anti-Actin	Sigma	WB 1:1000
MAb human anti-CD63 (H5C6) IgG_1	BD Pharmingen	IF 1:100
MAb mouse anti-CMV (I.E.A.)	Argene	1:100
MAb mouse anti-γ-Adaptin IgG_{2B}	Sigma-Aldrich	IF 1:1000
MAb mouse anti-HA F-7	Santa Cruz	EM 1:200
PAb rabbit anti-HA Y-11	Santa Cruz	EM 1:200
MAb mouse anti-pp65 65-33	kindly provided by W. Britt, Alabama University, Birmingham	EM 1:5 WB 1:5
MAb mouse anti-gB 2F12 IgG_1	Santa Cruz	IF 1:1500

Table 3. Secondary antibodies applied in this study for immunofluorescence analyses (IF), Western blotting (WB) and electron microscopy (EM).

Secondary Antibody	**Manufacturer**	**Dilution**
goat Alexa-488 anti-mouse IgG_1	Invitrogen	IF 1:1000
goat Alexa-555 anti-mouse IgG_{2A}	Invitrogen	IF 1:1000
goat Alexa-488 anti-mouse $f(ab')_2$	Invitrogen	IF 1:1000
goat Alexa-488 anti-rabbit $f(ab')_2$	Invitrogen	IF 1:1000
goat Alexa-555 anti-mouse $f(ab')_2$	Invitrogen	IF 1:1000
goat Alexa-555 anti-rabbit $f(ab')_2$	Invitrogen	IF 1:1000
swine HRP anti-rabbit	DAKO	WB 1:3000
rabbit HRP anti-mouse	DAKO	WB 1:5000
goat 10 nm gold anti-rabbit	Aurion	EM 1:50
rabbit 10 nm gold anti-mouse	Aurion	EM 1:50
rabbit HRP anti-mouse	DAKO	WB 1:5000
goat 10 nm gold anti-rabbit	Aurion	EM 1:50
rabbit 10 nm gold anti-mouse	Aurion	EM 1:50

2.5 Chemicals and reagents

All chemicals and reagents not listed here were purchased from Sigma, Heidelberg, or from Merck, Darmstadt.

- EDTA: Biochrom KG
- Epon 812: Fluka, Buchs, Switzerland
- Glutamine: Biochrom KG
- Glutar aldehyde solution: Plano GmbH
- Glycerol: Roth
- Lead citrate: Atlanta Chemie Heidelberg
- Nitrogen (liquid): VWR International GmbH
- Non essential amino acids: Biochrom
- Paraformaldehyde (PFA): Fluka Chemie AG, Switzerland
- SDS (Sodiumdodecylsulfate): Serva

- TEMED (Tetramethylethylendiamin): Serva
- Tris (Trishydroxymethylaminomethan): USB, Cleveland, Ohio, USA
- Tris(dimethylaminomethyl)phenol: Fluka, Buchs, Switzerland
- Triton X-100: Serva
- Trypsin-EDTA-solution: Gibco BRL

2.6 Other materials

- *Taq*-DNA-Polymerase: Biolabs, USA
- Restriction enzymes: New England Biolabs GmbH and MBI Fermentas
- Phusion® Hot Start High-Fidelity Polymerase: Finnzymes Oy, Finland
- Chloramphenicol: Serva
- Kanamycin: Serva
- Penicillin: Seromed
- Streptomycin: Seromed
- 1µ-Slide 8 well ibi Treat: Ibidi
- 10 mM dNTPs: MBI Fermentas
- Endotoxin-free Plasmid DNA Purification Kit (NucleoBond XtraMidi EF): Macherey-Nagel
- Eppendorf-Tubes: Eppendorf
- Falcon Tubes: Becton Dickinson, NJ, USA
- Flasks and multi-wells for cell culture: Greiner Bio-One
- Monocyte Isolation Kit II: Miltenyi Biotec GmbH
- Plasmid DNA Purification Kits: Nucleospin Plasmid Quick Pure and NucleoBond XtraMidi: Macherey-Nagel
- Protein Standard prestained: Biorad, Hercules, CA, USA
- Agar: Difco, Detroit, USA
- Fetal calf serum (FCS): Gibco BRL
- Opti-MEM: Gibco BRL, Gaithersburg, MD, USA
- Trypsin: Seromed
- X-ray film Cronex 5: AGFA

2.7 Molecular biological standard methods

The methods listed here are considered standard methods of molecular biology and were performed according to Sambrook and Russel (2001). Thus, they will not be explained in further detail here.

- Alcohol precipitation of DNA
- Phenol-chlorophorm extraction
- Determination of DNA concentration by photometric measurement
- DNA restriction
- Agarose gel electrophoresis

2.8 DNA sequencing

DNA sequencing was performed by the Sanger method using a 310 Perkin Elmer capillary sequencer (Applied Biosystems ASI, Switzerland) and the Big Dye Cycle Sequencing Kit (Applied Biosystems ASI, Switzerland). The sequencing range was about 500 nucleotides. Amplification and labeling of DNA fragments was done using 750 ng template DNA, 4 µl Big Dye Sequencing Mixture, 4 µl 5x Sequencing Buffer, 2 µl primers (10 pmol/µl), H_2O ad 20 µl with the following PCR protocol:

30 sec	96 °C	
10 sec	96 °C	25 cycles
10 sec	50 °C	
4 min	60 °C	
∞	4 °C	

2.9 Immuno blotting

SDS-PAGE. To detect viral proteins in infected cells, SDS-PAGE was performed, followed by Western blotting. Infected cells were collected in ice cold PBS by scraping the cells off the culture dish after removing the cell medium and washing with cold PBS two times. The cells were then centrifuged for 5 min and 4000 rpm at 4 °C, and the pellet was diluted in an appropriate amount of RIPA buffer. The sample was then frozen at -20 °C and thawed by sonication for 1 min to lyse the cells. This freeze-thaw cycle was repeated at least two times, until the sample was inviscid. The sample was then diluted in 4x SDS buffer, proteins were denatured at 95 °C for five minutes and cell debris was pelleted by centrifugation at 13.000 rpm for one minute prior to loading onto a SDS-PA gel. 10%

separating gels and 4% collection gels were made according to protocol and inserted into the run chamber. Pockets were loaded with appropriate amounts of sample or 4 µl of prestained protein ladder. The gel was then run at 200 V for 30 minutes in Lämmli-buffer.

Western blotting. In order to enable detection of specific proteins, the proteins had to be transferred from the SDS-PA gel to a PVDF membrane by semi-dry blotting. The PVDF membrane (Millipore GmbH, Germany) was activated for 1 minute in methanol and equilibrated in blotting buffer together with the gel and 3 mm Whatman filter papers (Whatman, UK). Gel and PVDF membrane were then transferred to the semi-dry blotter (Panther, Thermo Scientific) embedded between the wet Whatman papers. Depending on the molecular weight of the proteins, a voltage of 10 mV was applied at a current of approximately 2 mA/cm^2 for 1 to 2 hours. The transfer was controlled by a prestained protein ladder. After the transfer the membrane was shaken in blocking solution (5% milk powder, 0.3% Tween in PBS) for 2 hours at room temperature or alternatively overnight at 4 °C to saturate unspecific binding sites. The membrane was then incubated with primary antibodies diluted in blocking solution for 60 min at room temperature. After washing the membrane three times for 10 min each in PBS, the specific HRP conjugated secondary antibodies were incubated at room temperature for 60 min, followed by three further washing steps with PBS and one time washing in tris-HCl buffer. Detection of proteins was done using immobilion western HRP substrate (Millipore GmbH, Germany) as recommended by the manufacturer. Chemiluminescence was detected using X-ray film, which was exposed to the membrane for several seconds to minutes, followed by film development in a AGFA automated developer.

2.10 BAC-mutagenesis

Production of recombination- and electro-competent *E. coli*. DH10B were grown with respective antibiotics in 5 ml LB-medium at 32 °C overnight. The next day, 200 ml LB with antibiotics was inoculated with the overnight culture and grown at 32 °C until OD_{600} was reached. Then, the cells were incubated in a 42 °C water bath shaker for 15 min and shaken on ice for further 15 min. The cells were then transferred into pre cooled centrifugation tubes and centrifuged at 4000 rpm and 4 °C for 10 min. The pellet was resuspended in sterile, ice-cold 10 % glycerol, transferred into a new centrifugation tube with 10 % glycerol and centrifuged at 4000 rpm and 4 °C for 5 min. This washing step was repeated 3 times each with centrifugation at 4000 rpm and 4 °C for 10 min. The pellet was

then resuspended in 1 ml glycerol and 50 µl aliquots of the cell suspension were transferred to pre-cooled (–20 °C) 1,5 ml Eppendorf tubes, shock frozen in liquid nitrogen and stored at -80 °C.

Generation of the recombination construct. The linear recombination constructs, which are needed as templates for the homolog recombination steps were generated by PCR. These contained the sequences of interest (which were provided by the specifically designed primers) with an inserted positive selection marker (aphAI, which confers kanamycin resistance), an adjoining I-SceI site and a duplication of a short sequence of the sequences of interest. The plasmid pEP-kan-S (Tischer et al. 2006) was used as the DNA-template. Amplification was done using 20 ng pEP-kan-S, 1 µl forward primer GATACCCTTTGTGGGTTCCGCGCGTGAACTCAGGGGCGTGTGAAGAAAAAGAA ACCCACGGCGAGGATGACGACGATAAGTAGGG (5'-3'; 1 µM), 1 µl reverse primer GCGGAGGACAGCAAGGCCGCCGCCGTGGGTTTCTTTTTCTTCACACGCCCCTG AGTTCACGCGCAACCAATTAACCAATTCTGATTAG (5'-3'; 1 µM), 1 µl dNTPs (20 mM), 5 µl 10x PCR buffer (ThermoPol), 0.5 µl taq polymerase (Biolabs, USA), H_2O ad 50 µl with the following PCR protocol:

3 min	95 °C	
30 sec	95 °C	15 cycles
30 sec	47 °C	
90 sec	68 °C	
30 sec	95 °C	20 cycles
2 min	68 °C	
7 min	68 °C	
∞	4 °C	

The PCR product was purified after agarose gel electrophoresis.

Integration of the recombination construct. To integrate the recombination construct into the HCMV genome, the purified PCR product was transformed by electroporation into competent *E. coli* that contained the TB40-BAC4. 250 ng of purified recombination construct was added to *E. coli* thawed on ice, and carefully mixed by stirring. The bacteria were then transferred into pre-cooled 2 mm electroporation cuvettes (Molecular Bio

Products Inc.) and inserted into the electroporation device (Gene Pulser and Pulse Controller, Biorad, USA), where the cells were briefly shocked in an electric field (1.25 kV, 25 µF, 200 Ω). The cells were then immediately transferred into SOC medium, shaken at 37 °C for 1 hour, plated on agar containing kanamycin/chloramphenicol and incubated at 32 °C over night.

Resolution of marker sequences. To induce resolution and remove the marker sequences from the BACs, the colonies of integrate BACs were inoculated in 1 ml LB containing chloramphenicol and incubated in a bacteria shaker at 32 °C. After one hour 1 ml 2 % arabinose in LB with chloramphenicol was added, followed by 30 min of shaking at 32 °C, 20 min shaking at 42 °C in the water bath and 45 min shaking at 32 °C. A small amount of the cells (~2 µl at an OD of 0.4) was then diluted in LB containing chloramphenicol and 30 µl of the suspension was then plated on 1 % arabinose/chloramphenicol agar plates. The DNA of selected kanamycin sensitive colonies was checked by sequencing.

Transfection of resoluted BACs into fibroblasts. To transfect MRC-5 cells with the BACs, 2-4 µg of purified BAC-DNA and 1µg of the plasmid pcDNA3-UL82 were diluted in ddH_2O to a total volume of 40 µl. MRC-5 were trypsinized and washed in PBS by centrifugation for 5 min at 1200 rpm. The pellet was resuspended in 750 µl Opti-MEM. 40 µl of DNA dilution was then added to 250 µl of the cell suspension and transferred into a 4 mm electroporation cuvette (Molecular Bio Products Inc.), followed by pulsing the cells at 260 V and 1050 µF with a EasyjecT Optima (EquiBio Ltd., UK). The cells were immediately transferred into a cell flask with pre-warmed medium and incubated at 37 °C and 5 % CO_2. The virus was further reconstituted on fibroblasts by spreading infectious supernatant to HFF.

2.11 Cultivation of cells

Working with cells and viruses was done in a sterile environment under S2 conditions, using sterile materials and solutions. All cells were cultivated at 37 °C and 5 % CO_2 atmosphere in an incubator. The cells were grown in T25, T75 or T175 cell flasks. Passaging of fibroblasts was standardly done by washing the cells three times with warm PBS/EDTA, trypsinizing and splitting the cells 1:3 into new cell flasks containing respective fresh medium. Passaging of HUVEC was done as described for fibroblasts, but

the cell flasks were coated with collagen beforehand. For that, cell flasks were covered with collagen in PBS and incubated for 1 hour at 37 °C.

2.12 Production of cell free virus stocks and titration

Fibroblasts were infected with virus solution or transfected with BAC-DNA. The cells were further passaged and cultivated at 37 °C/5 % CO_2 until cytopathic effects were visible in about 90 % of all cells. The supernatant was collected, centrifuged for 10 min at 4000 rpm to remove cell debris and then the supernatant was transferred to 1.5 ml Eppendorf tubes and frozen at -80 °C.

To assess the titer of a virus stock, HFF were infected with serial dilutions of the stock. The cells were spread at a confluency of 80 % in a 96-well one day before infection. At the day of infection, 1:10 serial dilutions of the virus stock were prepared, the old medium was removed from the cells and replaced by dilutions of virus suspension. 2 to 3 days post infection the cells were fixed for 10 min at -20 °C with pre-cooled methanol. The methanol was removed and the cells were dried completely at room temperature, followed by two times washing with 0.01 M PBS and incubation for one hour with mouse antibodies directed against IE. The cells were then washed three times with PBS, before incubation for one hour with secondary anti-mouse antibodies conjugated to HRP. After washing the cells three times with PBS, AEC solution was spread on the cells until the staining was clearly visible. The cells were then washed a last time with PBS, and infected cells were counted for each dilution. Viral infectivity was determined by plaque counting and expressed as plaque forming units (PFU) per ml.

2.13 Production of monocyte derived macrophages

Isolation of peripheral blood mononuclear cells (PBMC). Buffy coats obtained from HCMV-seronegative blood donors (provided by Institut für Klinische Transfusionsmedizin und Immunogenetik Ulm GmbH) were used to isolate PBMC by Ficoll-Paque density centrifugation. Density gradients were generated by the 400 kDa hydrophilic polymer Ficoll, which sedimented during centrifugation. The blood was mixed with 50 ml of D-PBS (Dulbecco`s PBS). Then 35 ml of the blood-PBS mix was transferred carefully into a 50 ml Falcon centrifugation tube containing 15 ml of lymphocyte separation medium LSM 1077 (PAA Laboratories, Germany) without mixing the liquids. Centrifugation for 25 min at 1750 rpm at room temperature without braking separated the blood into different phases, with the PBMC in the interphase between blood plasma and separation solution. The

PBMC phase was extracted by pipetting and transferred into a new centrifugation tube. Then D-PBS was added ad 50 ml, followed by centrifugation for 7 min at 1450 rpm at room temperature without brake, to remove potential residues of Ficoll. The cell pellet was resuspended with 10 ml of 1 % (w/v) EDTA in PBS without Ca^{2+} and Mg^{2+} (Biochrom AG, Germany) and D-PBS was added ad 50 ml, followed by centrifugation for 7 min at 900 rpm at room temperature without brake. The pellet was then resuspended and D-PBS was added ad 50 ml. The washing was repeated twice, to remove the platelets which could interfere with the selection procedure and activate cells in culture. Finally, the cell pellet was resuspended in 30 ml of D-PBS and a 1:50 dilution of the cells with Trypan blue (Carl Roth GmbH & Co. KG, Germany) was made to count living cells using a Neubauer counting chamber. A total of $1.5x10^8$ cells were used for monocyte isolation.

Isolation of monocytes from PBMC. The Monocyte Isolation Kit II (Miltenyi Biotec GmbH) was used to isolate monocytes by negative selection. This works by labeling of non-monocytes with magnetic microbeads, which retains them in a MACS column in the magnetic field of a MACS separator, while monocytes are passing the column. PBMC suspension was transferred into a new Falcon centrifugation tube, and D-PBS was added ad 50 ml. After centrifugation for 7 min at 1200 rpm at room temperature, the pellet was resuspended in 450 µl of Miltenyi buffer. The following steps were performed on ice. First, 150 µl of FcR blocking reagent was added, to block bindings of antibodies to the human Fc receptor. Then, 150 µl of monocyte biotin antibody cocktail was added to label non-monocytes by the biotin-conjugated monoclonal antibodies against CD3, CD7, CD16, CD19, CD56 and glycophorin, followed by a 10 min incubation on ice. Then, 450 µl of Miltenyi buffer was added and mixed by pipetting. The second labeling step was done by addition of 280 µl anti-biotin micro beads and subsequent incubation on ice for 15 min. Miltenyi buffer was added ad 50 ml, followed by centrifugation for 7 min at 1200 rpm at room temperature. In the meanwhile, a MACS LS column was placed in the magnetic field of a MACS separator and rinsed with 3 ml of Miltenyi buffer. The pellet was then resuspended in 750 µl of Miltenyi buffer, and the cell suspension was applied onto the column. The whole flow-through was collected in a new Falcon tube on ice. Remaining cells were washed from the column by additionally rinsing the column 3 times with 3 ml of Miltenyi buffer. After another centrifugation step for 7 min at 1200 rpm at room temperature, the pellet was resuspended in 2 ml of RPMI 1640 complete medium

supplemented with 10% (v/v) fetal calf serum (FCS) (GIBCO Invitrogen, USA) and the cells were counted as described for PBMC. Monocytes were kept at 37 °C.

Macrophage differentiation *in vitro*. A total of $3x10^6$ monocytes per ml were kept on hydrophobic lummox dishes (Greiner Bio-One GmbH, Germany) at 37 °C for seven days in RPMI 1640 complete medium supplemented with 10 % (v/v) FCS in presence of macrophage-colony stimulating factor (M-CSF). The addition of 100 ng/ml recombinant human M-CSF (R&D Systems) allowed differentiation into monocyte derived M2-macrophages (MDM). The old medium was replaced by fresh medium supplemented with growth factors after three days. Four days later, macrophages were completely differentiated and could be used for the experiments. 1 ml of D-PBS was added to the dish and incubated for 5 min at 37 °C, followed by pipetting repeatedly to detach the cells and transferring them into a centrifugation tube with medium. This was repeated until all cells were removed from the dish. After centrifugation for 7 min at 1200 rpm at room temperature, the pellet was resuspended in 1 ml of RPMI 1640 complete medium supplemented with 1 % (v/v) FCS. Macrophages were counted in a Neubauer chamber and 10^5 to $2x10^5$ cells per cm^2 were seeded for fluorescence staining or TEM analyses.

2.14 Fluorescence microscopy

For immune fluorescence stainings, $2x10^4$ to $2.5x10^4$ fibroblasts or HUVEC per cm^2, or $1.5x10^5$ to $2x10^5$ MDM per cm^2 were seeded in 8 well ibidi-slides (ibidi GmbH, Martinsried) and kept at 37 °C/5 % CO_2 followed by infection the other day. The following steps were done at room temperature. The cells were washed twice with PBS at the desired time post infection, fixed with 4 % (w/v) PFA in PBS for 10 min, washed with PBS and permeabilized by treatment with 0.1 % (v/v) Triton in PBS. The cells were then washed with PBS three times and blocking was done with blocking solution (5 % human serum, 1 % BSA in PBS) for 30 min, followed by incubation with primary antibodies diluted in blocking solution for 45 min and three times washing with washing solution (1 % BSA in PBS). Then, secondary antibodies diluted in blocking solution were applied for 30 min, followed by washing three times with washing solution. Finally, staining of DNA was done by applying DAPI diluted in PBS for 5 min, followed by three times washing with PBS and analyses using the Axio-Observer.Z1 fluorescence microscope (Zeiss, Germany) equipped with the AxioCam MRm and an apotome. Pictures were edited using Zeiss' software AxioVision LE 4.8.2.

2.15 Electron microscopy

Preparation of sapphire discs and cells. The sapphire discs were cleaned by sonication for 15 minutes each in 60 % sulphuric acid, water, soapy water and in acetone. The discs were kept in acetone until usage. Then, the discs were allowed to dry, followed by coating with a carbon layer of approximately 20 nm by electron beam evaporation in a BAF 300 (Bal-Tech, Principality of Liechtenstein). After marking the orientation of the discs by carving the number "2" into the carbon layer, the discs were incubated for 8 hours at 120 °C to increase the stability of the carbon film. The discs were then ionized in a special device (Edwards High Vacuum, Leica Microsystems GmbH) to increase the hydrophility of the discs, followed by sterilization under UV-light. The carbon coated sapphire discs were then immersed in cell culture medium and the cells were seeded on the discs. Cells were then incubated at 37 °C and 5 % CO_2 and infected the next day. The medium was then replaced by fresh medium 1.5 to 3 h post infection.

High pressure freezing. Cryofixation of biological samples provides a better picture of tissue and cells as chemical fixation (Shimoni and Müller 1998; Szczesny et al. 1996; Kaneko and Walther 1995; Roos and Morgan 1990). Freezing at high pressures reduces the occurrence of ice artifacts significantly (Moor and Riehle 1968; Studer et al. 1989; Dubochet and Sartori Blanc 2001). Thus, samples were cryofixed by high pressure freezing with a HPM01 (Engineering Office M. Wohlwend, Switzerland) after a certain time post infection (pi). Two aluminum planchettes (3 mm diameter; Engineering Office M. Wohlwend, Switzerland), a lower flat one and an upper with a cavity of 100 µm were immersed in 1-hexadecene and used to "sandwich" the sapphire disc. First, the flat planchette was inserted into the sample holder. Then, the sapphire disc with the adherent cells was removed from the culture dish, shortly deposited on a filter paper to remove excess medium, immersed in hexadecene and placed in the sample holder. Last, the upper planchette was put on top of the disc with the cavity enclosing the cells. The sample was then put into the high pressure freezing machine, where it was cryofixed with liquid nitrogen at a pressure of approximately 2100 bar. After the freezing process the samples were quickly transferred into liquid nitrogen where they were stored until freeze-substitution.

Freeze-substitution and plastic embedding. To substitute the water in the sample with an organic solvent, the sapphire discs were put in a substitution mixture pre-cooled to -90 °C.

For standard ultrastructural analysis and embedding in Epon, acetone containing 2 % (w/v) osmium tetroxide, 0.1 % (w/v) uranyl acetate and 5 % (v/v) water was used (Steinbrecht and Müller 1987; Plattner and Zingsheim 1987; Walther and Ziegler, 2002). The substitution mixture was allowed to precool to –90 °C in a self-made substitution apparatus (Fritz and Ziegler, unpublished). The samples were then quickly transferred from liquid nitrogen to the substitution mixture. Substitution was carried out by raising the temperature from -90 to 0 °C over 16 to 19 hours with an exponential temperature profile. After the substitution the samples were incubated at room temperature for 1 hour and washed 3 times with acetone. Infiltration with Epon was done with 50 % (v/v) Epon in acetone for 3 to 6 hours and pure Epon overnight. The next day, the sapphire discs were transferred into fresh Epon in 0.5 ml Eppendorf tubes –cells pointing up- and incubated at 60 °C for 2 to 4 days to allow the Epon to polymerize.

For embedding in LR-Gold and immunolabeling, substitution was done in acetone containing 0.05 % (w/v) uranyl acetate and 5 % (v/v) water. Substitution was carried out from –90 to –0 °C over 16 to 19 hours. The samples were left at 0 °C for 1 hour and washed with pre-cooled acetone before infiltration with 50 % LR-Gold in acetone on ice for 1 hour and pure LR-Gold for 1 hour in closed and completely filled 0.5 ml Eppendorf tubes. LR-Gold was prepared with 0.1 % (w/w) benzil and 0.1 % (w/w) benzoylperoxide and handled in a nitrogen atmosphere to exclude oxygen. The samples were then transferred into fresh LR-Gold in 0.5 ml Eppendorf tubes –cells pointing up- and incubated in a self-made polymerization device (Fritz and Ziegler, unpublished) and polymerized under UV-light for 48 hours at –20 °C.

Sectioning. The samples embedded in Epon were immersed in liquid nitrogen to remove the sapphire disk. LR-Gold samples were only briefly exposed to nitrogen atmosphere since cooling damages this plastic. The resulting surface was then trimmed with a razor to fit to a microtome diamond (Diatome Ultra, DiS-Galetzka) and sectioned with a Leica Ultracut UCT Microtom (Leica, Germany) to a thickness of 70 nm for standard TEM applications, 100 nm for immuno-gold labeling or 500 nm for tomography. The sections were then transferred to 300 mesh copper grids in case of Epon sections or on formvar / carbon coated copper grids in case of LR-Gold samples. If necessary, sections were contrasted 2 to 4 minutes with 2 % (w/v) uranyl acetate, washed in water 3 times, contrasted in 2 % (w/v) lead citrate, washed in water 3 times and allowed to dry before

imaging in a Zeiss EM10 or a JEOL JEM-1400 transmission electron microscope at an acceleration voltage of 80 kV.

Tomography. For electron tomography, 500-nm-thick sections were imaged in a Titan (FEI, Eindhoven) 300-kV field emission transmission electron microscope in scanning transmission mode using a high-angle annular dark field (HAADF) detector (Fischione Instruments, Horley, United Kingdom). A total of 71 images were recorded at tilt angles from +70° to -70°. The volume was reconstructed by weighted back projection using the IMOD software (Kremer et al. 1996), with the help of 15-nm colloidal gold as fiducial markers for alignment. For segmentation and data display, the AMIRA and the IMOD software were used.

Immunogold labeling. Immunogold labeling of 100 nm thin LR-Gold sections was performed at room temperature. Unspecific binding sites were blocked by a 10 min incubation of the sections in blocking buffer [0.15 M NaCl and 0.01 M Na_2HPO_4 adjusted to pH 7.0, supplemented with 0.05 % (v/v) TWEEN 20 and 0.05 % (w/v) BSA], followed by an incubation for 30 min with primary antibodies diluted in blocking buffer. The sections were washed four times for 3 min in blocking buffer and subsequently incubated for 30 min with secondary antibodies [either goat anti-mouse (Aurion) or goat anti-rabbit (Aurion), diluted in blocking buffer] conjugated to 10 nm colloidal gold. Sections were washed two times for 3 min in blocking buffer and four times for 1.5 min in aqua dest prior to imaging with the TEM.

Image Processing. In case of the Zeiss EM10 TEM, images were recorded on negative film and digitalized with a Duoscan f40 (AGFA). Digital pictures were processed with Photoshop (Adobe, USA). Only contrast enhancement and adjustment of brightness was done.

3 Results

3.1 Cytomegalovirus morphogenesis in fibroblasts, endothelial cells and macrophages

Adherent fibroblasts are commonly used to study HCMV morphogenesis in cell culture. *In vivo*, however, HCMV replicates in different cell types, including endothelial cells and macrophages. Replication of HCMV in endothelial cells and macrophages plays an important role for the establishment of HCMV infection *in vivo* (Jarvis and Nelson 2002; Adler and Sinzger 2009), making these cell types an important target for research of virus morphogenesis. We wanted to clarify whether morphogenesis of HCMV is similar in fibroblasts, endothelial cells and macrophages. Therefore, human lung fibroblasts (MRC-5), human foreskin fibroblasts (HFF), human umbilical vein endothelial cells (HUVEC), and monocyte derived macrophages (MDM) were infected with HCMV wild-type virus and the morphogenesis was compared between these cell types.

First, we wanted to clarify whether the viral assembly compartment (AC) was established in all cell types. The AC is the cytoplasmic region in which the viral particles assemble and secondary envelopment takes place. The viral protein pp28 was used as a marker of this virus induced region in immunofluorescence analyses. Furthermore, an antibody raised against the C-terminus of the HCMV tegument protein pUL71 (Schauflinger et al. 2011) was used to detect the localization of pUL71, the protein of interest of this study. Overlapping signals of pp28 and pUL71 could be found in a circular region near the cell nuclei at 5 days post infection in HFF (FIG. 5). These results demonstrated that pUL71 was localized to the AC at late times of infection. Similar localization patterns of pp28 and pUL71 were observed in fibroblasts, endothelial cells and macrophages, confirming a similar establishment of the AC as well as a similar localization of pUL71 in these cell types (FIG. 5).

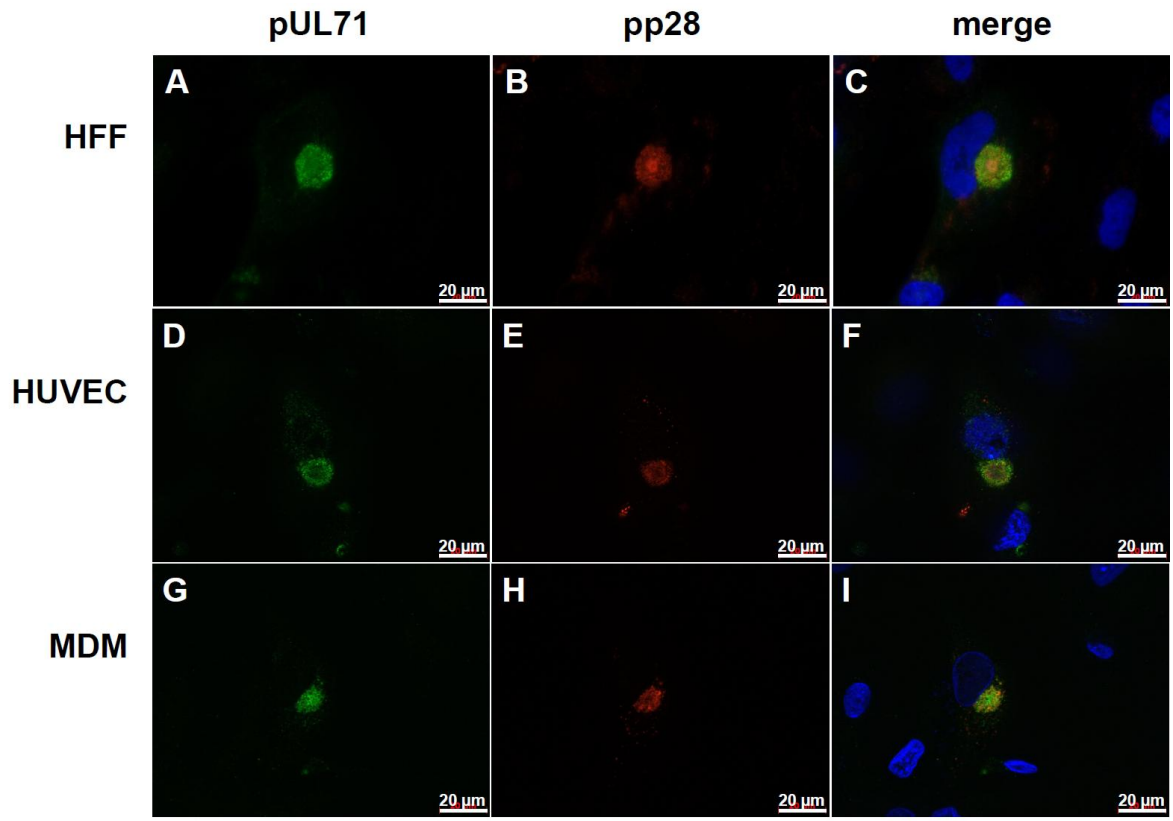


FIG. 5. Fibroblasts, HUVEC and MDM exhibit a similar establishment of the assembly compartment as well as similar localization pattern of pUL71. The subcellular localization of the viral proteins pUL71 and pp28 after infection with wild-type virus is shown in HFF (MOI 0.5) **(A-C)**, in HUVEC (MOI 5) **(D-F)** and in MDM (MOI 5) **(G-I)**, respectively. Cells were fixed with 4 % PFA in PBS at 5 dpi (HFF) or 6 dpi (HUVEC and MDM). pUL71 and pp28 were detected by the respective antibodies and visualized by secondary antibodies conjugated to Alexa Fluor 488 (for pUL71) and 555 (for pp28). Cell nuclei were visualized by DAPI.

Since immunofluorescence analyses suggested a similar establishment of the AC in fibroblasts, HUVEC and MDM, we aimed to compare HCMV wild-type infection in these different cell types in more detail by transmission electron microscopic (TEM) analyses. Therefore, cells were grown on carbon coated sapphire discs and infected with wild-type virus. At late times of infection cells were cryofixed by high pressure freezing, freeze-substituted and embedded in Epon. The plastic embedded cells were then thin sectioned and analyzed in a TEM. Ultrastructural analysis of cells at late stages of HCMV infection allowed a detailed insight into viral morphogenesis. Investigation of the viral morphogenesis in fibroblasts was ideal at 5 dpi, since many virus particles were assembled at the AC at this stage. In contrast, it was difficult to find sufficient amounts of viral particles in HUVEC and MDM at 5 dpi. Thus, cryofixation of HUVEC and MDM was performed at 6 dpi, which better resembled the stage of infection in fibroblasts at 5 dpi.

First we focused on the appearance of the AC, which was easy to recognize on an ultrastructural level, since it was free of mitochondria and surrounded by Golgi cisternae. This compartment was a concentric area, arranged around the microtubule organizing centre (MTOC) of the cell and often located at the indentation of a kidney shaped nucleus (FIG. 6). The AC contained large numbers of various vesicles with different shapes and sizes. Furthermore, protein aggregates -such as dense bodies- as well as the majority of cytoplasmic viral particles was found at the AC.

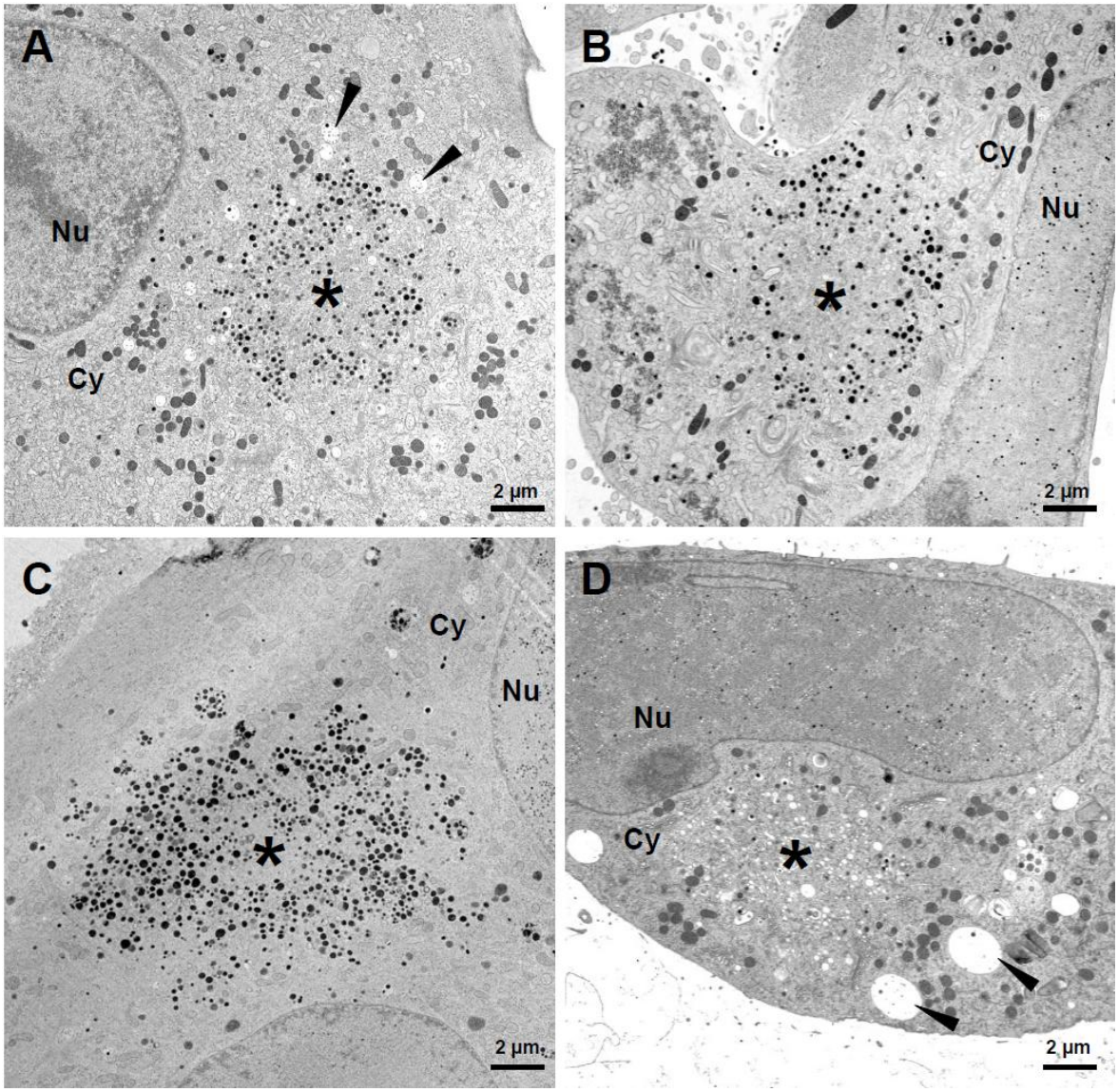


FIG. 6. HCMV induces the establishment of a viral assembly compartment in fibroblasts, HUVEC and MDM at late stages of infection. Overviews of wild-type infected cells with the viral AC in the centre are shown. **(A)** HFF at 5 dpi, **(B)** MRC-5 at 5 dpi, **(C)** HUVEC at 6 dpi, **(D)** MDM at 6 dpi. The asterisk indicates the centre of the AC. Note that multivesicular endosomes (black arrowheads) are relatively larger in MDM than in other cell types. Nu nucleus, Cy cytoplasm.

HFF and MRC-5 fibroblast cells exhibited strong similarities in their ultrastructural appearances, and no noticeable differences between these two cell lines were detectable. The cells of both fibroblast lines exhibited usually an oblong shape. Infection with an MOI of 0.5 to 1 was sufficient to establish infection in the majority of the cells, allowing efficient TEM analyses. Infected cells were enlarged in size compared to uninfected cells and showed a well recognizable AC at 5 dpi (FIG. 6 A, B). A closer look at the viral AC revealed that the majority of virus particles were fully enveloped and contained within a small vesicle. Budding processes occurred usually into small crescent shaped vesicles for both, MRC-5 (FIG. 7 A-D) and HFF (FIG. 7 F).

Next, wild-type virus infected HUVEC were prepared for TEM analyses at 6 dpi. Due to the low infectability of endothelial cells a higher MOI of 5 to 10 had to be used to establish a sufficient number of infected cells. HUVEC had about the same size as fibroblasts but were not as elongated as fibroblasts. Yet, both HUVEC and fibroblasts looked similar on an ultrastructural level. Most virus particles within the AC were completely enveloped and only few were found in a process of budding into small crescent shaped vesicles (FIG. 7 G). These findings resembled the ultrastructural phenotype of wild-type virus in fibroblasts.

To study HCMV morphogenesis in macrophages, MDM were prepared from blood of HCMV seronegative donors, by isolation of monocytes and their subsequent differentiation into macrophages. MDM were seeded on sapphire discs seven days after differentiation, infected with HCMV wild-type virus and processed for TEM analyses at 6 dpi. These cells were difficult to investigate, due to their low infectability and their tendency to detach from the sapphire discs. MDM were found to exhibit two main cell shapes. First, there were small and round cells with very irregular shapes due to their lamellipodiae. Second, bigger and fusiform cells with a smoother cell surface were found, which were mainly the ones that showed infection. In general, macrophages were smaller in size than fibroblasts or endothelial cells. Consistently, the AC seemed to occupy a smaller area and to contain less viral particles compared to fibroblasts and HUVEC (FIG. 6 D). However, in general more and larger endosome like vesicles such as multivesicular bodies (MVBs) were found in the cytoplasm of HCMV infected MDM, especially in the periphery of the AC (FIG. 6 D). Like in fibroblasts and HUVEC, the viral particles were mainly found within the AC in infected MDM. The majority of these particles was already enveloped and found within small vesicles (FIG. 7 H). In addition, virus particles were

observed in the lumen of larger vesicles or MVBs, which was less common in fibroblasts or HUVEC (FIG. 7 I).

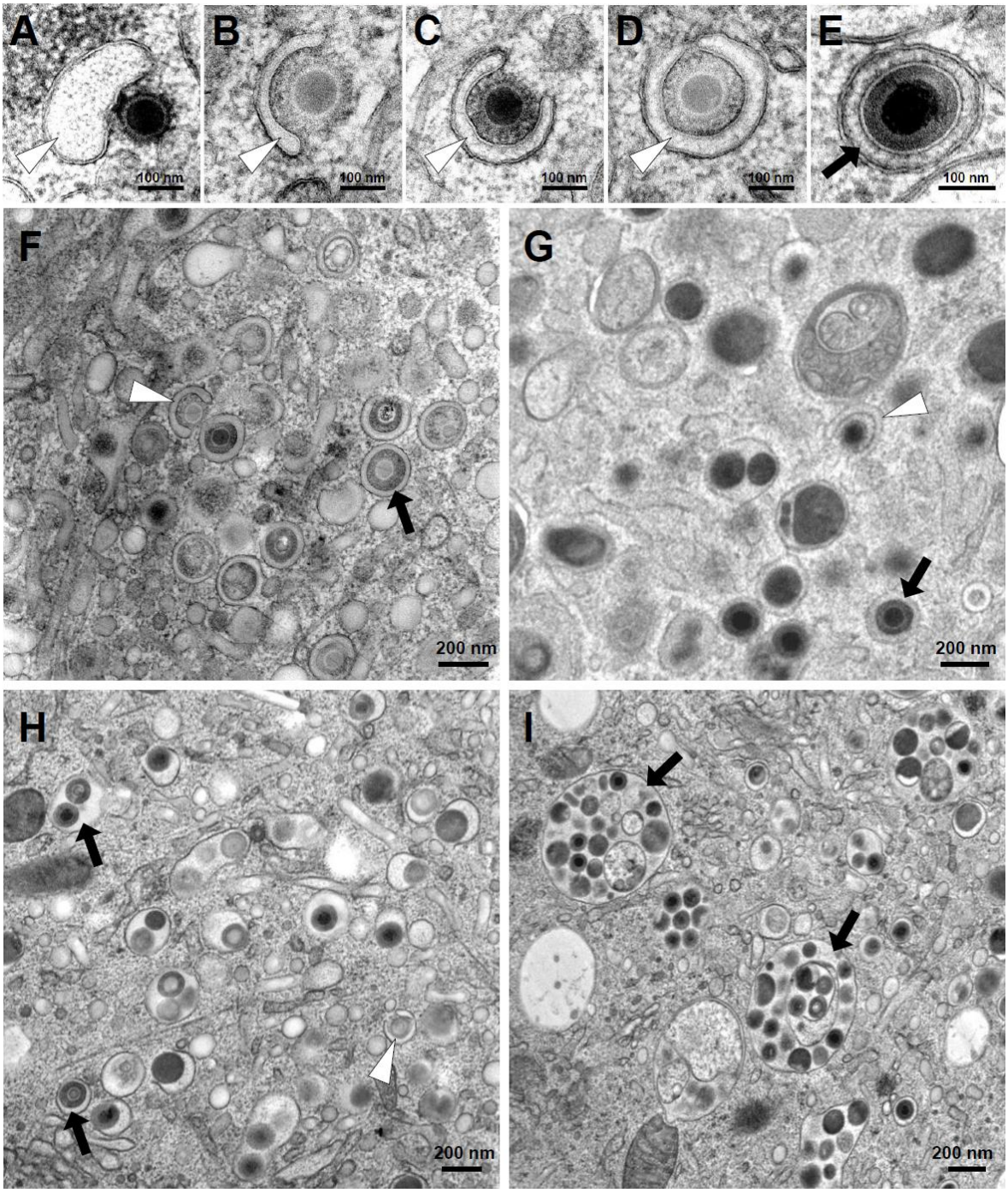


FIG. 7. Typical budding vesicles in wild-type infected cells are small and crescent shaped. **(A-D)** Budding vesicles (white arrowheads) wrap around a capsid in MRC-5 cells. **(E)** When the process of envelopment is completed, the enveloped virus is contained within a vesicle (black arrow), which originates from the prior budding process. Fully enveloped viruses are commonly found in HFF at 5 dpi **(F)**, HUVEC at 6 dpi **(G)** and MDM at 6 dpi **(H)**, while only few budding processes can be observed. **(I)** Bigger, endosome-like vesicles containing virus particles are seen in MDM at 6 dpi.

Next, it was investigated whether secondary envelopment processes are equally efficient in fibroblasts, endothelial cells and macrophages. HCMV virions acquire their envelope from the infected host cell. In the case of HCMV the final envelopment process starts with a budding of a cytoplasmic capsid into a vesicle. The lipid membrane of this vesicle wraps around the capsid (FIG. 7 A-D). To finish the envelopment, a fusion process has to take place, resulting in the formation of the viral envelope and a vesicle surrounding the enveloped virus particle (FIG. 7 E). This envelopment process happens preferably within the AC and its stages can only be observed with the help of electron microscopy. The ability of the virus to get efficiently enveloped in the host cell is a requirement for the production of infectious virus progeny.

To compare HCMV envelopment in different cell types and to quantify final envelopment stages, micrographs were randomly taken of the AC or areas of the AC from more than 20 cells from at least two independent experiments per cell type. The stages of envelopment of virus particles within the AC were assessed based on their classification into three categories: (a) fully enveloped particles, which already had acquired an envelope and therefore were found within a vesicle (FIG. 7 E); (b) capsids, which were associated with cellular membranes, but had not acquired their envelope yet (FIG. 7 A-D); and (c) naked cytoplasmic capsids, which showed no association with a membrane (FIG. 17, page 43). To compare the frequency of those envelopment stages in the different cell types, relative ratios of enveloped, budding and naked particles were calculated for wild-type virus infected fibroblasts, HUVEC and MDM, respectively. All HCMV infected cell types had in common, that the vast majority of particles within the AC were already fully enveloped and only a small portion was found in budding processes, while the amount of naked capsids was neglectable (Table 4). These data suggested that the process of HCMV final envelopment was equally efficient in all these cell types.

Table 4. Quantification of envelopment stages of HCMV wild-type virus particles in the AC of HFF (5 dpi), MRC-5 (5 dpi), HUVEC (6 dpi) and MDM (6 dpi), respectively. The data was assessed from randomly chosen areas of ACs within n cells from at least two independent experiments per cell type.

			mean % particles ± SD		
cell type	n	# particles	enveloped	budding	naked
HFF	27	929	86.6 ± 14.8	13.0 ± 14.7	0.4 ± 1.7
MRC-5	23	1130	84.7 ± 8.6	13.1 ± 6.6	2.2 ± 4.2
HUVEC	30	750	74.5 ± 11.4	23.4 ± 10.7	2.1 ± 3.6
MDM	25	438	88.2 ± 7.5	10.9 ± 7.1	0.9 ± 2.7

As described above, these data were assessed from randomly chosen areas of different ACs, since it was often not possible to assess the state of all particles within one AC. This was mainly due to ACs being only partly visible, because they were covered by the copper grid which served as carrier for the ultra-thin plastic sections, or because of bad preservation of the ultrastructure. To exclude that choosing areas of the AC falsified the quantification, we investigated whether budding events are equally distributed within the area of the AC or whether budding occurs preferentially in certain areas of the AC. Since the circular AC is organized in a symmetrical manner i.e. an outer area with mainly Golgi and *trans*-Golgi vesicles and an inner area with mainly early endosomes (Das et al. 2007), we believed that it was sufficient to compare the outer and inner area of the AC. The location of budding events within the AC was analyzed in micrographs of wild-type virus infected HFF with completely visible ACs. The AC was defined by an elliptic shape, enclosed by Golgi membranes, multivesicular compartments and mitochondria (FIG. 8). This area was further divided by another ellipse with the identical shape and same centre but only half of the main diameter, leading to an AC artificially subdivided into an inner and an outer area. The envelopment stages of the viral particles were assessed separately for both areas and the numbers of enveloped, budding and naked particles were compared for the two regions (Table 5). No significant differences between the two compartments were found, suggesting that secondary envelopment is happening evenly throughout the whole AC. Thus, the investigation of only areas of the AC of one given cells should return valid data about the frequency of budding events within the entire AC of this cell.

Table 5. Envelopment stages of viral particles were assessed separately for the inner and the outer area of the viral assembly compartment on micrographs of wild-type infected HFF at 5 days post infection. A total of 1050 particles were counted in 11 cells and the fractions of enveloped, budding and naked capsids were calculated separately for the inner and outer AC areas.

	mean % particles ± SD		
	enveloped	budding	naked
inner AC	81.1 ± 11.6	18.9 ± 11.6	0.0 ± 0.0
outer AC	80.0 ± 6.8	19.6 ± 6.2	0.5 ± 0.7

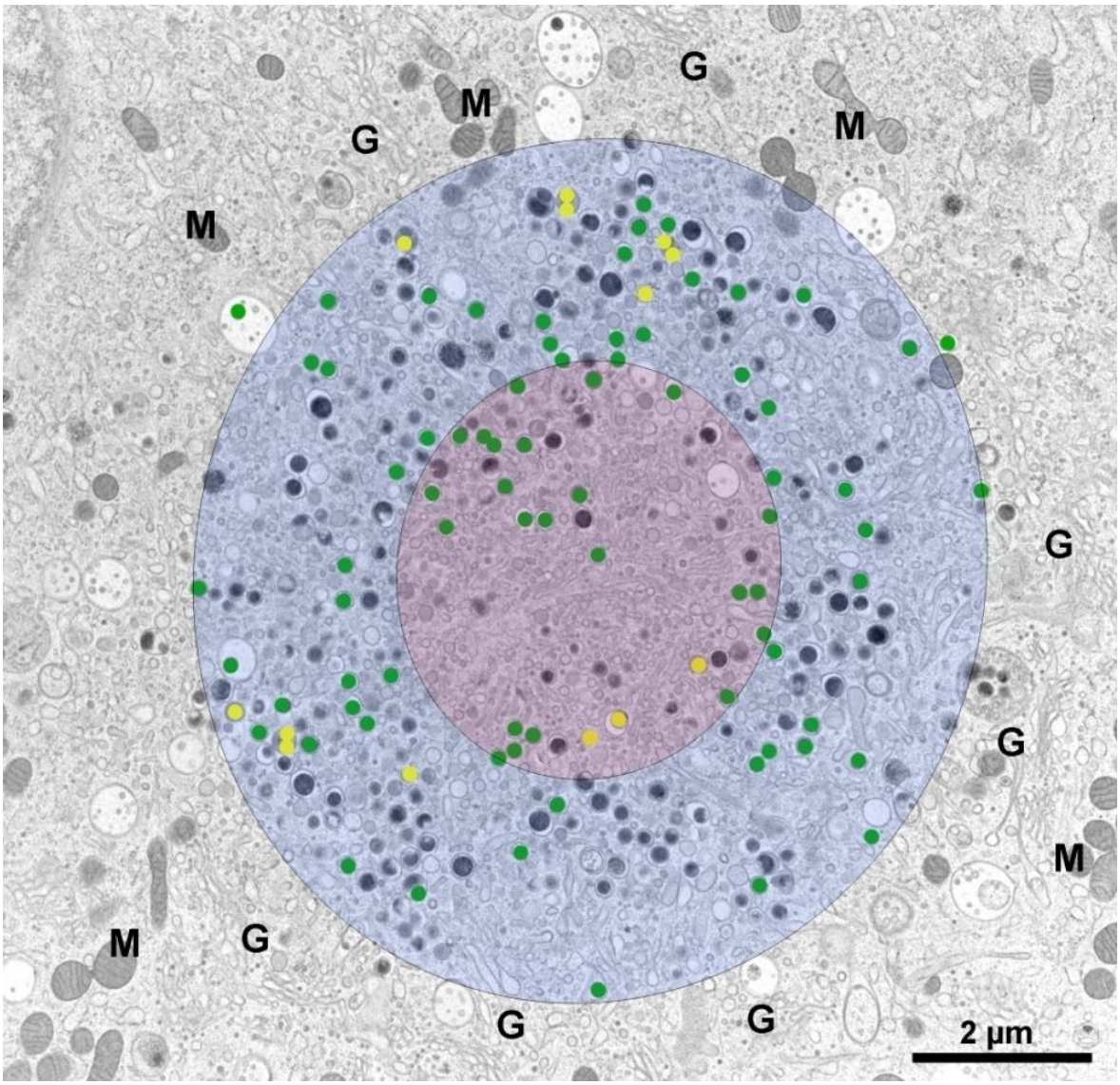


FIG. 8. Budding processes are equally distributed within the inner and outer area of the viral assembly compartment. The AC was artificially subdivided into an inner area (light red) and outer area (light blue) on this micrograph of a wild-type virus infected HFF at 5dpi; it contains fully enveloped (labeled green) and budding (labeled yellow) viral particles and is surrounded by stacks of the Golgi apparatus and Mitochondria. M Mitochondria, G Golgi stacks.

In summary, HCMV infection led to the establishment of a viral AC in fibroblasts, HUVEC and MDM. Fibroblasts and HUVEC appeared similar on an ultrastructural level, while macrophages were characterized by a different cell size and shape, and the distinct presence of multivesicular endosomes. A vast majority of cytoplasmic virus particles of wild-type virus infected fibroblasts, endothelial cells and macrophages was completely enveloped, indicating an efficient secondary envelopment process in all investigated cell types.

3.2 Subcellular localization of pUL71

The subcellular localization of a viral protein within the host cell could be also an indicator for the role that this protein might play during virus morphogenesis. Thus, the subcellular localization of pUL71 was investigated in more detail. At 5 dpi pUL71 was located within the AC of wild-type virus infected HFF as shown by immunofluorescence analyses (FIG. 9). pUL71 was either evenly distributed within the area of the AC or showed a ring like pattern, i.e. with stronger signals in the outer area of the AC. The localization pattern of pUL71 was slightly different from that of viral proteins pp28 and glycoprotein B (gB). Interestingly, signals for pUL71 were overlapping or co-localizing with signals of the cellular protein γ-Adaptin, which is a marker for the *trans*-Golgi network (TGN) (FIG. 9). These data suggested that pUL71 might be associated with membranes.

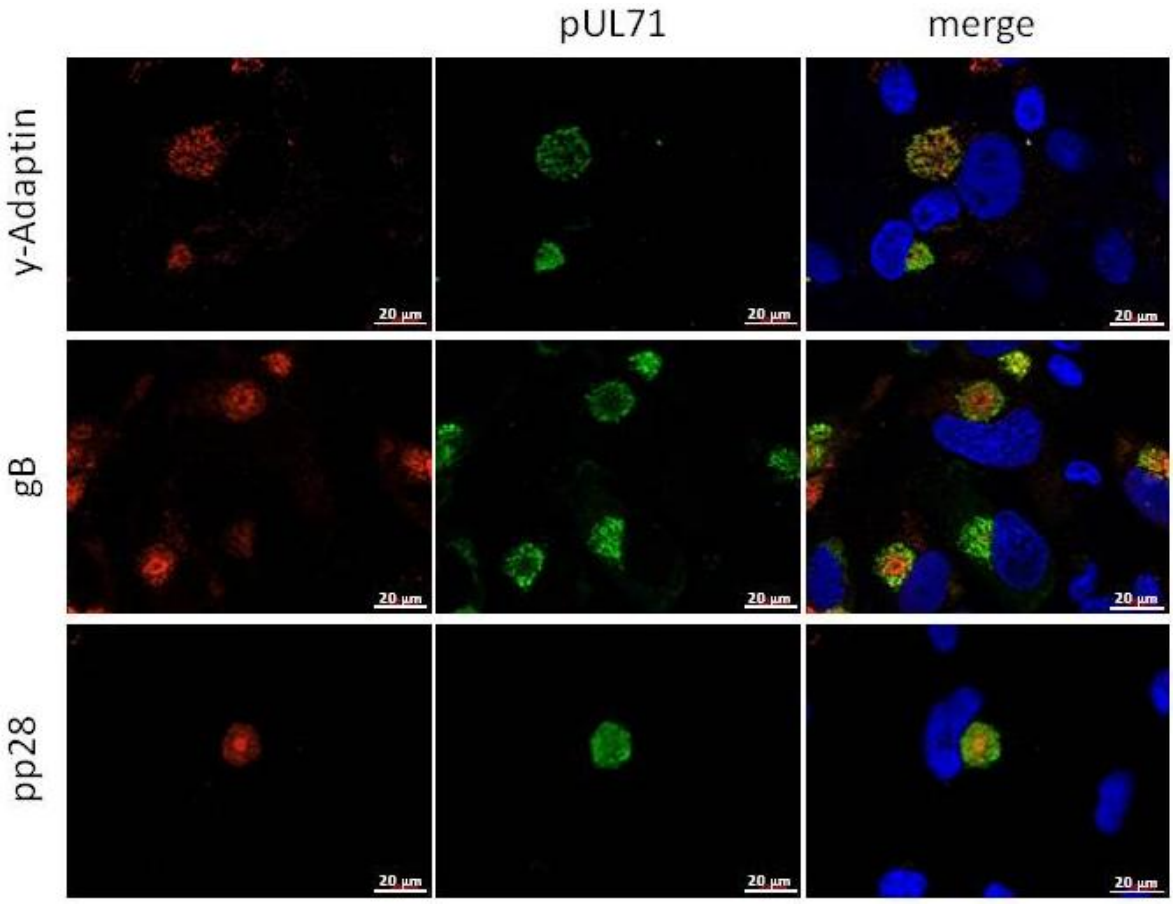


FIG. 9. pUL71 co-localizes with the TGN-marker y-Adaptin. The localization of cellular (y-Adaptin) and viral (gB, pp28, pUL71) proteins in wild-type virus infected HFF (MOI 0.5) is shown. Cells were fixed with 4 % PFA at 5 days post infection. Proteins were detected by the respective primary antibodies and visualized by secondary antibodies conjugated to Alexa Fluor 488 and 555. Nuclei were stained with DAPI.

To investigate the subcellular localization of pUL71 during infection on an ultrastructural level, HFF were infected with a recombinant virus TB71HA, which expresses a C-terminally HA tagged pUL71. As assessed by immunofluorescence, the localization of pUL71 was not affected by the C-terminal HA-tag (Jens von Einem, unpublished data). TB71HA infected cells were cryofixed at 5 dpi and freeze-substituted with glutar aldehyde as fixative but without osmium-tetroxide to preserve immunogenicity. The cells were then embedded in LR-Gold and thin sections were prepared for immuno-gold labeling. Ultra thin sections were labeled against either pUL71 or the HA epitope using the respective primary antibodies followed by secondary antibodies conjugated to 10 nm colloidal gold. Freeze substitution without osmium-tetroxide but only glutar aldehyde as fixative followed by LR-gold embedding of the samples provided sufficient structural preservation to distinguish single membranes (FIG. 10).

Signals for pUL71, detected with either anti-HA or anti-pUL71 antibodies, were found almost exclusively at membranes (FIG. 10 A-D). Gold particles were mostly found at the viral envelope or at membranes of vesicles which contained virus particles, but also at other membranes of round or tubular vesicles within the AC. In some cases these membranous structures seemed to be MVBs or Golgi cisternae, but in many cases the nature of these vesicles was not clear. Most gold particles were found within the AC, whereas outside of the AC hardly any gold particles could be found. Additionally, except for signals at extracellular virus particles no signals for pUL71 were obtained in the extracellular space (FIG. 10 D), suggesting specific labeling with low background. Since the overall labeling density was relatively low, the specificity of the labeling method was further confirmed by using an antibody directed against the most abundant HCMV tegument protein pp65. As expected, signals for pp65 showed a higher labeling density compared to the pUL71 labeling. Gold particles were found at electron dense material - most likely protein aggregates- and dense bodies in the cytoplasm, as well as in the extracellular space (FIG. 10 E-F).

Taken together, the combined data of immunofluorescence stainings and immuno-gold labeling of HCMV infected fibroblasts revealed that pUL71 is associated with membranes within the viral AC, which might be Golgi-derived.

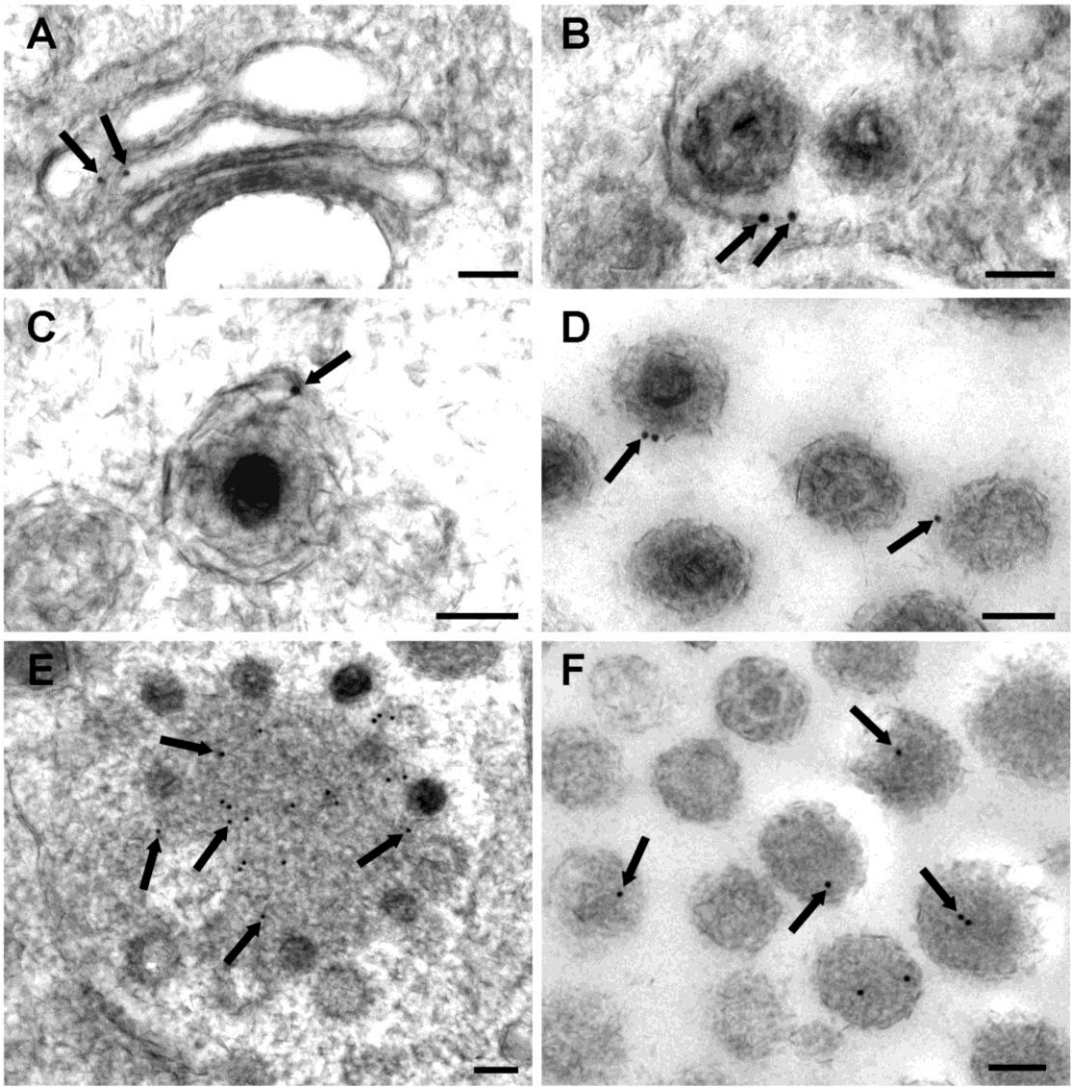


FIG. 10. pUL71 is located at membranes. The location of viral proteins was detected on an ultrastructural level by immuno-gold labeling of thin sections of LR-Gold embedded HFF 5 days after infection with TB71HA. Primary antibodies against HA **(A, B)**, against pUL71 **(C, D)** and against pp65 **(E, F)** were used, followed by secondary antibodies conjugated to 10 nm colloidal gold (arrows). pUL71 is found on the membranes of Golgi apparatus stacks **(A)**, on membranes surrounding viral particles in the cytoplasm **(B, C)**, as well as on the viral envelope of released viral particles **(D)**. Signals for pp65 are detected at protein aggregates surrounded by viral capsids **(E)**, as well as in viral dense bodies in the extracellular space **(F)**. Each bar represents 100 nm.

3.3 Cytomegalovirus morphogenesis in absence of pUL71

To investigate the function of the HCMV tegument protein pUL71, a UL71stop mutant virus (TB71stop) had been generated and analyzed previously (Schauflinger 2008). Since the expression of full-length pUL71 is disabled in the TB71stop virus, it is feasible to draw conclusions about the function of pUL71 by comparing TB71stop to HCMV wild-type

virus. Experiments with TB71stop virus infected cells were performed to learn in detail how the absence of pUL71 affected viral growth and also whether pUL71 knock-out caused similar effects in fibroblasts, endothelial cells and macrophages. First, immunofluorescence analyses were performed to compare the establishment of the viral AC between TB71stop virus infected fibroblasts, HUVEC and MDM. Staining against pp28 was used to mark the AC in TB71stop virus infected fibroblasts at 5 dpi, often revealing an altered appearance of the viral AC compared to wild-type virus infected cells (FIG. 11). Signals for pp28 were often found to accumulate in the periphery of the AC, sometimes at large intracellular vesicles in close proximity to the AC. The same results were obtained for TB71stop virus infected HUVEC and MDM, confirming the abnormal AC arrangement in all investigated cell types (FIG. 11).

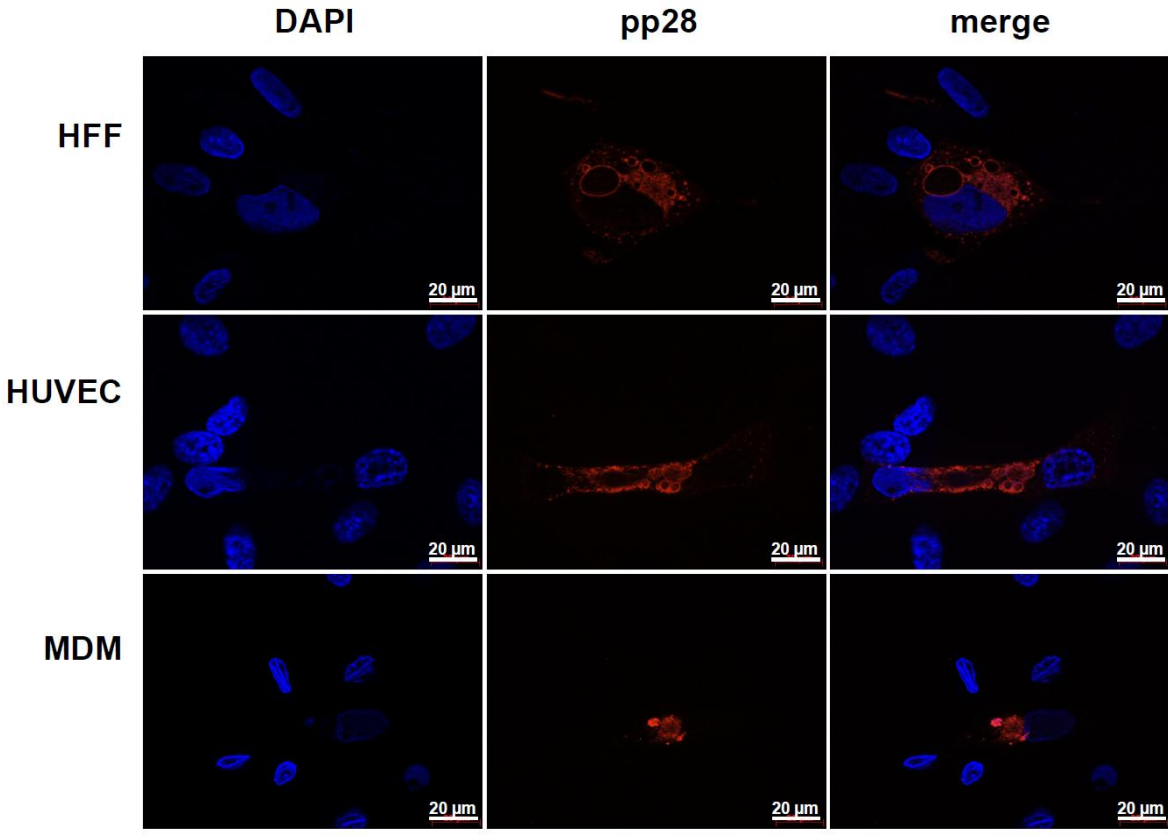


FIG. 11. Absence of pUL71 during HCMV infection leads to the formation of abnormal assembly compartments in fibroblasts, HUVEC and MDM. The subcellular localization of pp28 is shown in TB71stop virus infected HFF (MOI 0.5), HUVEC (MOI 5) and MDM (MOI 5), respectively. Cells were fixed with 4 % PFA in PBS at 5 dpi (HFF) or 6 dpi (HUVEC and MDM). The viral protein pp28 was detected by the respective antibody and visualized by secondary antibodies conjugated to Alexa Fluor 555. Cell nuclei were visualized by DAPI.

Apparently, the appearances of viral ACs were not restricted to a single phenotype at late stages of infection with TB71stop virus. Immunofluorescence stainings revealed the formation of large vesicles and strong accumulations of the viral protein pp28 in the periphery of the AC. To gather more data about the appearances and frequencies of the AC phenotypes in TB71stop virus infected cells, further immunofluorescence assays were performed. For that, HFF were infected with TB71stop virus and fixed at 5 dpi. Staining against the viral protein pp150 served as a marker for viral particles, since pp150 is associated with HCMV capsids in the cytoplasm. Additionally, DNA was labeled with the fluorescent stain DAPI. Then, the state of the AC in infected HFF was assessed. AC phenotypes were classified into three categories. Type I AC showed a characteristic circular or broad-ring like pattern, comparable to the typical appearance of ACs in wild-type virus infected cells (FIG. 12 A). Type II AC was marked by strong accumulations of viral particles and/or vesicles with diameters smaller than 5 µm, especially in the periphery of the AC (FIG. 12 B). Finally, type III AC was characterized by large vesicles with diameters of more than 5 µm in close distance to the AC (FIG. 12 C), often accompanied by accumulations of viral particles as observed in type II AC.

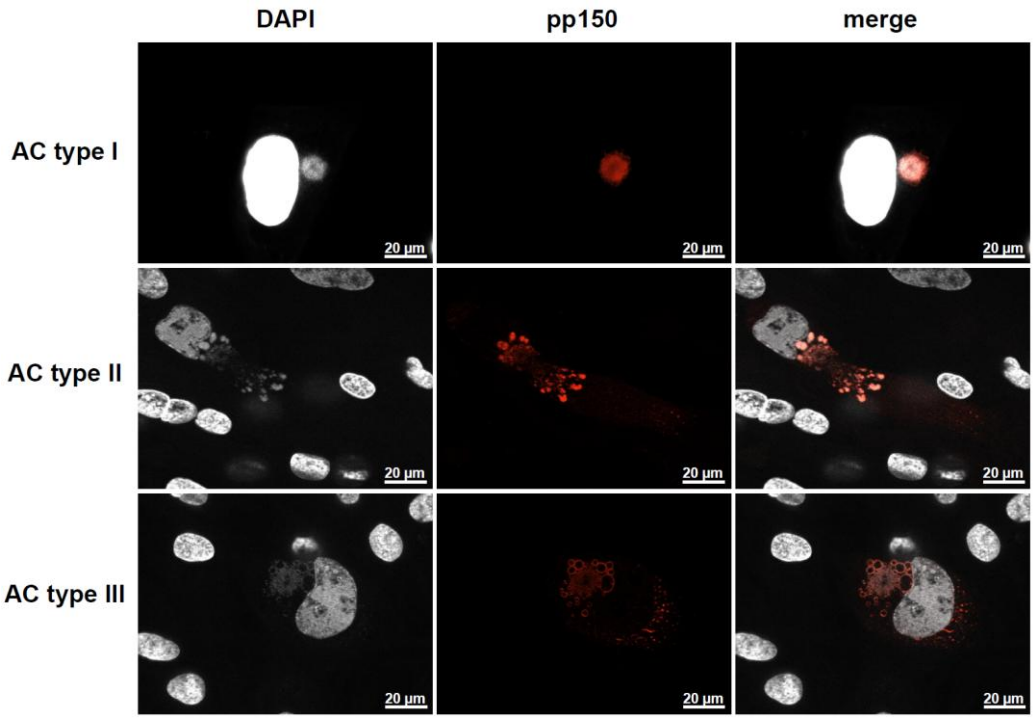


FIG. 12. The appearances of viral assembly compartments are distinguished into three major types: type I is wild-type like, type II is characterized by accumulations of viral proteins, and type III by large vesicles in the periphery of the AC. HFF were infected with TB71stop and fixed with 4 % PFA in PBS at 5dpi. DNA was visualized with DAPI. The viral protein pp150 was detected with the specific primary antibody and visualized with secondary antibodies conjugated to Alexa Fluor 555.

To determine the frequencies of the three different AC phenotypes in TB71stop virus infected fibroblasts, immunofluorescence pictures were randomly taken from infected cells with clearly visible DAPI and pp150 signal in the AC, and a quantification of the AC types was performed. The same was done for wild-type virus infected HFF at 5 dpi which served as reference. Not surprisingly, wild-type virus infection led to the establishment of a type I AC in more than 90 % of the cells, while only few cells exhibited type II AC, and no type III ACs could be observed (FIG. 13 A). In contrast, TB71stop virus infection in HFF led to the establishment of a wild-type like AC type I in ca. 30 % of the cells, while more than 40 % of the cells showed enlarged vesicles of type III, and type II ACs were found in about 20 % of TB71stop virus infected cells (FIG. 13 A).

We wanted to know whether these phenotypes were dependent on the time of infection and on the cell type, respectively. Thus, HFF and HUVEC were infected with wild-type and TB71stop virus, respectively, fixed at 7 dpi, and the AC types were assessed as described above. Again, the majority of wild-type virus infected cells showed a type I AC, while TB71stop virus infection led to the establishment of abnormal AC type II in more than 20 % of the cells and AC type III in about 40 % of the cells. This was found for HFF (FIG. 13 B) as well as for HUVEC (FIG. 13 C) at 7 dpi, suggesting that these AC phenotypes occurred with a similar frequency in different cell types at late times post infection.

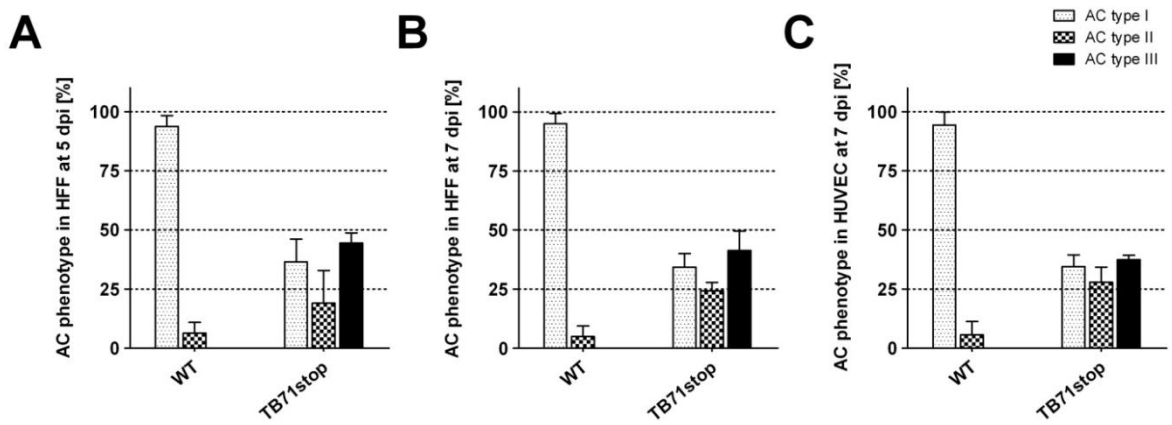


FIG. 13. Frequencies of AC type I (dotted), type II (checkered) and type III (black) were assessed for wild-type and TB71stop virus infected cells, respectively. **(A)** HFF at 5 dpi, **(B)** HFF at 7 dpi, **(C)** HUVEC at 7 dpi. A MOI of 0.1 to 0.5 was used to infect HFF, and a MOI of 1 to 5 was used to infect HUVEC. To visualize the ACs, the cells were stained against the viral protein pp150 with the respective antibodies and DNA was visualized with DAPI. Three independent experiments were performed for each time point and the AC types were assessed in pictures randomly taken from infected cells. The columns show the mean relative ratio of AC phenotypes and the bars give the SD.

Interestingly, the previous ultrastructural analyses of TB71stop infected fibroblasts already showed the occurrence of large vesicles in the periphery of the AC (Schauflinger 2008). These vesicles appeared to be multivesicular bodies (MVBs), since their lumen contained intraluminal vesicles typically found in multivesicular endosomes. To clarify the nature of these vesicles, staining against the cellular protein CD63 served as a marker for MVBs in an immunofluorescence study. CD63 is a tetraspanin abundantly present in late endosomes and lysosomes and is enriched on intraluminal vesicles of MVBs (Pols and Klumpermann, 2009). In TB71stop virus infected HFF, CD63 signals accumulated in the lumen of large vesicles which were also stained positive for pp28, indicating that these enlarged structures were MVBs (FIG. 14).

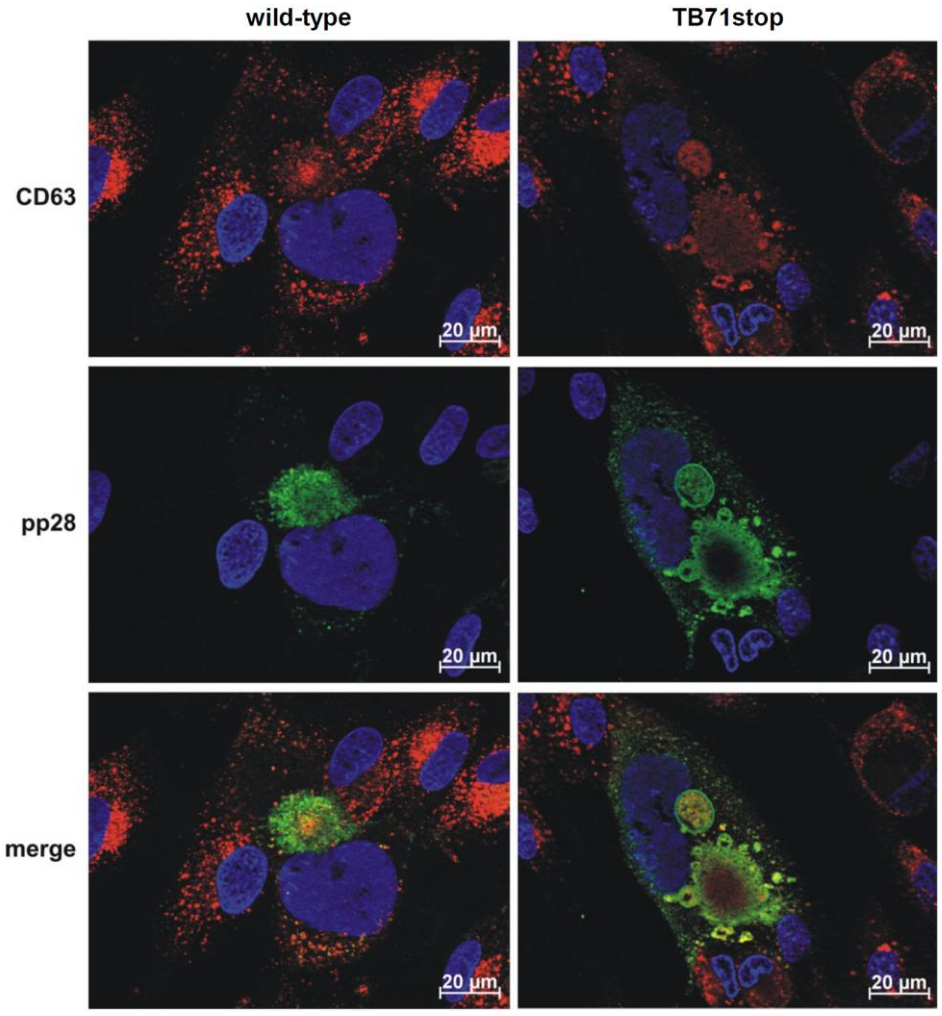


FIG. 14. The MVB marker CD63 accumulates in enlarged vesicles of TB71stop infected cells. The subcellular localization of CD63 and viral pp28 in wild-type and TB71stop virus infected HFF (MOI 0.1 to 0.5) is shown. Cells were fixed with 4 % PFA in PBS at 7 days post infection. CD63 and pp28 were detected by the respective antibodies and visualized by isotype-specific secondary antibodies conjugated to Alexa Fluor 488 (for pp28) and 555 (for CD63). Cell nuclei were visualized by DAPI.

To get a better insight into TB71stop virus infected cells, the phenotypes between the different cell types were compared by TEM analyses. Thus, HFF and MRC-5 were cryofixed at 5 dpi, whereas HUVEC and MDM were cryofixed at 6 dpi, embedded in Epon and further processed for TEM analyses. The phenotype in fibroblasts was assessed first. Not surprisingly, both fibroblast lines looked very similar on an ultrastructural level. Infection with TB71stop virus led to the formation of a viral AC in the host cells, which seemed to be larger in size than in wild-type virus infected cells (FIG. 15 A, B). As indicated by the immunofluorescence data, the abundance and size of MVBs was increased in many TB71stop virus infected fibroblasts. Sometimes vastly enlarged MVBs with diameters of significantly more than 5 µm were found, which was never observed in wild-type virus infected cells. These endosomes accumulated preferably in the periphery of the AC. The viral particles within the AC of TB71stop virus infected fibroblasts were mainly found in the process of budding. The vesicles used for budding were usually bigger than compared to wild-type virus infected fibroblasts, and multiple budding processes into elongated and irregular shaped vesicles was common (FIG. 16 A; see also FIG. 18). Furthermore, TB71stop particles were sometimes budding into MVBs in large numbers (FIG. 16 E). This confirmed the previously observed phenotype and defect of secondary envelopment in fibroblasts (Schauflinger 2008).

Next, these findings were compared to the TEM data of endothelial cells. TB71stop virus infection of HUVEC led to comparable effects as those observed in fibroblasts. Similarly, the AC was often characterized by the appearance of MVBs in the periphery of the AC (FIG. 15 C). Interestingly, also in TB71stop virus infected HUVEC many particles within the AC were seen mostly in different stages of budding, indicating an impairment of final particle envelopment. However, the changed appearance of budding vesicles in TB71stop virus infected HUVEC did not seem to be as pronounced as in fibroblasts. Multiple budding events into bigger vesicles were found also in HUVEC, but not as frequently as in fibroblasts. Budding occurred usually into thinner, tubular vesicles (FIG. 16 B).

Finally, the phenotype of TB71stop virus infected macrophages was assessed. As with fibroblasts and endothelial cells, MDM exhibited often vastly enlarged endosomal vesicles in the periphery of the AC (FIG. 15 D). Out of all cell types investigated, the difference between wild-type and TB71stop virus infection was most pronounced in MDM. Not only was the frequent appearance of MVBs around the viral AC very prominent, but also the inner area of the AC was very densely packed with vesicles used as

budding site by many TB71stop virus particles (FIG. 16 C). Located usually more in the outer area of the AC, sometimes greatly enlarged irregular shaped vesicles were found and many virus particles were attached to those vesicles (FIG. 16 D). This could be found also in TB71stop virus infected fibroblasts and occasionally in HUVEC, and might correspond to the accumulations of the type II AC seen in immunofluorescence stainings (compare to FIG. 12), but this feature was noticeably more prominent in MDM. So far, the data showed a similar phenotype and impairment of secondary envelopment in TB71stop virus infected fibroblasts, endothelial cells and macrophages due to the absence of pUL71.

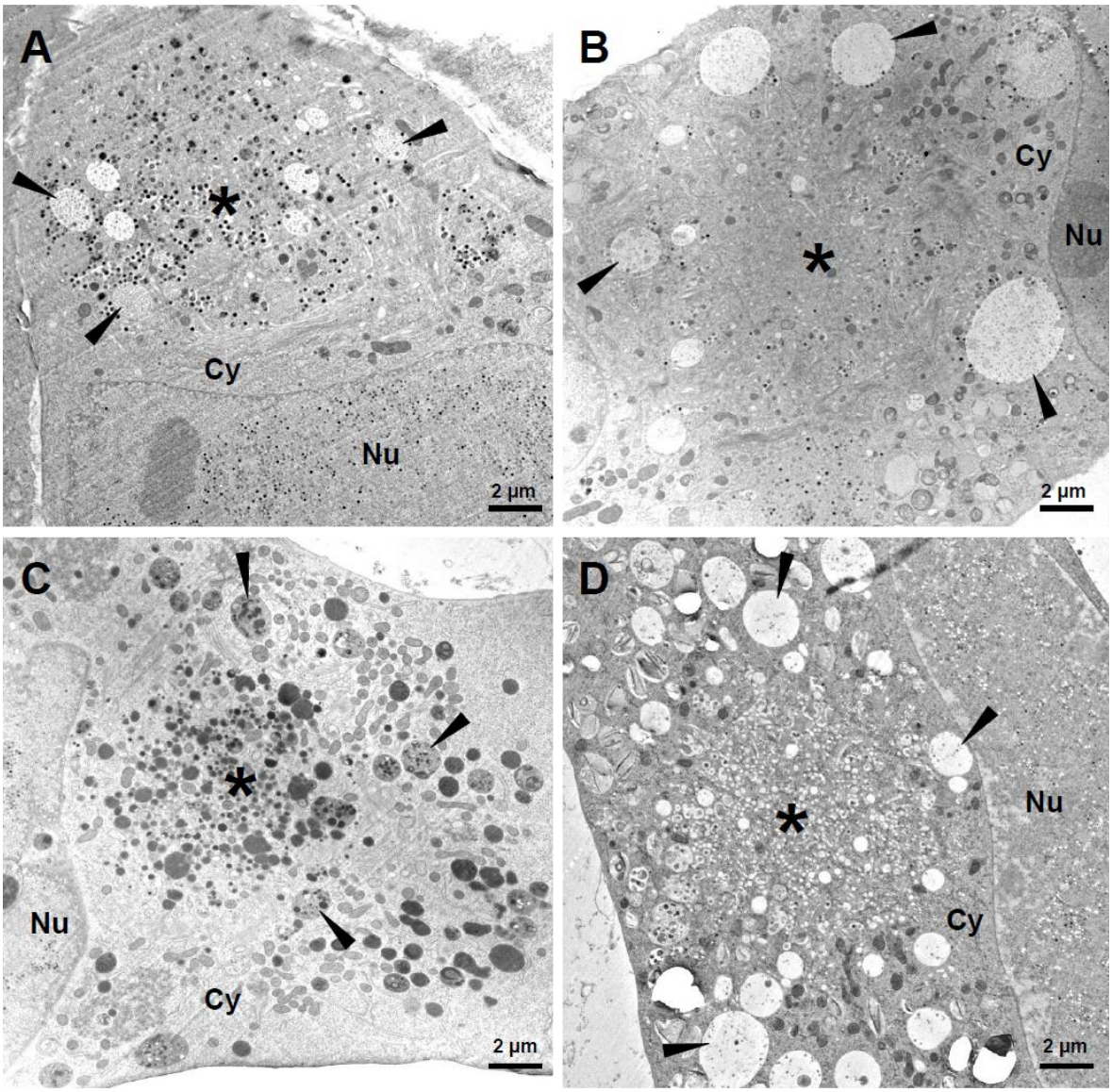


FIG. 15. Absence of pUL71 during HCMV infection leads to the formation of large vesicles in fibroblasts, HUVEC and MDM. Overviews of TB71stop infected cells with the viral AC in the centre are shown. **(A)** HFF at 5 dpi, **(B)** MRC-5 at 5 dpi, **(C)** HUVEC at 6 dpi, **(D)** MDM at 6 dpi The asterisk indicates the centre of the AC. Note that relatively large MVBs (black arrowheads) in the periphery of the AC are a property of many TB71stop virus infected cells, independent from the cell type. Nu nucleus, Cy cytoplasm.

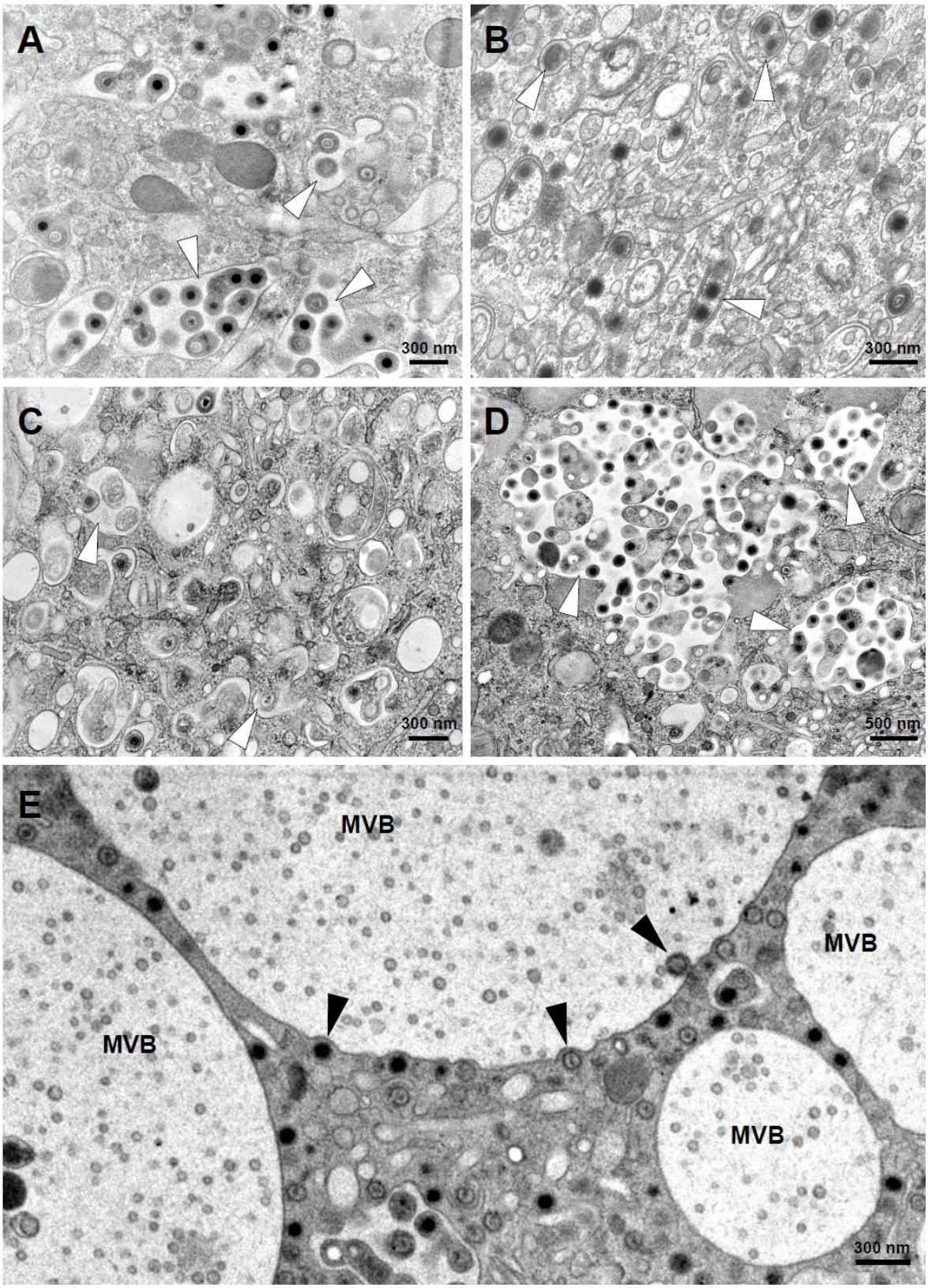


FIG. 16. Budding vesicles (white arrowheads) in TB71stop virus infected cells are often enlarged and irregular shaped. **(A)** Enlarged budding vesicles in HFF at 5 dpi. **(B)** Smaller, tubular or crescent shaped vesicles in HUVEC at 6 dpi. **(C)** Budding vesicles in the central area of the AC, and **(D)** larger vesicles in the periphery of the AC in MDM at 6 dpi. **(E)** Multivesicular bodies (MVBs) are associated to multiple budding TB71stop particles (black arrowheads) in MRC-5 at 5 dpi.

To quantify the impairment of secondary envelopment, the various stages of particle envelopment in the AC were categorized for TB71stop virus infected cells. As with wild-type virus infected cells (chapter 3.1), particles were classified into three different categories: (a) fully enveloped particles, (b) capsids in the process of budding, and (c) naked capsids. While the distinction of the three categories was quite clear for wild-type particles, it was more difficult for the TB71stop particles which were associated with enlarged irregular shaped budding vesicles (FIG. 16; FIG. 17).

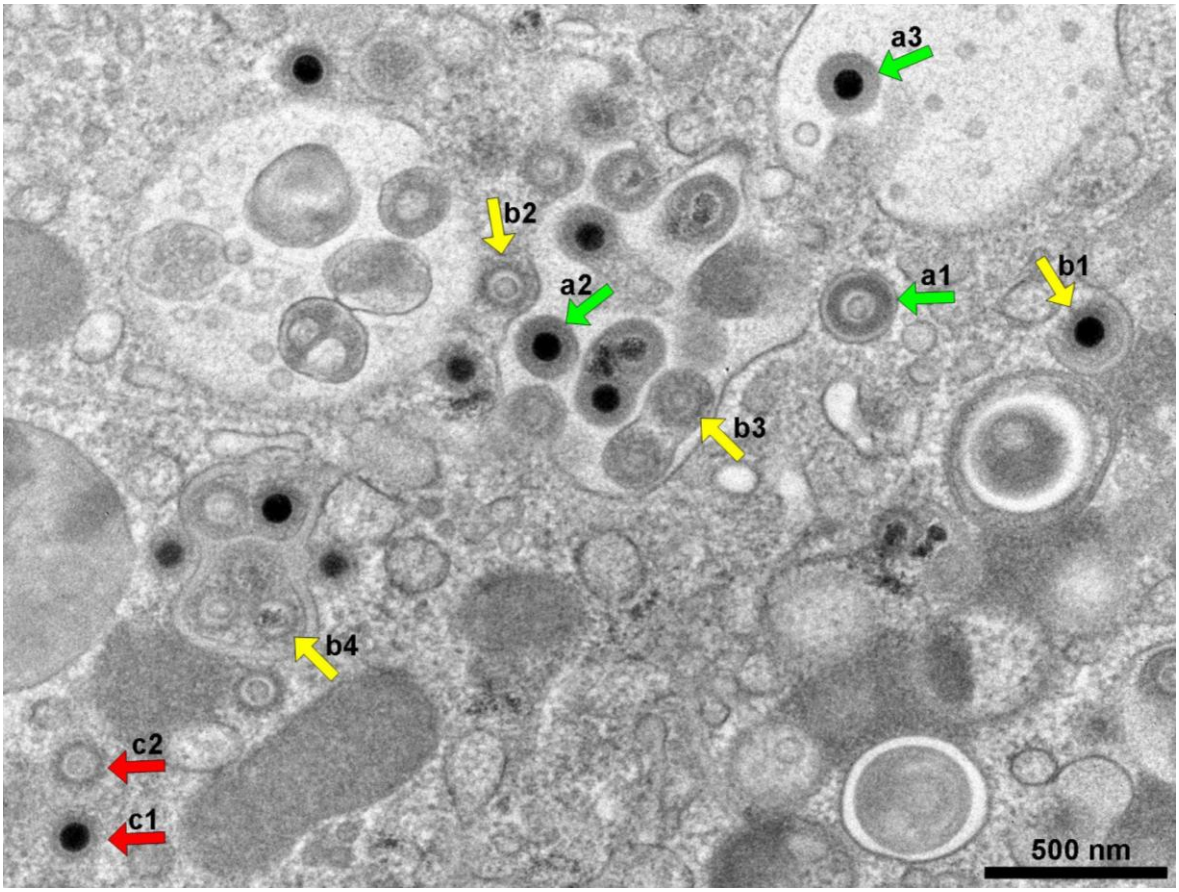


FIG. 17. The various states of HCMV particles within the assembly compartment can be seen in this micrograph of a TB71stop infected HFF at 5dpi. Fully enveloped particles (green arrows) within a small vesicle (a1), a bigger vesicle (a2) and within an endosome (a3). Particles associated to membranes but are not fully enveloped (yellow arrows) are budding into a small crescent shaped vesicle (b1), into a bigger vesicle (b2), or budding together with one (b3) or more viral particles (b4). Naked capsids (red arrows) free in the cytoplasm (c1) and associated to a protein aggregate (c2). Both, nucleocapsids containing DNA (a2, a3, b1, c1) as well as empty particles (a1, b2, b3, b4, c2) can be found in the viral assembly compartment.

It was important to precisely distinguish between the different stages of envelopment. However, judging three dimensional processes such as envelopment from a two dimensional micrograph is difficult. Thus, electron tomography was performed to gather

three dimensional data. For that, 500 to 800 µm thick sections were prepared from Epon embedded TB71stop virus infected HFF and imaged in a Titan 300-kV field emission transmission electron microscope in scanning transmission mode. A total of 71 images were recorded at tilt angles from +70° to -70° and the three dimensional image data was reconstructed. The tomography analysis was focused on the particles that were associated to enlarged budding vesicles in the AC. Very often particles were found in long tubules, which prolonged into these vesicles. On some occasions it was unclear whether a particle was yet fully enveloped or still in the process of budding, e.g. the particles b3 and b4 in FIG. 17. To get a better picture of such particles, membranes and capsids were manually labeled in the three dimensions of the electron tomogram, resulting in a three dimensional computer visualization of budding processes (FIG. 18). Obviously these particles were not fully enveloped, since the membrane fusion had not been completed. Another feature of those non enveloped particles was that their tegument layer was usually not densely associated to the surrounding membrane, but had a rather spiked appearance. This was in contrast to fully enveloped particles, where the tegument evenly filled the space between the viral capsid and the surrounding membrane.

Based on these data, a quantification of enveloped, budding and naked capsids was performed on TB71stop virus infected fibroblasts, HUVEC and MDM, by analyzing micrographs of the AC and categorizing the particles accordingly. The absence of pUL71 during HCMV infection led to a severe envelopment defect in all cell types, which was marked by a mean amount of enveloped particles of less than 25 % (Table 6).

Table 6. Quantification of envelopment stages of TB71stop virus particles in the AC of HFF (5 dpi), MRC-5 (5 dpi), HUVEC (6 dpi) and MDM (6 dpi), respectively. The data was assessed from randomly chosen areas of ACs within n cells from at least two independent experiments per cell type.

			mean % particles ± SD		
cell type	n	# particles	enveloped	budding	naked
HFF	18	1063	24.6 ± 8.6	73.2 ± 9.7	2.3 ± 4.3
MRC-5	19	1244	20.4 ± 10.2	77.6 ± 9.4	2.0 ± 3.6
HUVEC	20	565	18.2 ± 6.6	74.2 ± 6.6	7.1 ± 10.8
MDM	24	1121	16.0 ± 9.2	83.8 ± 9.1	0.3 ± 0.8

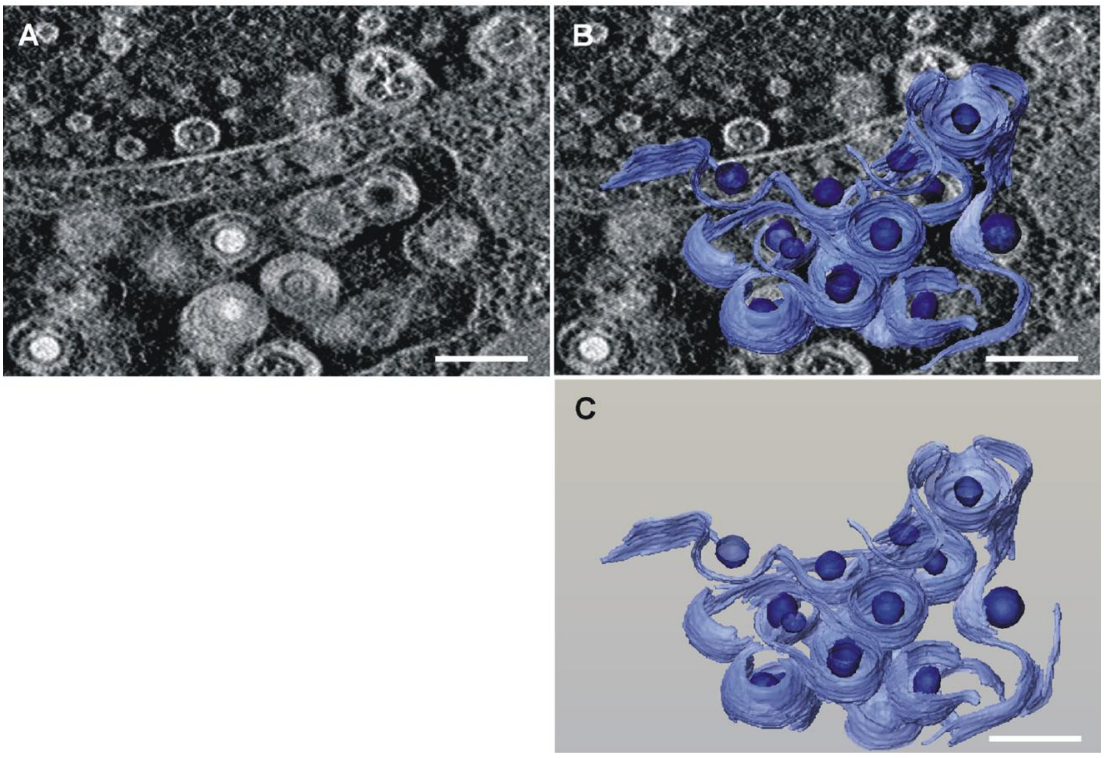


FIG. 18. A three dimensional reconstruction of membranes and viral capsids from tomography of TB71stop infected HFF at 5 days post infection provides information about budding events. Areas with high mass density, such as membranes occur bright in the dark-field STEM tomogram. **(A)** A single slice from the three-dimensional tomogram shows a big vesicle in which multiple budding processes of TB71stop virus particles take place. **(B)** Membranes used as budding sites as well as viral capsids were reconstructed and superimposed on the original micrograph. Membranes are depicted in light blue; viral capsids are indicated in dark blue. **(C)** Reconstruction of the budding processes only. Bars, 200 nm.

Since an impairment of secondary envelopment was found and often a larger amount of viral particles seemed to accumulate in TB71stop virus infected cells, we hypothesized that the number of virus particles in the cytoplasm was higher in TB71stop virus infected cells than in wild-type virus infected cells. Thus, the total amount of virus particles was assessed from micrographs of completely visible ACs of 11 wild-type virus infected HFF and 12 TB71stop virus infected HFF from more than three independent experiments. While in wild-type virus infected fibroblasts an average of 95 virus particles was found within one section of the AC, TB71stop virus infected cells exhibited a more than 3-fold increase in the average number of cytoplasmic particles (FIG. 19). These data confirmed that TB71stop particles were accumulating in the cytoplasm in vast numbers. Interestingly, the number of viral particles seemed to correlate to the phenotype of the AC. Two TB71stop virus infected cells with ACs morphologically similar to wild-type ACs (AC type I, FIG. 19 B) exhibited no significant increase of particle numbers within the AC. However, five

TB71stop virus infected HFF with strong accumulations of viral particles at the AC (AC type II, FIG. 19 B) exhibited a more than two-fold increase in the number of viral particles compared to wild-type virus. The number of virus particles within five ACs that were characterized by large MVBs (AC type III, FIG. 19 B) was increased more than five-fold compared to wild-type virus.

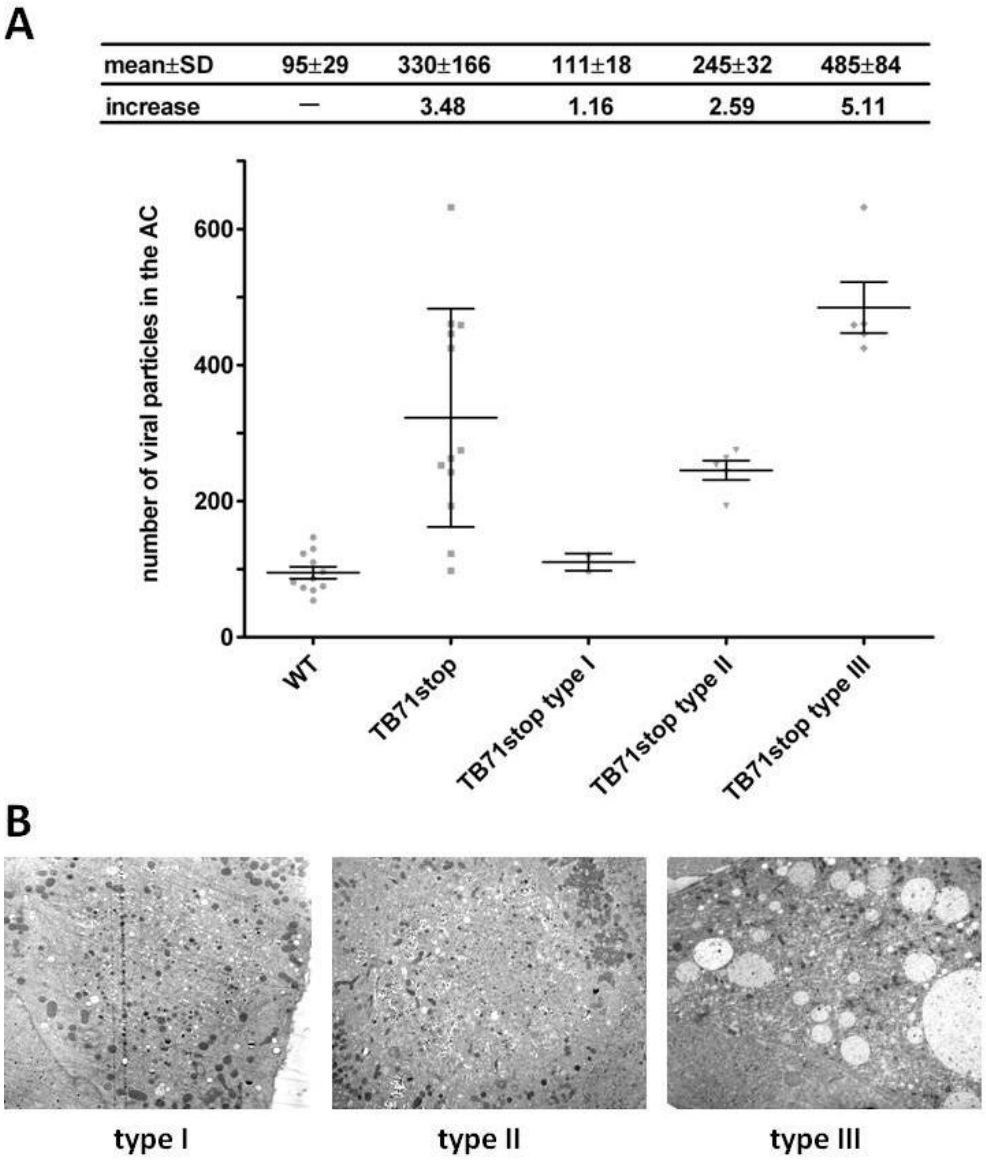


FIG. 19. TB71stop virus infected cells exhibit a more than 3-fold increase in the average number of cytoplasmic particles compared to wild-type virus infected cells. The number of viral particles was counted on two-dimensional slices through ACs at 5 days post infection. 11 wild-type virus infected HFF and 12 TB71stop virus infected HFF from at least four independent experiments per virus were investigated. **(A)** Single data points are represented by light grey symbols, the mean ± SD is indicated by the black bars and explicitly given in the table above each group, together with the factor on which the number of TB71stop particles is increased compared to wild-type virus. **(B)** The data for TB71stop virus infected cells was further distinguished into three different AC phenotypes. Type I AC appears similar as in wild-type virus infected cells, type II is marked by distinct particle accumulations and type III is characterized by large MVBs.

Virus particles in the cytoplasm can also be distinguished on the basis of their DNA content. The packaging of the HCMV genome into the viral capsids is a prerequisite for the production of infectious virus particles. However, in reality not all capsids in the nucleus are loaded with a genome, and also empty capsids can leave the nucleus. Therefore, viral particles which contain either genomic DNA (the so called nucleocapsids) or are empty (i.e. derived from B- or A-capsids) can be found in the cytoplasm. Particles containing the viral genome appear black on TEM micrographs, while empty particles appear bright and are either characterized by a protein ring structure within the capsid or completely empty (FIG. 17). We wanted to clarify, whether there was a difference in the amount of nucleocapsids and empty capsids between wild-type and TB71stop virus infected cells, respectively. Thus, micrographs of ACs of wild-type and TB71stop virus infected HFF were analyzed at 5 dpi and the found particles were categorized as either empty or DNA filled. Approximately 70 % of all viral particles within the AC of wild-type virus infected cells were nucleocapsids (Table 7). Surprisingly, only 40 % of the TB71stop particles contained DNA, showing that the absence of pUL71 caused a significant reduction of cytoplasmic nucleocapsids.

Table 7. The fraction of nucleocapsids out of the total amount of particles in random regions of ACs of 19 wild-type and 9 TB71stop virus infected cells were assessed from more than 3 independent experiments at 5 dpi.

virus	# particles	mean % nucleocapsids ± SD
wild-type	623	72.5 ± 10.6
TB71stop	715	40.8 ± 13.7

Viral genome packaging into capsids occurs in the nucleus. To clarify whether the reduction of cytoplasmic nucleocapsids in the absence of pUL71 is based on a defect in genome packaging, HFF were infected with wild-type HCMV and TB71stop virus, respectively, and processed for TEM analysis 5 dpi. Micrographs of nuclei of wild-type and TB71stop virus infected HFF were randomly taken and the numbers of DNA containing C-capsids, of their precursors (B-capsids), and of empty A-capsids were counted. The most abundant type of nuclear particles were B-capsids, followed by C-capsids, while the amount of A-capsids was low. This was true for both, wild-type and TB71stop virus infected cells (FIG. 20). Consistent with this observation, no significant

differences between wild-type and TB71stop virus were found, suggesting that pUL71 is not involved in genome packaging.

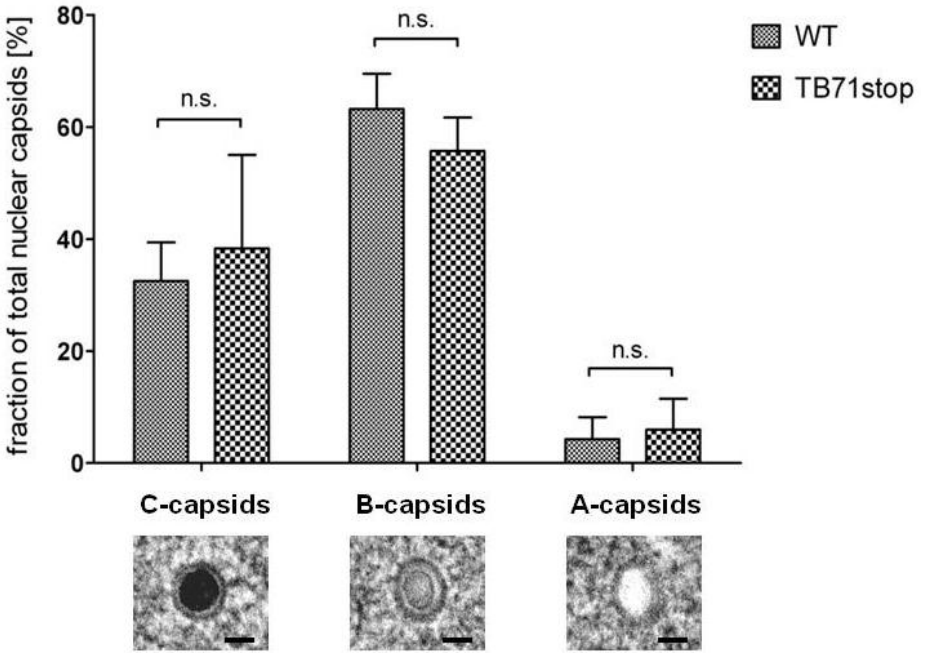


FIG. 20. The relative amounts of nuclear A-, B- and C-capsids, respectively, do not differ between wild-type and TB71stop virus infected HFF. The data for each group was assessed from micrographs taken from the nuclei of HFF 5 days post infection from at least three independent experiments per group. A total amount of 1220 capsids from 8 nuclei for wild-type virus and 2002 capsids from 10 nuclei for TB71stop virus were counted, and the fractions of A-, B- and C-capsids were statistically compared by unpaired t-testing using GraphPad Prism V5.01. No significant differences ($p < 0.05$) between the fractions of capsids of wild-type and TB71stop viruses were found. Micrographs of a C-, B- and A-capsid are depicted beneath the respective group. Bars 50 nm.

Since the absence of pUL71 had no effect on genome packaging, we wondered whether empty capsids were less efficiently enveloped than nucleocapsids and thus accumulated within the cytoplasm, since only enveloped particles are capable to leave the host cell. Therefore it was investigated whether the DNA content of a capsid affected its capability to acquire an envelope. Micrographs of ACs of wild-type and TB71stop virus infected HFF were analyzed at 5 dpi. Virus particles were classified as either empty or DNA-filled, and further distinguished into enveloped or non-enveloped. In wild-type virus infected cells approximately one third of the total particles analyzed were empty, while almost two thirds of the particles in the AC were nucleocapsids (FIG. 21). About the same ratio of empty particles to nucleocapsids was found within the population of enveloped particles. The percentage of nucleocapsids within the group of non-enveloped particles was lower

compared to the other groups, but not significantly different. Similarly, in TB71stop virus infected HFF the percentage of nucleocapsids within the groups of total, enveloped, and non-enveloped particles was about the same, with no significant differences between those groups (FIG. 21). This data suggested that envelopment of particles was independent of their packaging status, despite the tendency of nucleocapsids being more often found enveloped than non-enveloped.

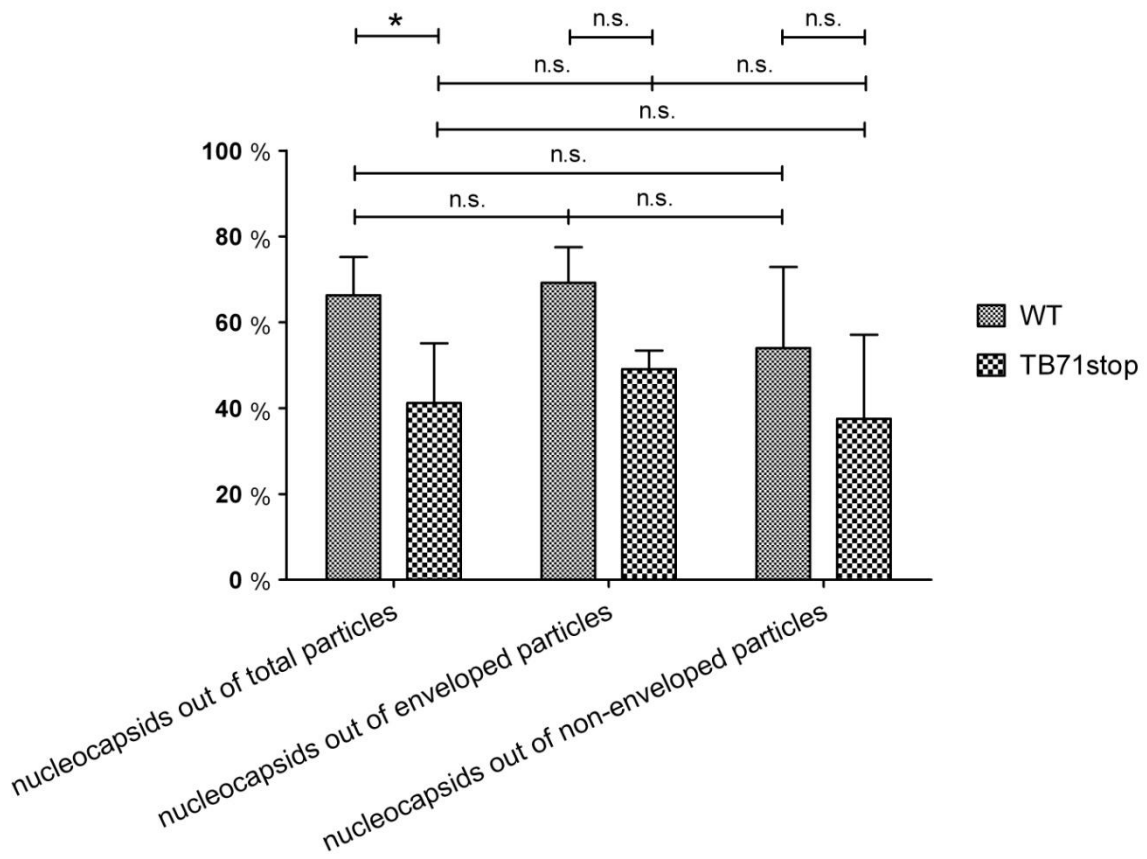


FIG. 21. Envelopment of HCMV particles is independent of the DNA content of the particles. The fractions of nucleocapsids out of the total cytoplasmic particles, out of all enveloped particles and out of all non-enveloped particles, respectively, were determined in wild-type and TB71stop virus infected HFF. Particles were counted on micrographs taken from areas of ACs at 5 days post infection from at least three independent experiments. 247 particles for wild-type virus and 427 particles for TB71stop virus were counted. Data groups were statistically compared using the Mann-Whitney test in GraphPad Prism V5.01. Bars: standard deviation, n.s. not significant, * $p < 0.05$.

Since more empty capsids than nucleocapsids accumulated in the cytoplasm of TB71stop virus infected cells, and those cells were characterized by a pronounced occurrence of multivesicular endosomes, we aimed to investigate whether nucleocapsids were more likely to be degraded and thus found inside of multivesicular bodies (MVBs). Therefore the proportions of nucleocapsids and empty particles, which were attached to the limiting membranes of MVBs or intraluminal of MVBs were determined in micrographs of TB71stop virus infected HFF (Table 8). While the majority of particles at membranes of MVBs were empty capsids, particles in the lumen of MVBs were mainly nucleocapsids, suggesting a more efficient uptake of nucleocapsids compared to empty capsids at MVB membranes. This may also explain the low amount of nucleocapsids in TB71stop virus infected cells.

Table 8. Determination of the proportion of nucleocapsids and empty particles (containing no DNA) found attached to membranes of MVBs or inside MVBs in micrographs of TB71stop infected HFF at 5dpi. The table contains data of 4 independent experiments.

particles attached to MVBs counted	293
nucleocapsids of attached particles	27.3 %
empty capsids of attached particles	72.7 %
particles inside MVBs counted	99
nucleocapsids of particles inside MVBs	57.6 %
empty capsids of particles inside MVBs	42.4 %

Taken together, these data showed that absence of HCMV pUL71 caused various alterations of the morphology of infected fibroblasts, endothelial cells and macrophages, which differed from the morphology of HCMV wild-type infected cells. These alterations were characterized by the pronounced occurrence of multivesicular bodies and by a noticable accumulation of non-enveloped viral particles within the AC. The impairment of secondary envelopment went along with an altered appearance of vesicles that were used for budding. Furthermore, the relative amount of nucleocapsids in the cytoplasm of TB71stop virus infected fibroblasts was reduced compared to wild-type virus infected cells, although no influence of pUL71 on genome packaging in the nucleus could be detected.

3.4 Investigation of potential N-terminal pUL71 palmitoylation sites

While the phenotype caused by pUL71 deficient HCMV was well characterized by now, it was not clear whether these found defects were related to a single pUL71 function or rather to a combination of multiple pUL71 functions. To clarify this, recombinant viruses with mutations within known or potential functional domains within the sequence of pUL71 were investigated. First, we focused on the pUL71 N-terminus.

Deletion of the pUL71 N-terminus led to a cytoplasmic distribution of this protein (Fischer 2008), suggesting that the N-terminus determines the localization of pUL71 at membranes. Interestingly, all known proteins homologous to pUL71 have in common a conserved palmitoylation site at the N-terminus (Nozawa et al. 2005), and palmitoylation of a protein can determine its association to membranes, possibly influencing the subcellular localization (Resh, 1999). The software CSS-Palm 3.0 which evaluates potential palmitoylation sites based on a given protein sequence (Ren et al. 2008), predicted two N-terminal palmitoylation sites for two pUL71 cysteines at positions 8 and 13 (Table 9). Previous investigations of the double point mutant virus TB71C8/13A where the cysteines on position 8 and 13 had been replaced by alanines showed a growth defect and reduced plaque size in infected HFF (Böck 2010). To clarify on the contributions of the individual cysteines, recombinant viruses TB71C8A and TB71C13A had been generated, by mutating either C8 or C13 into alanine (Suffner 2011). In this study, the double mutant TB71C8/13A and the respective single point mutant viruses TB71C8A and TB71C13A were investigated in more detail to gain information about the importance of the two potential pUL71 palmitoylation sites for HCMV morphogenesis.

Table 9. Two potential N-terminal palmitoylation sites within the sequence of pUL71 were predicted by the software CSS-Palm 3.0 (http://csspalm.biocuckoo.org).

Position	Peptide	Score	Cutoff	Cluster
8	MQLAQRLCELLMCRR	2,496	1,225	Cluster C
13	RLCELLMCRRKAAPV	1,338	0,308	Cluster A

Since post-translational palmitoylation of pUL71 might be responsible for its localization, immunofluorescence analyses were performed in cells infected with TB71C8/13A, TB71C13A and TB71C13A, respectively, to determine effects of the mutations C8A and C13A on the localization of pUL71 (FIG. 22). Antibodies against pUL71 were used to visualize this protein, while labeling of HCMV tegument protein pp28 was used to mark the viral AC. In wild-type virus infected cells, the signals for pUL71 and pp28 partially

overlapped, demonstrating the localization of pUL71 at the AC (FIG. 22 A-C). The same results were obtained for TB71C8A virus infected cells, indicating that mutation of C8 did not affect pUL71 localization (FIG. 22 G-I). Interestingly, the signal intensity for pUL71 was very low in both, TB71C8/13A (FIG. 22 D-F) and TB71C13A (FIG. 22 J-L) virus infected cells. Weak pUL71 signals in those cells could be found in the area of the AC, along with very weak pUL71 signals in the surrounding cytoplasm. These results were confirmed for HFF at 5 dpi (data not shown) as well as for HUVEC seven days after infection with TB71C8/13A, TB71C8A and TB71C13A (FIG. 22).

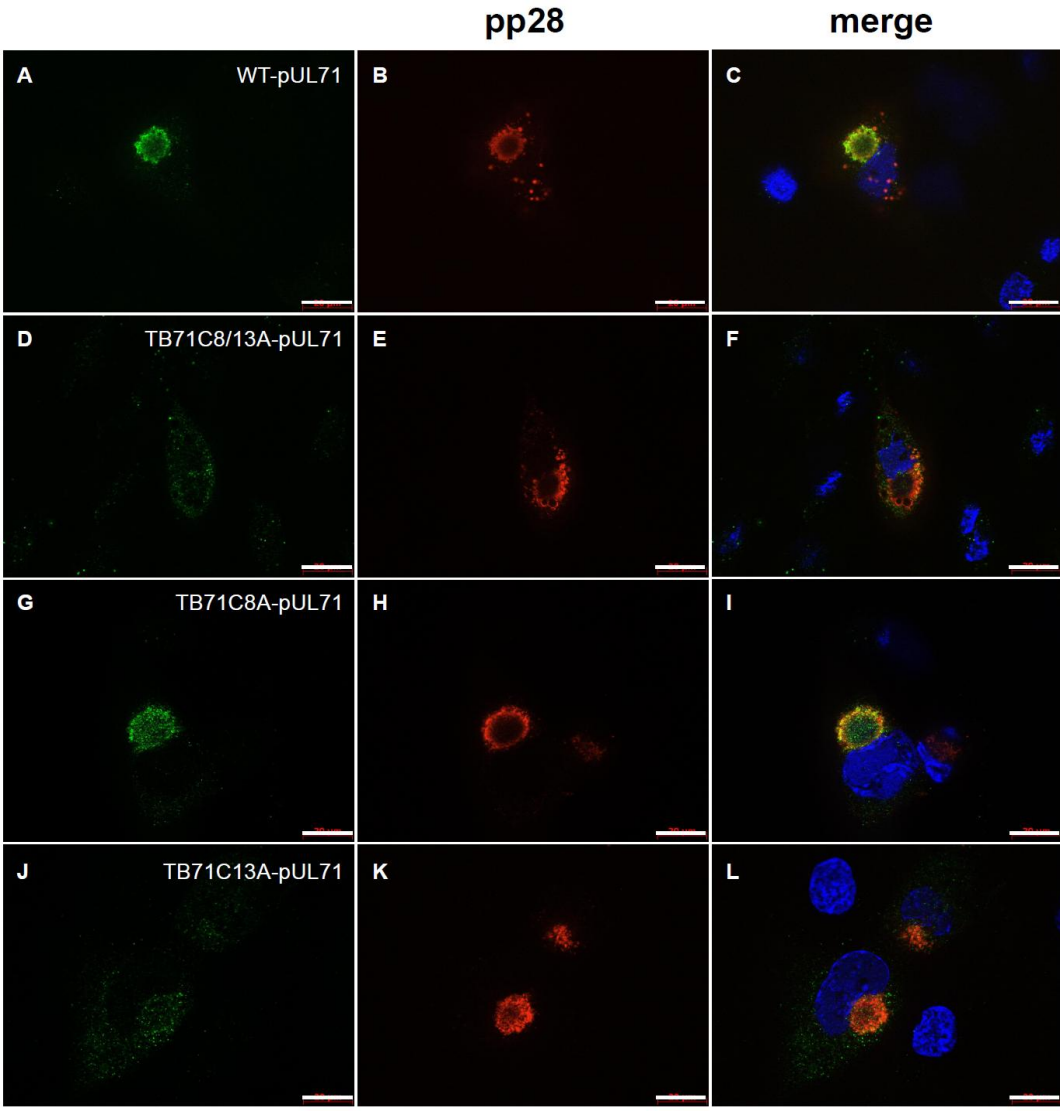


FIG. 22. Only weak pUL71 signals are seen when pUL71 C13 is impaired. The localization of pUL71 and pp28 in infected HUVEC infected with wild-type virus **(A-C)**, TB71C8/13A **(D-F)**, TB71C8A **(G-I)** and TB71C13A **(J-L)** at an MOI of 5 is shown. Cells were fixed with 4 % PFA in PBS at 7 dpi. The viral proteins pUL71 and pp28 were detected by the respective antibodies and visualized by respective secondary antibodies conjugated to Alexa Fluor 488 (for pUL71) and 555 (for pp28). Cell nuclei were visualized by DAPI. Bars 20 µm.

The data obtained by immunofluorescence studies suggested decreased amounts of pUL71 in the cytoplasm of cells infected with TB71C8/13A and TB71C13A, rather than a delocalization of the protein. To compare the pUL71 levels between wild-type, TB71C8A and TB71C13A virus infected HFF, lysates of infected cells were processed for immuno-blotting at 5 dpi. pUL71 was detected by the respective antibody. No pUL71 signals could be detected in the lysate of TB71C13A virus infected cells, while clear signals were obtained in lysates of wild-type and TB71C8A virus infected HFF (FIG. 23). However, pUL71 signals seemed to be reduced in TB71C8A virus infected cells as well, possibly indicating a similar, but less pronounced effect in the reduction of pUL71 levels as in TB71C13A virus infected cells. Equal infection rates were confirmed by detecting pp65, and the loading of equal amounts of cell lysate was controlled by the detection of cellular actin (FIG. 23).

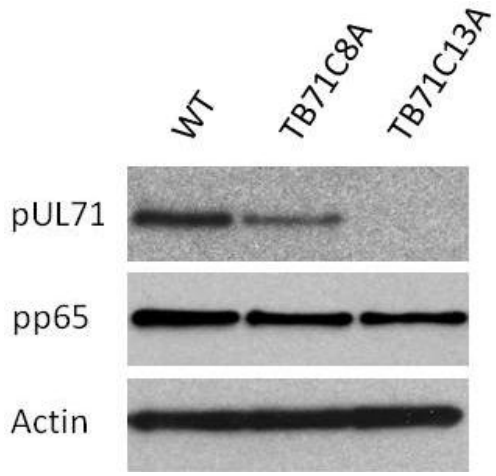


FIG. 23. pUL71 is not detectable when pUL71 cysteine 13 is mutated to alanine. A Western blot was performed with lysates of wild-type, TB71C8A, and TB71C13A virus infected HFF at 5 dpi. Antibodies against pUL71, pp65 and actin were used to detect the respective proteins, followed by the respective secondary antibodies conjugated to HRP.

Immunofluorescence stainings of TB71C8/13A and TB71C13A virus infected cells at 7 dpi not only revealed weaker signals for pUL71, but also enlarged vesicles in the periphery of the AC could be observed, resembling the MVBs found in analyses of the TB71stop virus. These vesicles were found in both TB71C8/13A and TB71C13A virus infected HFF (data not shown) and HUVEC (FIG. 24), but not in TB71C8A virus infected cells. We hypothesized, that these vesicles corresponded to the MVBs which were observed in our previous analyses of TB71stop virus infected cells. To investigate the nature of these enlarged vesicles, antibodies against the cellular MVB marker CD63 were

used. Indeed, accumulation of CD63 could be observed inside the enlarged vesicles in TB71C8/13A and TB71C13A virus infected HUVEC (FIG. 24), suggesting that these vesicles were MVBs and that the observed phenotype corresponded to the phenotype in TB71stop virus infected cells.

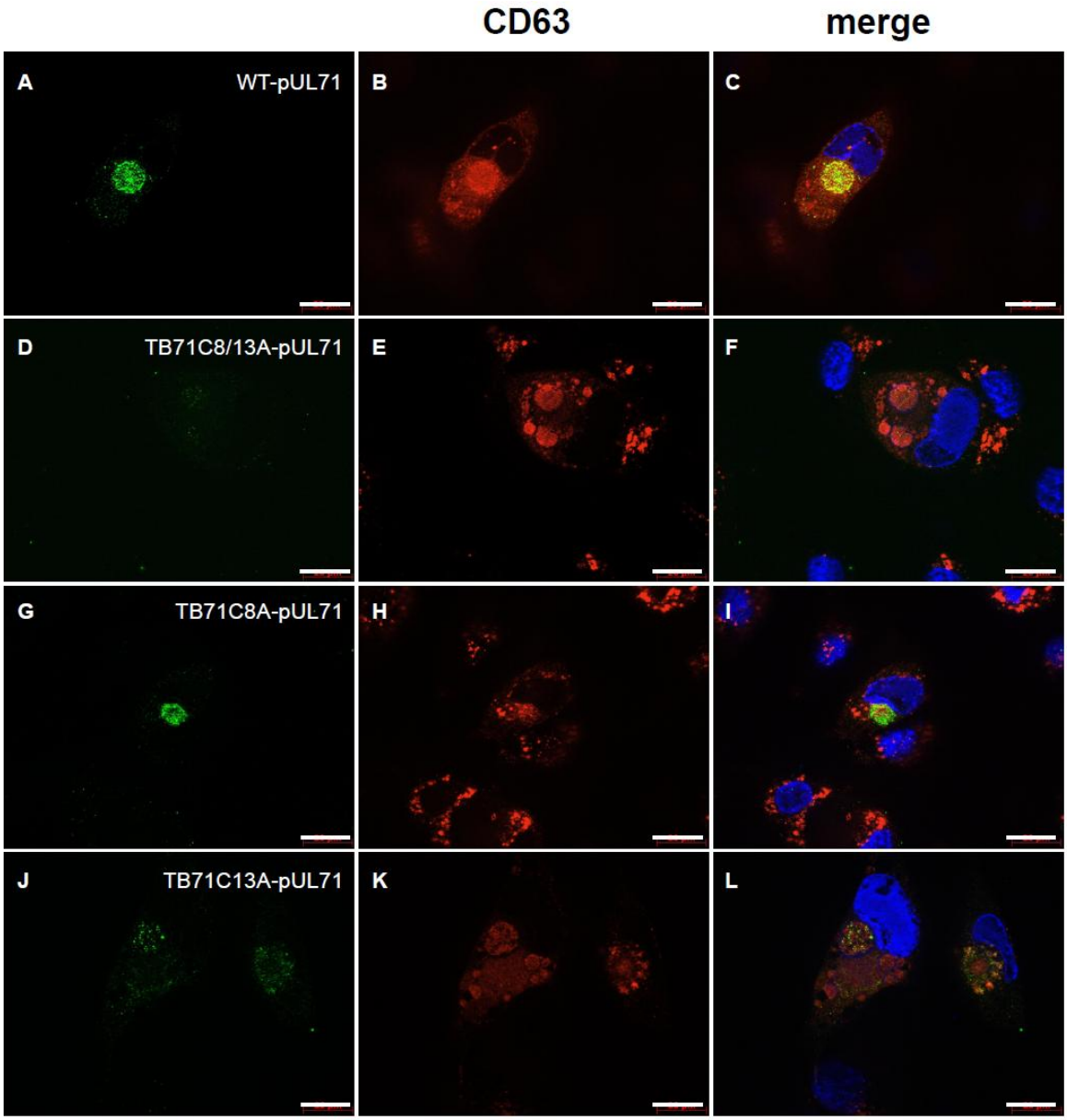


FIG. 24. Large MVBs occur when pUL71 C13 is mutated to A13. The subcellular localizations of MVB marker CD63 and pUL71 are shown in wild-type **(A-C)**, TB71C8/13A **(D-F)**, TB71C8A **(G-I)** and TB71C13A **(J-L)** virus infected HUVEC (MOI 5). Cells were fixed with 4 % PFA in PBS at 7 dpi. pUL71 and CD63 were detected by the respective antibodies and visualized by respective secondary antibodies conjugated to Alexa Fluor 488 (for pUL71) and 555 (for CD63). Cell nuclei were visualized by DAPI. Bars 20 µm.

However, these large MVBs could only be observed in a fraction of the cells infected with TB71C13A and TB71C8/13A viruses, respectively. Further immunofluorescence studies were performed to assess the frequency of these phenotypes, as already described for TB71stop virus infected cells, and the ACs were categorized as type I, II, or III, respectively (compare to FIG. 12 in chapter 3.3). Infection with the viruses TB71C8/13A and TB71C13A caused a similar picture as seen in TB71stop virus infected cells (FIG. 25). It was characterized by type III ACs in 30 % of infected cells and a smaller amount of cells that exhibited type II AC, while less than 40 % of the cells showed wild-type like type I ACs. On the contrary, the recombinant virus TB71C8A showed a picture similar to wild-type virus, with type I ACs found in more than 80 % of infected cells and a minor percentage of type II ACs. Quantification of AC types in HFF at 5 and 7 dpi, as well as in HUVEC at 7 dpi confirmed the wild-type like characteristics of TB71C8A, and the TB71stop like characteristics of TB71C8/13A and TB71C13A (FIG. 25). These findings demonstrated the importance of pUL71 C13, while the cysteine at position 8 did not seem to affect the function of pUL71.

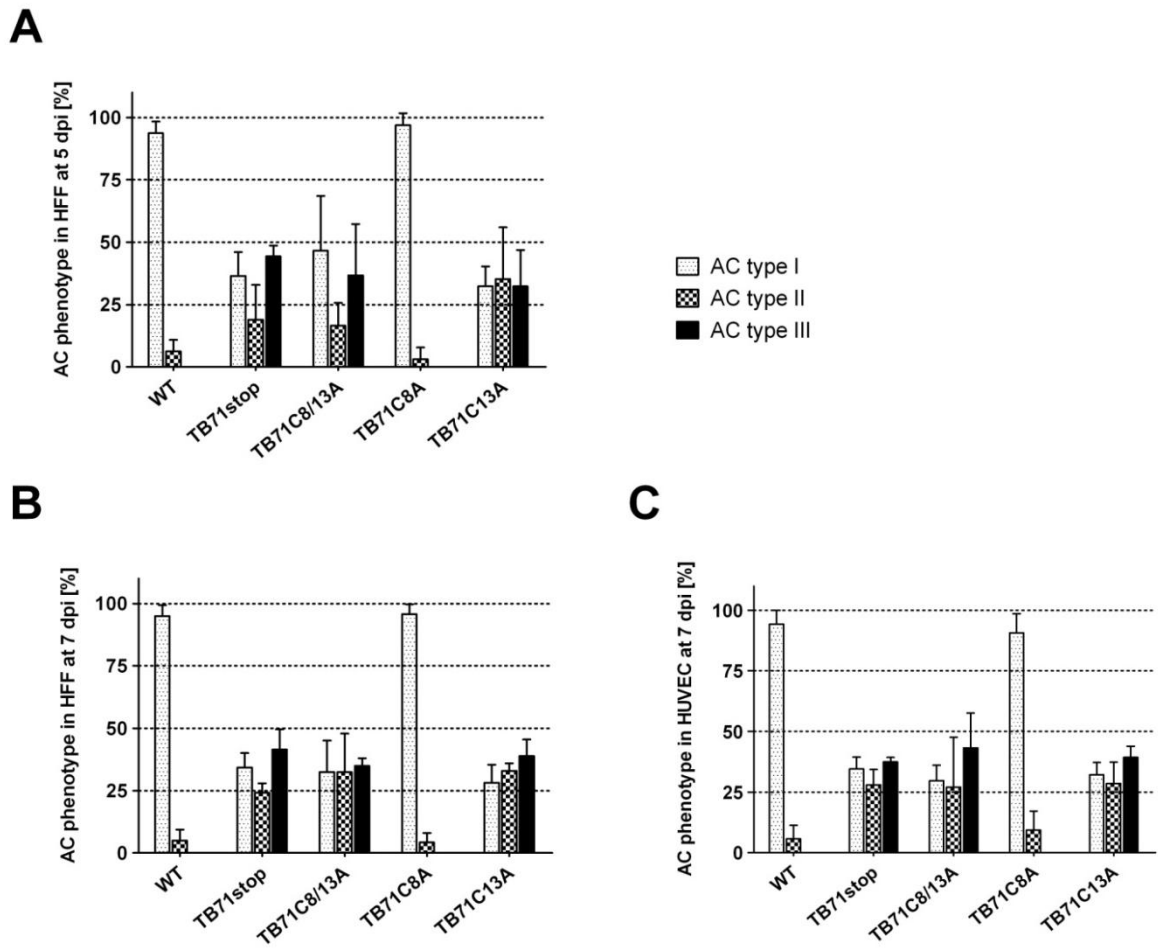


FIG. 25. Frequencies of AC type I (dotted), type II (checkered) and type III (black) were assessed for wild-type, TB71stop, TB71C8/13A, TB71C13A and TB71C13A infected cells, respectively. **(A)** HFF at 5 dpi, **(B)** HFF at 7 dpi, **(C)** HUVEC at 7 dpi. A MOI of 0.1 to 0.5 was used to infect HFF, and a MOI of 1 to 5 was used to infect HUVEC. To visualize the ACs, the cells were stained against the viral protein pp150 with the respective antibodies and DNA was visualized with DAPI. Three independent experiments were performed for each time point and the AC types were assessed in pictures randomly taken from infected cells. The columns show the mean relative ratio of AC phenotypes and the bars give the SD.

In order to analyze the effects of the point mutations within the potential palmitoylation sites on the morphogenesis of HCMV on an ultrastructural level, HFF were infected with TB71C8/13A, TB71C8A and TB71C13A viruses, and processed for TEM investigations 5 days post infection. TB71C8/13A and TB71C13A virus infected cells showed a similar phenotype. Both mutations led to a severe impairment of secondary envelopment: a vast majority of the particles within the AC were found in various stages of budding, while less than 21 % of TB71C8/13A and TB71C13A particles were fully enveloped (Table 10). This defect could also be observed in TB71C8/13A virus infected macrophages at 6 dpi, confirming a similar effect of the pUL71 cysteine mutation in these cells. Furthermore, the

vesicles used for budding were enlarged, comparable to the morphological phenotype of budding vesicles in TB71stop virus infection. This was in contrary to TB71C8A virus infected cells, where no obvious difference between wild-type virus infected cells was observed. 85 % of TB71C8A particles were found to be fully enveloped (Table 10). This confirmed that the mutation of the single amino acid at position 13 in the sequence of pUL71 was sufficient to induce a phenotype, which was virtually not distinguishable from the phenotype of TB71stop virus infected cells. On the other hand, mutation of the pUL71 cysteine at position 8 did not seem to make any difference from wild-type virus infection on an ultrastructural level.

Table 10. Quantification of envelopment stages of each TB71C8/13A, TB71C8A and TB71C13A virus particles in the AC of HFF (5 dpi) or MDM (6 dpi), respectively. The data was assessed from randomly chosen areas of ACs within n cells from at least two independent experiments per cell type and virus.

				mean % particles ± SD		
virus	cell type	n	# particles	enveloped	budding	naked
TB71C8/13A	HFF	8	211	20.8 ± 8.6	74.2 ± 11.2	4.9 ± 4.4
TB71C8/13A	MDM	3	101	18.1 ± 6.6	62.8 ± 3.6	19.1 ± 3.0
TB71C8A	HFF	15	220	85.0 ± 9.3	13.9 ± 9.0	1.1 ± 2.9
TB71C13A	HFF	16	485	14.3 ± 6.4	80.8 ± 10.0	4.9 ± 7.2

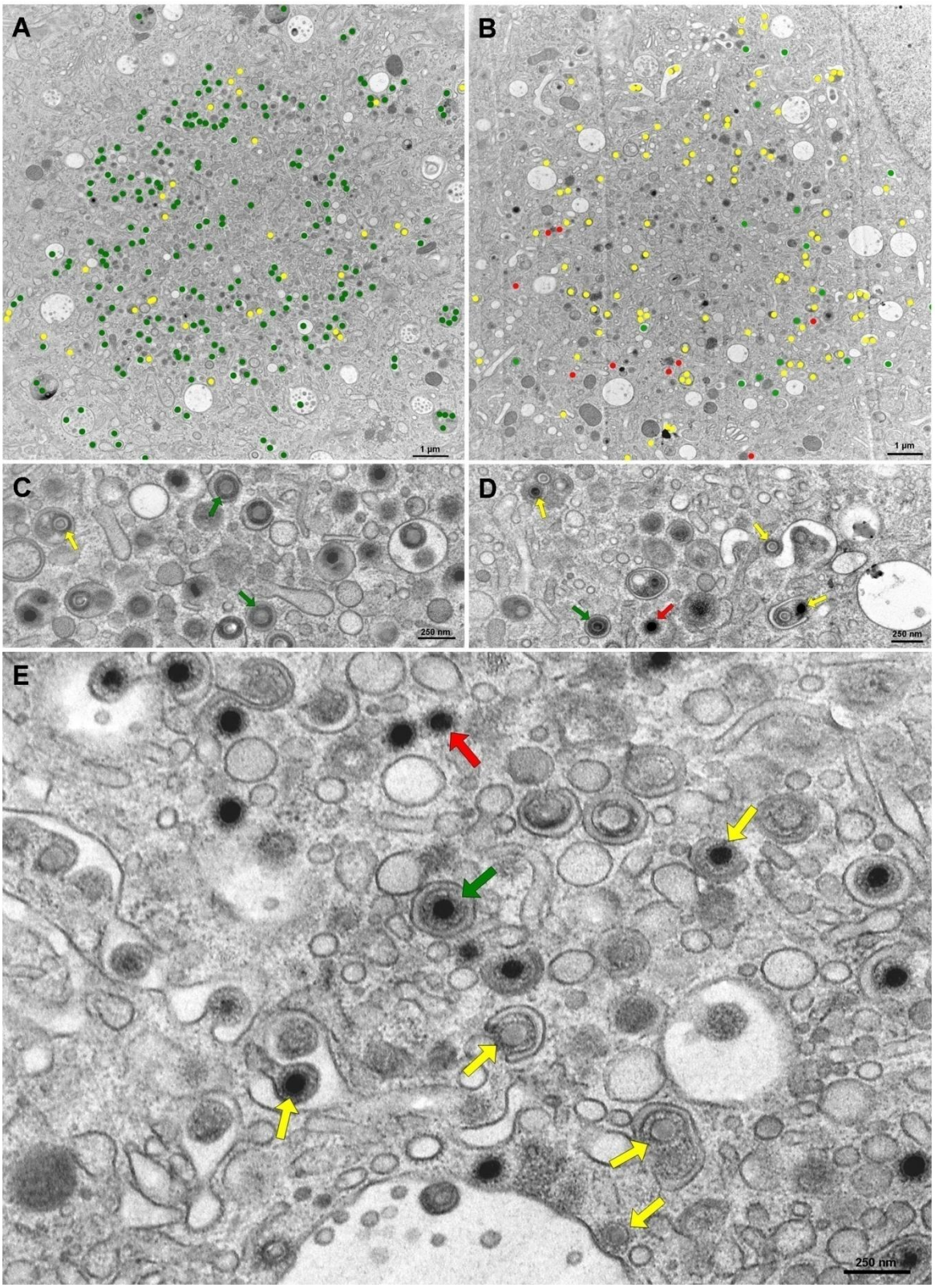


FIG. 26. TB71C8A **(A, C)**, TB71C13A **(B, D)** and TB71C8/13A **(E)** infected HFF at 5 dpi **(A, B)** Overviews of ACs show the distribution of fully enveloped particles (labeled green), budding particles (labeled yellow) and naked capsids (labeled red). **(C-E)** A greater magnification of the AC area reveals particles which are fully enveloped (green arrows), budding (yellow arrows) or naked (red arrows).

The number of nucleocapsids in the cytoplasm of TB71stop virus infected HFF was significantly reduced in comparison to wild-type virus infected cells (chapter 3.3, FIG. 21). To strengthen these findings and to further determine whether mutation of the potential pUL71 palmitoylation sites might cause a reduction of nucleocapsids, the number of nucleocapsids and empty capsids was assessed in micrographs of HFF infected with wild-type virus, TB71stop, TB71C8A and TB71C13A, respectively. Infection with TB71stop and TB71C13A but not TB71C8A led to a significant reduction of nucleocapsids compared to wild-type virus (FIG. 27), which demonstrated once more the outstanding importance of pUL71 C13.

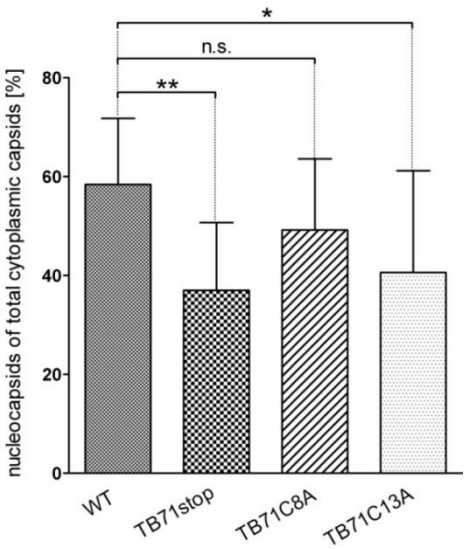


FIG. 27. The amount of cytoplasmic nucleocapsids is reduced when C13 is mutated. Fraction of DNA containing nucleocapsids in comparison to the total amount of capsids in the cytoplasm of HFF infected with wild-type, TB71stop, TB71C8A and TB71C13A, respectively. The data for each group was assessed from micrographs taken from the cytoplasm of infected cells at 5 dpi from at least two independent experiments per group. Data groups were statistically compared using an unpaired t-test in GraphPad Prism V5.01. Bars: standard deviation, n.s. not significant, * $p < 0.05$, ** $p<0.01$.

Taken together, the investigation of the pUL71 N-terminus revealed two potential palmitoylation sites at position 8 and 13. While mutation of C8 did not seem to affect HCMV morphogenesis, the mutation of a single cysteine at position 13 in pUL71 was sufficient to cause a phenotype similar as in TB71stop virus infected cells. This included the occurrence of enlarged MVBs, the alteration of budding vesicles and a significant reduction of nucleocapsids in the cytoplasm. The observed defects might be based on the low intracellular pUL71 levels in TB71C8/13A and TB71C13A virus infected cells.

3.5 Investigation of a pUL71 leucine zipper like motif

A leucine zipper like motif is located within the area of amino acids 34 to 55 of pUL71. Leucine zippers have been shown to enable protein-protein interactions, such as oligomerization (Landschulz et al. 1988). Preliminary investigations showed that pUL71 was able to oligomerize. While the leucine zipper provided this self-interaction of pUL71, mutation of leucines L34 and L41 was sufficient to inhibit this oligomerization (Meissner 2012). To determine the influence of the pUL71 leucine zipper, two recombinant viruses with mutations within the leucine zipper like motif were studied. TB71del34-41 virus exhibits a deletion of pUL71 amino acids 34 to 55, and the TB71L34/41A virus contains two point mutations exchanging the leucines at position 34 and 41 to alanines. First, immunofluorescence stainings of TB71del34-41 and TB71L34/41A virus infected cells were performed, to check the expression and localization of mutant pUL71. The viral proteins pUL71 and pp28 showed overlapping signals in the area of the AC of TB71del34-41 and TB71L34/41A virus infected HUVEC at 6 dpi (FIG. 28), and the signal strengths for pUL71 were comparable to those in wild-type infected cells.

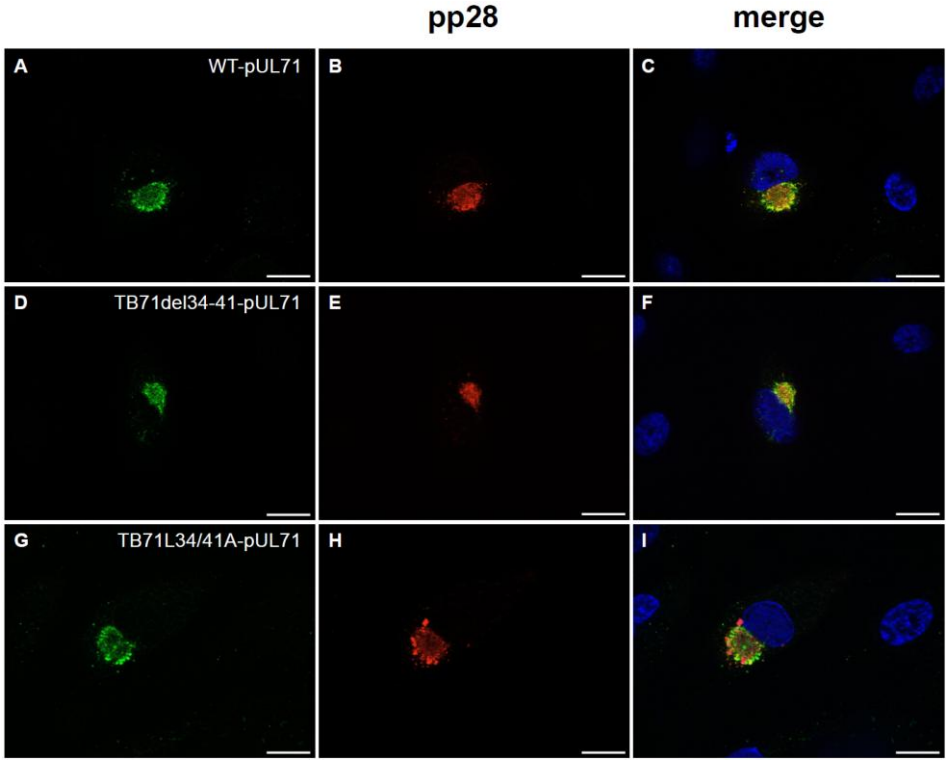


FIG. 28. Localization of pUL71 and pp28 in infected HUVEC infected with wild-type virus, TB71del34-41 and TB71L34/41A, respectively at an MOI of 5. Cells were fixed with 4 % PFA in PBS at 6 dpi. The viral proteins pUL71 and pp28 were detected by the respective antibodies and visualized by respective secondary antibodies conjugated to Alexa Fluor 488 (for pUL71) and 555 (for pp28). Cell nuclei were visualized by DAPI. Bars 20 µm.

In addition, the occurrence of enlarged MVBs could be observed in some cells infected with TB71del34-41 and TB71L34/41A viruses, respectively (data not shown). Thus, the frequency of the AC phenotypes I, II, and III, was assessed in further immunofluorescence studies as described for TB71stop virus infected cells (chapter 3.3, FIG. 12). Both viruses TB71del34-41 and TB71L34/41A showed a similar phenotype as TB71stop virus (FIG. 29), characterized by the occurrence of type III ACs in more than 25 % of TB71del34-41 and TB71L34/41A virus infected cells and about the same percentage of cells that exhibited AC type II. Less than 50 % of these cells showed an AC phenotype with wild-type characteristics. This effect was observed in both, HUVEC and HFF, at 5 and at 7 dpi, respectively (FIG. 29).

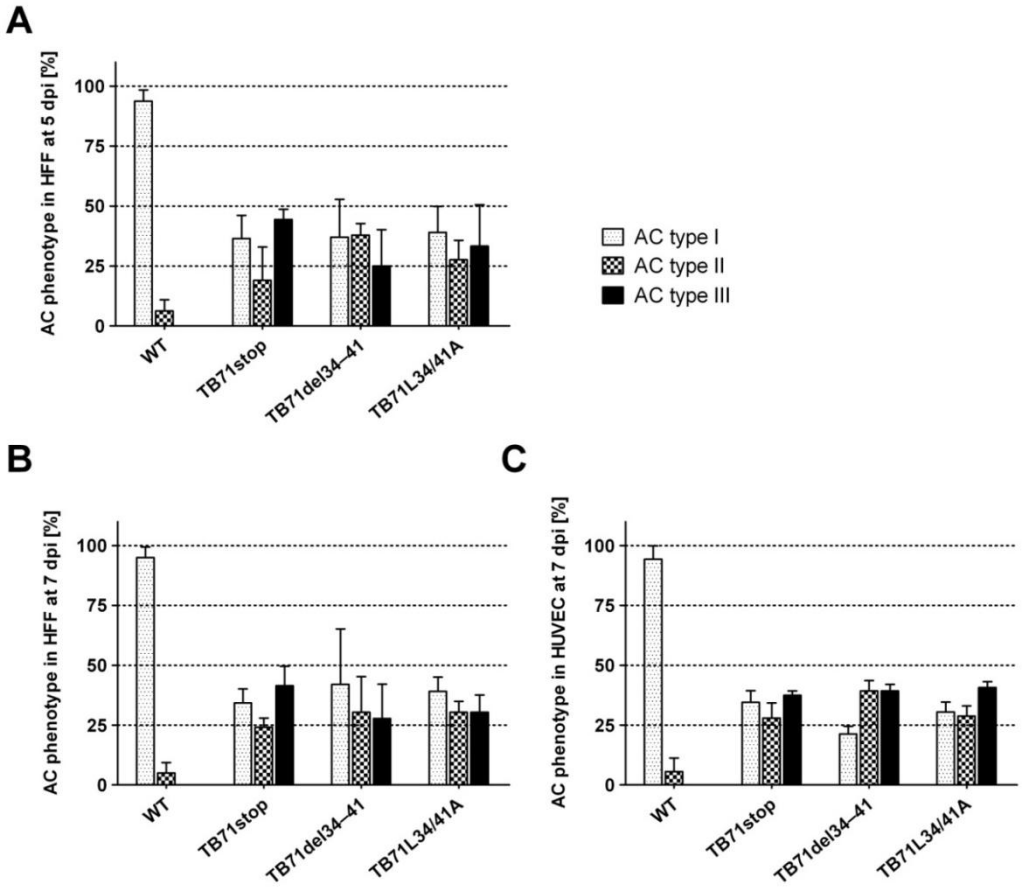


FIG. 29. Frequencies of AC type I (dotted), type II (checkered), and type III (black) were assessed for wild-type virus, TB71stop, TB71del34-41 and TB71L34/41A infected cells, respectively. **(A)** HFF at 5 dpi, **(B)** HFF at 7 dpi, **(C)** HUVEC at 7 dpi. A MOI of 0.1 to 0.5 was used to infect HFF, and a MOI of 1 to 5 was used to infect HUVEC. To visualize the ACs, the cells were stained against the viral protein pp150 with the respective antibodies and DNA was visualized with DAPI. Three independent experiments were performed for each time point and the AC types were assessed in pictures randomly taken from infected cells. The columns show the mean relative ratio of AC phenotypes and the bars give the SD.

To get a quantitative picture of the virus morphogenesis stages, the amount of fully enveloped, budding and naked particles was assessed in micrographs of TB71del34-41 and TB71L34/41A virus infected cells. In fibroblasts, less than 21 % of the TB71del34-41 and TB71L34/41A virus particles were enveloped (Table 11). A similar phenotype and envelopment defect was observed in TB71del34-41 virus infected HUVEC. After evaluation of enveloped, budding and naked particles in TB71L34/41A virus infected MDM, it seemed as if macrophages exhibited a less pronounced envelopment defect as fibroblasts, as about 40 % of the viral particles in the AC of MDM were counted as enveloped (Table 11). However, only a small number of TB71L34/41A virus infected macrophages were investigated and those were often characterized by an increased occurrence of larger vesicles in the periphery of the AC in a mild (FIG. 30 E) or greatly enhanced manner (FIG. 30 F). These irregular shaped vesicles contained many viral particles, which were counted as enveloped. In many TB71del34-41 and TB71L34/41A virus infected cells multiple budding processes took place on those larger vesicles (FIG. 30 C-F).

Table 11. Quantification of envelopment stages of each TB71del34-41 and TB71L34/41A virus particles in the AC of HFF (5 dpi), MDM (7 dpi) or HUVEC (6 dpi), respectively. The data was assessed from randomly chosen areas of ACs within n cells from at least two independent experiments per cell type and virus.

				mean % particles ± SD		
virus	cell type	n	# particles	enveloped	budding	naked
TB71del34-41	HFF	30	729	20.8 ± 8.6	75.7 ± 8.4	3.5 ± 5.2
TB71del34-41	HUVEC	15	527	28.0 ± 6.2	70.2 ± 7.7	1.8 ± 2.2
TB71L34/41A	HFF	17	532	18.9 ± 7.5	79.7 ± 7.3	1.4 ± 3.0
TB71L34/41A	MDM	7	389	40.5 ± 12.8	58.6 ± 12.2	0.9 ± 1.6

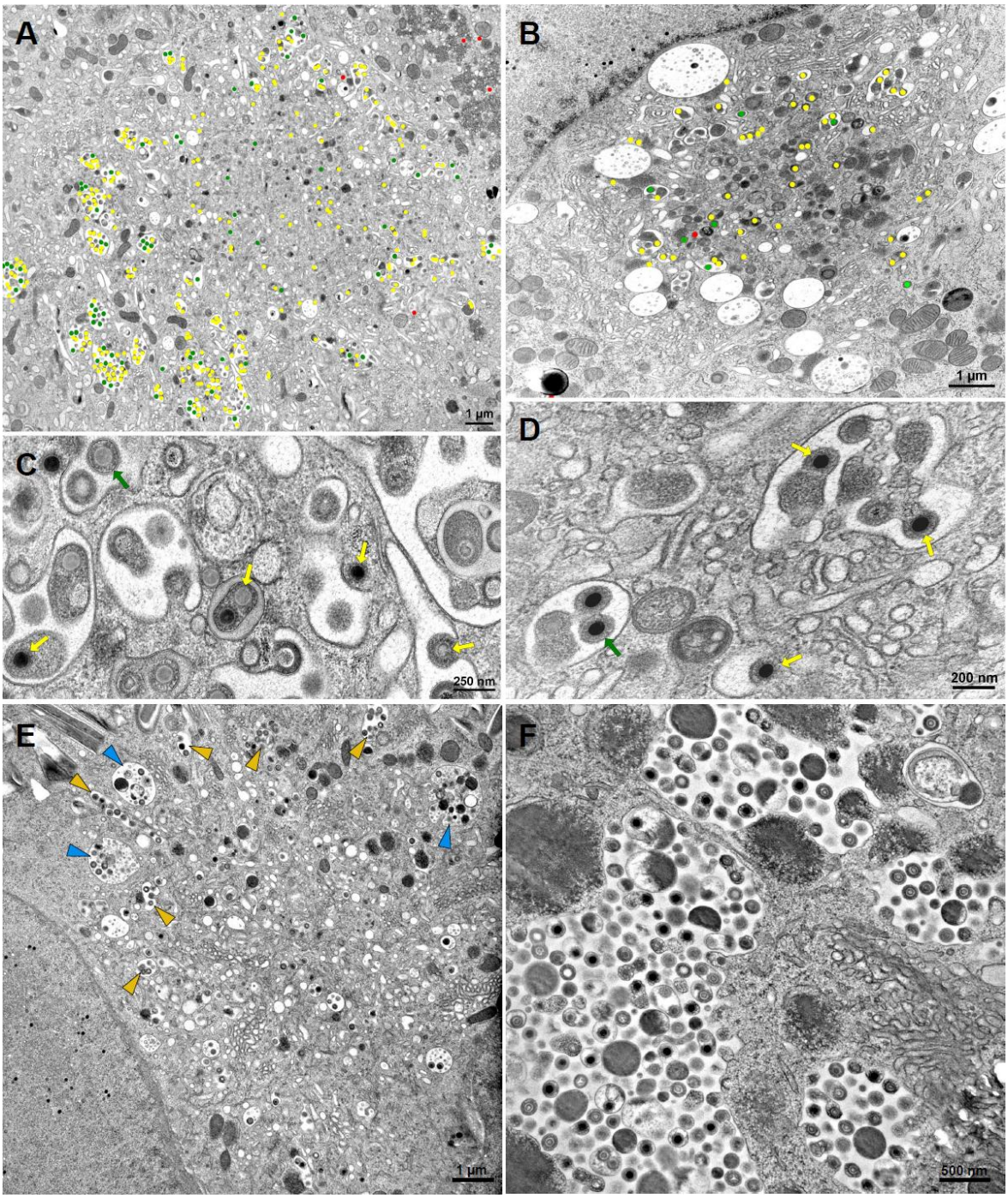


FIG. 30. Ultrastructural analysis of TB71del34-41 **(A, C)** and TB71L34/41A **(B, D)** virus infected HFF at 5 dpi **(A, B)** Overviews of ACs showing the distribution of fully enveloped particles (labeled green) and budding particles (labeled yellow). **(C, D)** A greater magnification of the AC area reveals particles which are fully enveloped (green arrows) or budding (yellow arrows). **(E)** Multivesicular vesicles (blue arrowheads) and irregular shaped vesicles (orange arrowheads) containing viral particles in a TB71L34/41A infected MDM at 6 dpi **(F)** Accumulation of viral particles in and at enlarged irregular shaped vesicles in the cytoplasm of a TB71L34/41A infected MDM at 6 dpi.

Since decreased numbers of cytoplasmic nucleocapsids were counted in HFF infected with TB71stop or TB71C13A viruses compared to wild-type virus (chapter 3.3, FIG. 21; chapter 3.4, FIG. 27), we determined whether the mutation of the pUL71 leucine zipper motif causes a similar phenotype. Thus, the amount of nucleocapsids and empty capsids was assessed in micrographs of HFF infected with wild-type virus, TB71stop, TB71del34-41 and TB71L34/41A, respectively. Both TB71del34-41 and TB71L34/41A viruses exhibited a significantly lower amount of nucleocapsids compared to the amount in wild-type virus infected HFF (FIG. 31). Deletion of pUL71 amino acids 34 to 41 showed the most pronounced effect, since only about 33 % of the particles contained a viral genome in the cytoplasm of TB71del34-41 virus infected cells.

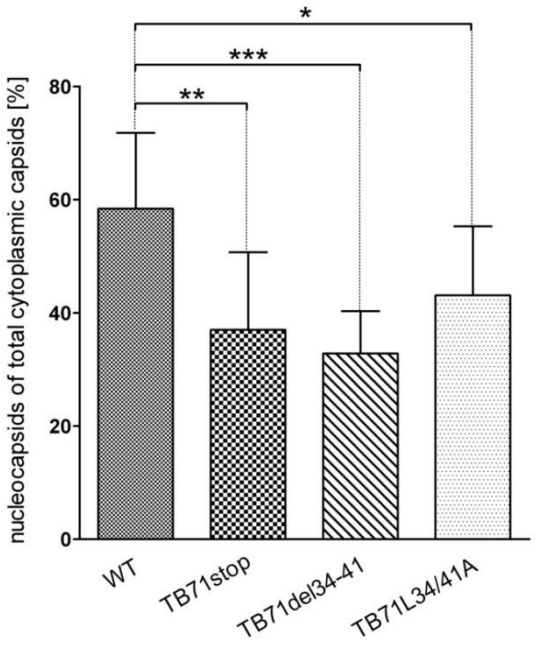


FIG. 31. The amount of cytoplasmic nucleocapsids is reduced when the pUL71 leucine zipper like motif is mutated. Fraction of DNA containing nucleocapsids in comparison to the total amount of capsids in the cytoplasm of HFF infected with wild-type virus, TB71stop, TB71del 34-41 and TB71L34/41A, respectively. The data for each group was assessed from micrographs taken from the cytoplasm of infected cells at 5 dpi from at least two independent experiments per group. Data groups were statistically compared using an unpaired t-test in GraphPad Prism V5.01. Bars: standard deviation, n.s. not significant, * $p < 0.05$, ** $p < 0.01$, *** $p < 0.001$.

In summary, the mutation of the pUL71 leucine zipper like motif led to a comparable impairment of viral morphogenesis in fibroblasts, endothelial cells and macrophages. The frequent occurrence of enlarged MVBs, the altered appearance of budding vesicles, the severe impairment of secondary envelopment, and the decrease of cytoplasmic

nucleocapsids in TB71del 34-41 and TB71L34/41A virus infected fibroblasts resemble the phenotype observed for the TB71stop virus. The mutation of two pUL71 leucines at position 34 and 41 was sufficient to cause those defects, highlighting the importance of the pUL71 leucine zipper like motif for HCMV morphogenesis.

3.6 Analysis of the pUL71 C-terminus

HCMV pUL71 is interacting with the cellular ATPase Vps4 through a PVDPRE motif at amino acid positions 315 to 320, thereby recruiting Vps4 to the viral AC (Böck 2010). To clarify on the meaning of this interaction, two recombinant viruses had been generated: one where the whole Vps4 interaction motif had been deleted (TB71del315–326 virus) and one where two prolines within the Vps4 interacting motif were mutated (TB71P315/318A virus) (Suffner 2011). The subcellular localization of pUL71 was not affected in TB71del315-326 and TB71P315/318A virus infected HFF, but the ability to recruit Vps4 to the AC was lost (Suffner 2011).

TEM analyses were performed to investigate the morphogenesis of both viruses. On an ultrastructural level TB71del315–326 virus infected fibroblasts exhibited a similar phenotype as wild-type virus infected cells. The AC and the cytoplasmic vesicles showed no abnormalities (FIG. 32 A). Budding process were usually observed at small vesicles (FIG. 32 C), and more than 80 % of the particles within the AC of TB71del315-326 virus infected HFF were already fully enveloped (Table 12). Consistent with previous results, infection of HFF and MDM with TB71P315/318A exhibited normal appearances of ACs (FIG. 32 B), budding vesicles (FIG. 32 D) and no effect on secondary envelopment was observed (Table 12). In short, both TB71del315–326 and TB71P315/318A viruses were undistinguishable from wild-type virus on an ultrastructural level.

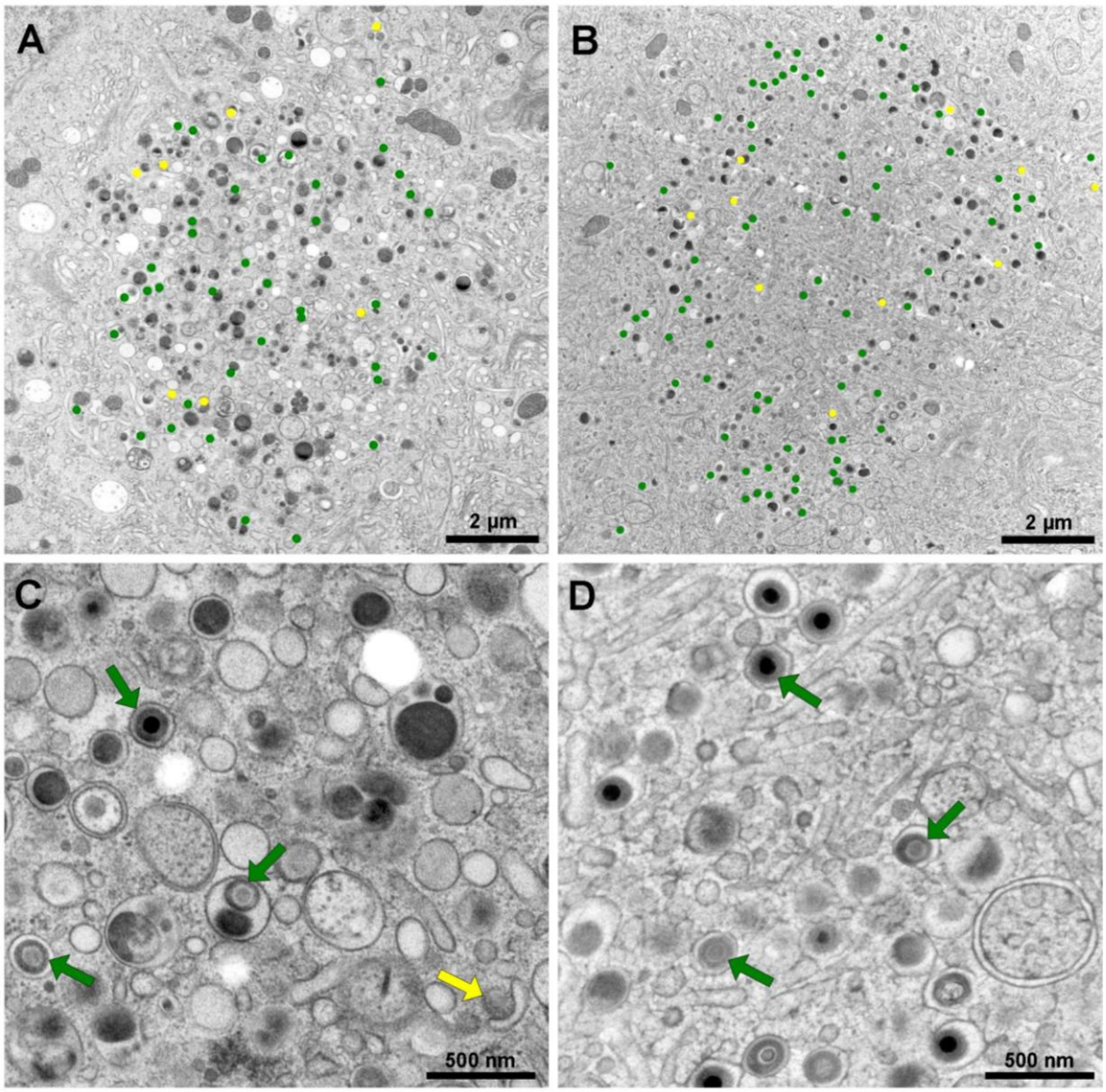


FIG. 32. TEM micrographs of HFF 5 days post infection with Vps4 mutant viruses TB71del315–326 **(A, C)** and TB71P315/318A **(B, D)**, respectively. **(A, B)** Overviews of ACs showing the distribution of fully enveloped particles (labeled green) and budding particles (labeled yellow). **(C-E)** A greater magnification of the AC area reveals particles which are fully enveloped (green arrows) or budding (yellow arrows).

To investigate whether the C-terminus of pUL71 provided any functional importance at all, two further recombinant viruses TB71del315-361 and TB71del327-361 had been generated and were investigated by TEM. These mutant viruses exhibit a complete deletion of the pUL71 C-terminus beginning from amino acid 315, and from amino acid 327, respectively.

In fibroblasts infected with TB71del315-361 the viral AC appeared to be normal (FIG. 33 A), since no enlarged endosomes in the periphery could be observed. The budding vesicles were often small and crescent shaped, as frequently seen in wild-type

infected cells. However, only about one third of the TB71del315-361 particles was completely enveloped (FIG. 33 C; Table 12). Furthermore, sometimes larger vesicles could be observed that were used as multiple budding site, as described for the TB71stop virus. This phenotype could not only be observed in TB71del315-361 virus infected fibroblasts, but also in HUVEC and MDM, confirming that the deletion of the pUL71 C-terminus from amino acids 315 to 361 led to the same defect in these cell types (Table 12).

Next, the effects of the deletion of the pUL71 amino acids 327 to 361 were investigated. The deleted region comprises the pUL71 C-terminus downstream of the Vps4 interacting motif. Infection of HFF with TB71del327-361 was very similar to the infection with TB71del315-361. No enlarged MVBs in the cytoplasm were detected (FIG. 33 B). Only about one third of particles in the AC were enveloped (FIG. 33 D; Table 12). These data demonstrated the importance of the pUL71 C-terminus for efficient secondary envelopment of HCMV.

Table 12. Quantification of envelopment stages of each TB71del315-326, TB71P315/318A, TB71del315-361 and TB71del327-361 virus particles in the AC of HFF (5 dpi), HUVEC (6 dpi) or MDM (6 dpi), respectively. Contains data of at least two independent experiments per cell type.

				mean % particles ± SD		
virus	cell type	n	# particles	enveloped	budding	naked
TB71del315-326	HFF	14	494	82.5 ± 10.8	17.1 ± 9.9	0.37 ± 1.4
TB71P315/318A	HFF	28	749	74.8 ± 13.1	21.9 ± 10.2	3.34 ± 5.8
TB71P315/318A	MDM	26	237	85.9 ± 11.0	11.5 ± 10.9	2.60 ± 7.0
TB71del315-361	HFF	27	997	33.4 ± 9.5	64.5 ± 9.2	2.1 ± 3.0
TB71del315-361	HUVEC	13	334	24.8 ± 9.9	68.4 ± 10.8	6.8 ± 5.3
TB71del315-361	MDM	26	576	33.0 ± 16.9	63.0 ± 15.0	4.1 ± 5.7
TB71del327-361	HFF	22	211	31.5 ± 18.9	65.5 ± 20.3	2.9 ± 5.3

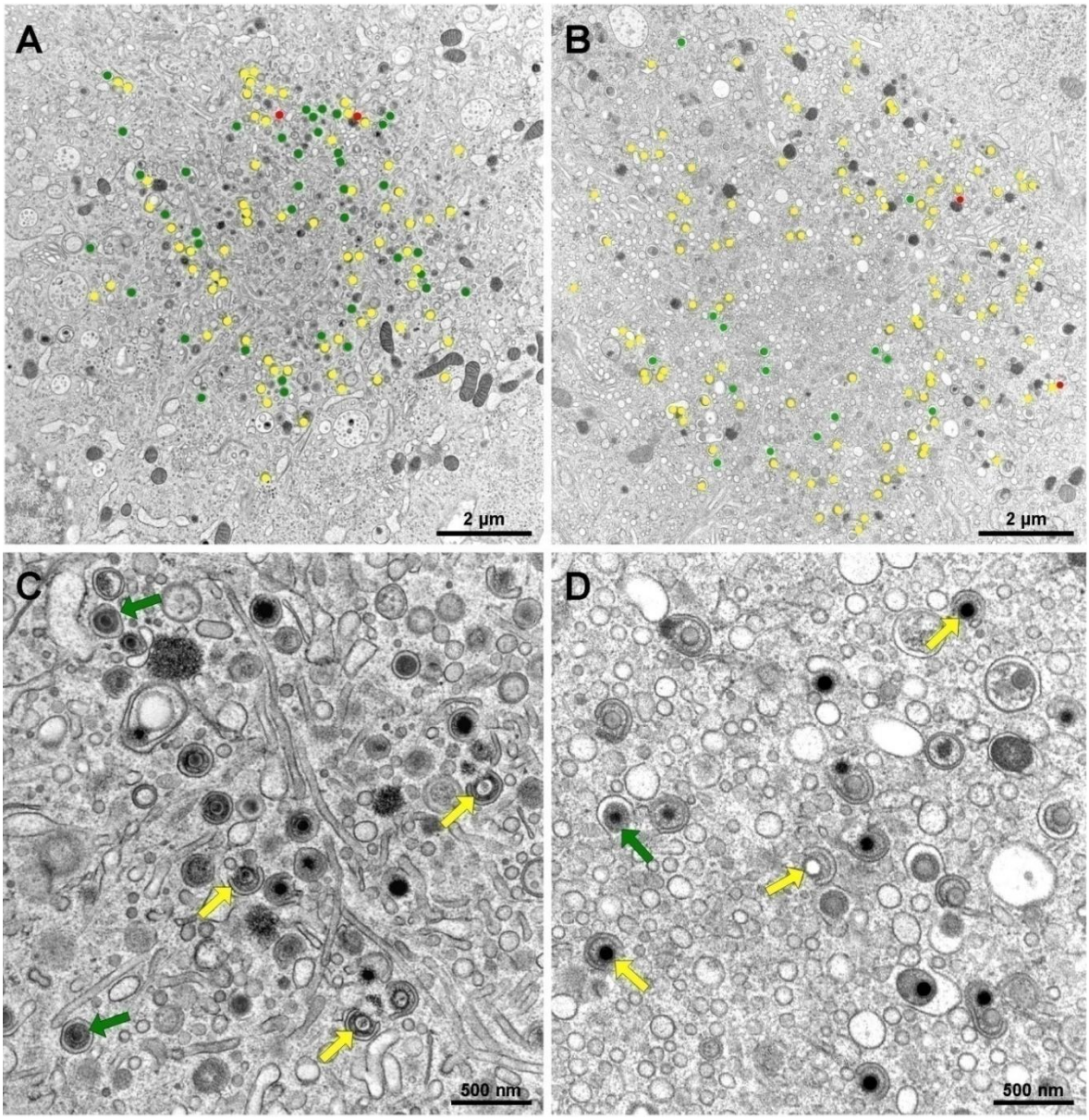


FIG. 33. TB71del315-361 **(A, C)** and TB71del327-361 **(B, D)** infected HFF at 5 dpi. **(A, B)** Overviews of ACs showing the distribution of fully enveloped particles (labeled green), budding particles (labeled yellow) and naked capsids (labeled red). **(C-E)** A greater magnification of the AC area reveals particles which are fully enveloped (green arrows) or budding (yellow arrows).

The ultrastructural data suggested that mutation or deletion of the C-terminus is not causative for an enlargement of MVBs as observed for the TB71stop virus. Therefore we hypothesized, that mostly AC types I and II (as defined in chapter 3.3, FIG. 12) would occur in TB71P315/318A, TB71del315-326, TB71del315-361, and TB71del327-361 virus infected cells, respectively. To clarify this, immunofluorescence experiments were performed to quantify the different AC phenotypes in infected HFF and HUVEC. As expected, the impairment of the pUL71 C-terminus led to establishment of wild-type like

type I ACs in the vast majority of infected cells (FIG. 34). Only few cells exhibited an AC phenotype II, and the occurrence of type III ACs was not significant (FIG. 34). This was true for both cell types and stages of infection, respectively, and confirmed that the pUL71 C-terminus only played a role for secondary envelopment of HCMV capsids.

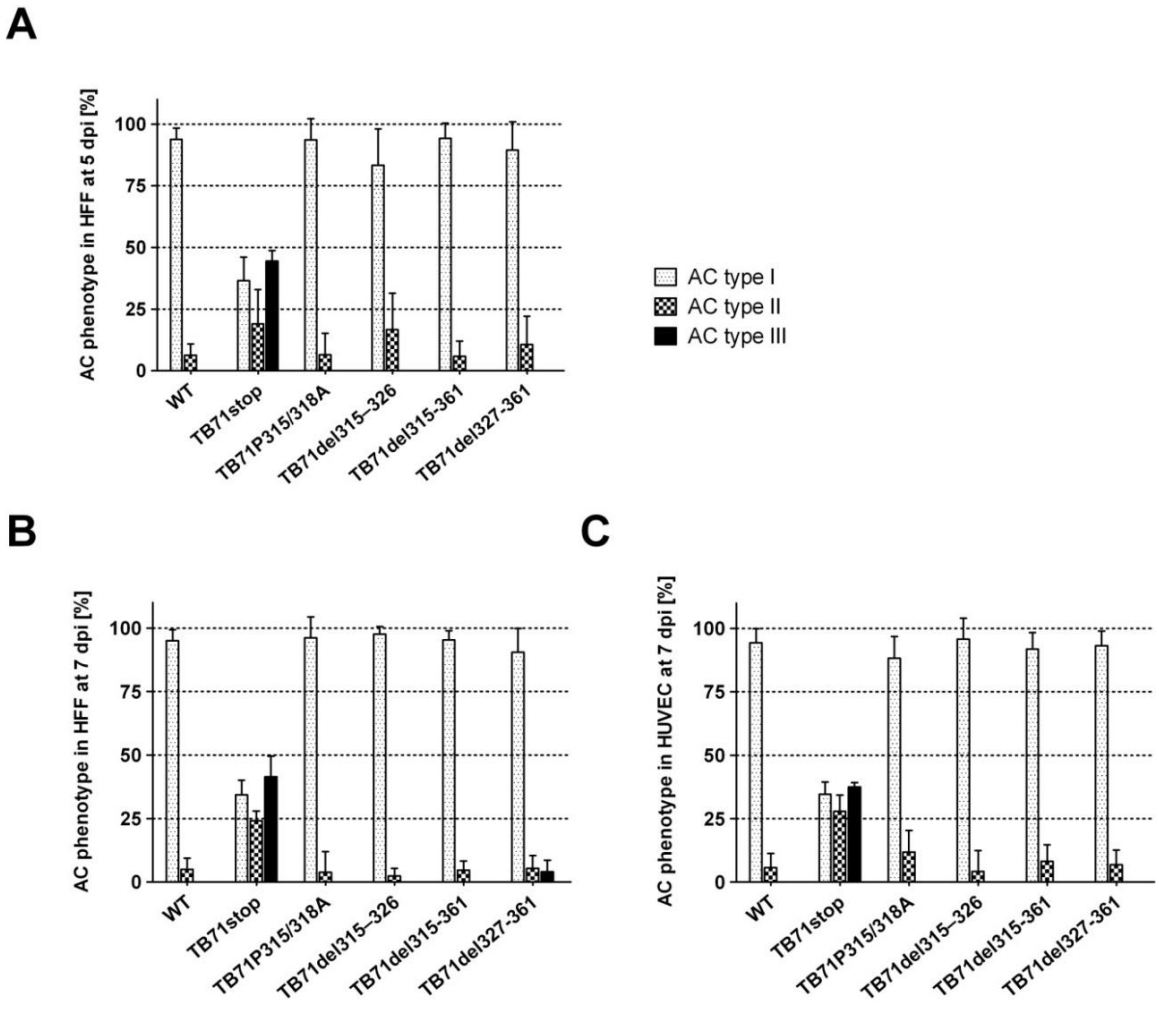


FIG. 34. Frequencies of AC type I (dotted), type II (checkered) and type III (black) were assessed for wild-type, TB71stop, TB71P315/318A, TB71del315–326, TB71del315-361 and TB71del327-361 infected cells, respectively. **(A)** HFF at 5 dpi, **(B)** HFF at 7 dpi, **(C)** HUVEC at 7 dpi. A MOI of 0.1 to 0.5 was used to infect HFF, and a MOI of 1 to 5 was used to infect HUVEC. To visualize the ACs, the cells were stained against the viral protein pp150 with the respective antibodies and DNA was visualized with DAPI. Three independent experiments were performed for each time point and the AC types were assessed in pictures randomly taken from infected cells. The columns show the mean relative ratio of AC phenotypes and the bars give the SD.

Impairment of the N-terminal pUL71 palmitoylation site and the leucine zipper like motif, respectively, led to a reduced amount of nucleocapsids in the cytoplasm of infected HFF compared to wild-type virus (chapter 3.4, FIG. 27; chapter 3.5, FIG. 31). To investigate, whether the deletion of the pUL71 C-terminus causes the same defect, the amount of nucleocapsids and empty capsids was assessed in micrographs of HFF infected with wild-type virus, TB71stop and TB71del315-361 viruses, respectively. However, the complete deletion of the endmost pUL71 C-terminal amino acids 315 to 361 had no effect on the relative amount of nucleocapsids in the cytoplasm (FIG. 35).

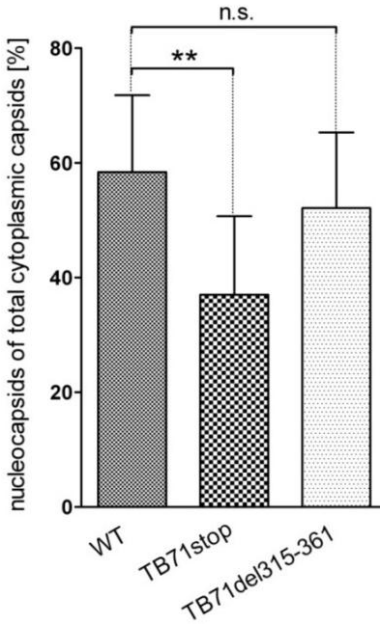


FIG. 35. The amount of cytoplasmic nucleocapsids is not reduced when the pUL71 C-terminus is truncated. Fraction of DNA containing nucleocapsids in comparison to the total amount of capsids in the cytoplasm of HFF infected with wild-type, TB71stop and TB71del315-361, respectively. The data for each group was assessed from micrographs taken from the cytoplasm of infected cells at 5 dpi from at least two independent experiments per group. Data groups were statistically compared using an unpaired t-test in GraphPad Prism V5.01. Bars: standard deviation, n.s. not significant, ** $p < 0.01$.

Taken together, the deletion of the pUL71 Vps4 interacting domain was neither affecting the appearance of the viral AC nor the secondary envelopment of virus particles. However, deletion of the C-terminus of pUL71 from amino acids 327 to 361 resulted in an impairment of final particle envelopment, without affecting MVBs. Also, the amount of cytoplasmic nucleocapsids was not reduced compared to wild-type virus. These data point towards a role of the pUL71 C-terminus for the process of secondary envelopment only.

3.7 Generation and investigation of a pUL71 C-terminal deletion virus

Since the data suggested an important but unknown motif within the last 35 C-terminal amino acids of pUL71, a HCMV mutant TB71del348-361 was created to further narrow down the motif important for secondary envelopment of HCMV. This mutant virus lacked the 14 endmost C-terminal amino acids of pUL71, caused by the introduction of a stop codon and following frame shift at amino acid position 348 of the UL71 gene (FIG. 36 A). As with all other mutants in this study, this was achieved through two step markerless BAC-mutagenesis (Tischer et al. 2006) of the HCMV TB40-BAC4 (Sinzger et al. 2008b). Restriction fragment length polymorphism (RFLP) analyses of the wild-type TB40-BAC4 and the TB71del348-361-BAC with restriction enzymes EcoRV and PstI resulted in identical restriction patterns, verifying the integrity of the generated BAC (FIG. 36 B). Furthermore, DNA sequencing of the specific area confirmed the correct introduction of the mutation (data not shown). The TB71del348-361-BAC DNA was then used to reconstitute the respective virus on fibroblasts. Immuno-blotting confirmed the smaller size of the protein pUL71del348-361 (FIG. 36 C).

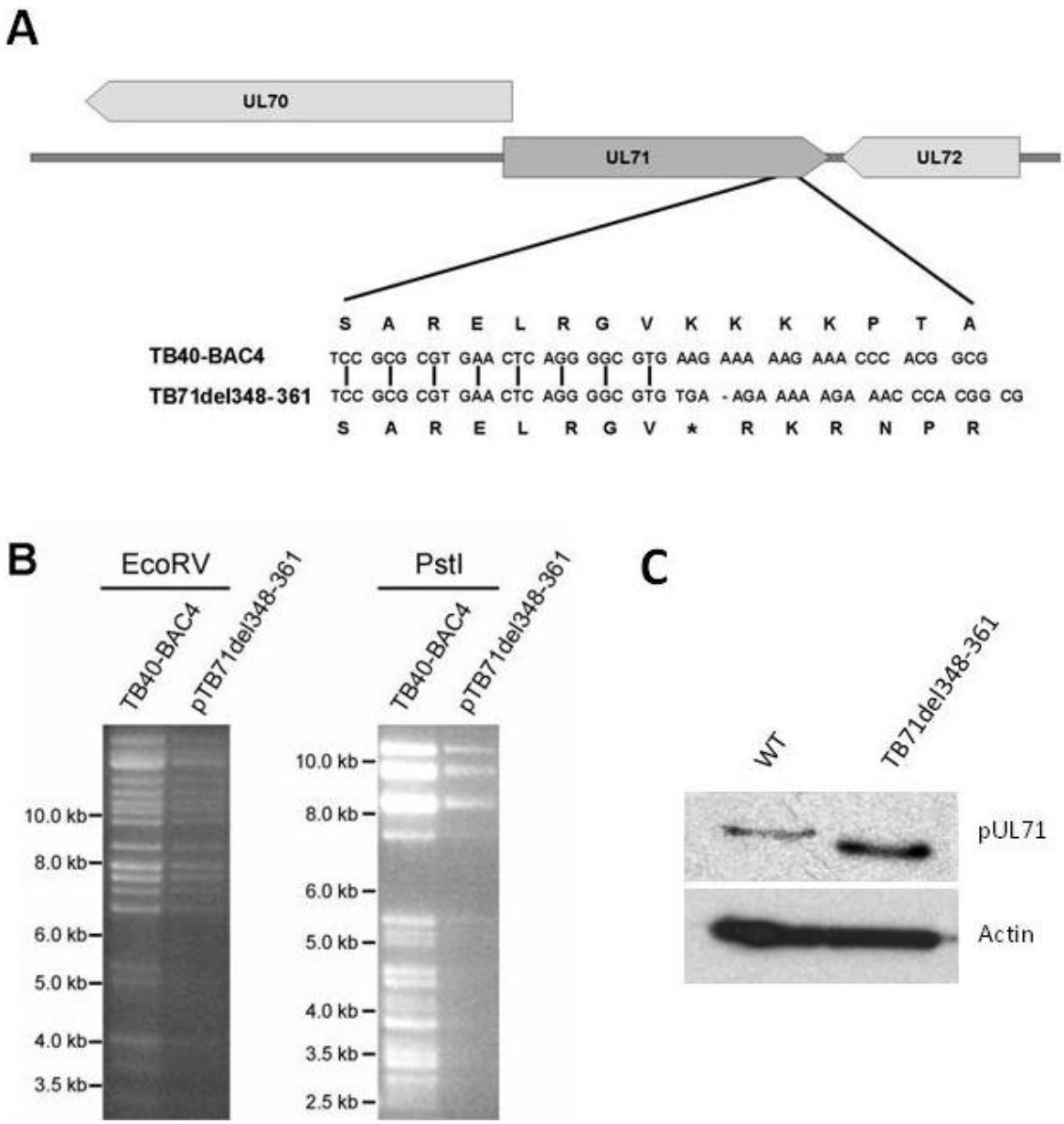


FIG. 36. Generation of the C-terminal deletion mutant TB71del348-361. **(A)** Position of the introduced stop codon at amino acid position 348 and the following frameshift mutation in the UL71 gene. **(B)** Restriction fragment length polymorphism analysis of BAC-DNAs of TB40-BAC4 (wild-type) and TB71del348-361-BAC with restriction enzymes EcoRV and PstI. The BAC-DNA was used to reconstitute the respective viruses. **(C)** HFF were lysed 5 days after infection with wild-type and TBdel348-361 viruses, respectively, and Western blotting was performed using antibodies against pUL71 and actin.

To compare the virus growth between TB71del348-361 and wild-type virus, the release of viral progeny into the supernatant was investigated by a high MOI kinetic for both viruses. 10-fold dilutions of the virus stocks were prepared and incubated on HFF. The supernatant of infected cells was collected daily for 7 days and titrated on HFF. The growth curves of

TB71del348-361 and wild-type virus exhibited no significant differences, demonstrating a similar growth of both viruses (FIG. 37).

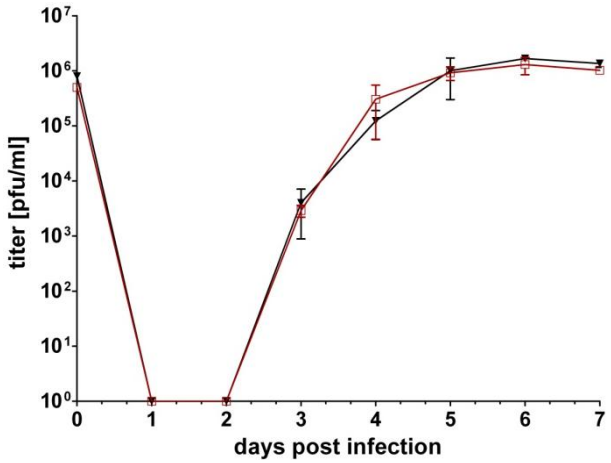


FIG. 37. TB71del348-361 and wild-type virus exhibit a similar growth kinetic. HFF were infected with wild-type (▼) and TB71del348-361 (□) virus at an MOI of 6. The supernatants were collected the following seven days and titrated on HFF to assess the amount of released infectivity. Day 0 represents the inoculum. Each data point represents the mean ± SD of two titrations.

Next and most importantly, we wanted to know whether the deletion of only 14 C-terminal amino acids of pUL71 was still sufficient to cause an impairment of secondary envelopment. Thus, electron microscopy was performed to assess the ultrastructural phenotype of TB71del348-361 virus infected cells. TB71del348-361 virus infected HFF showed a similar phenotype as described for TB71del315-361 and TB71del327-361 viruses. Less than 30 % of the particles were completely enveloped (Table 13), and no enlarged MVBs were observed (FIG. 38). Similar results were obtained in TB71del348-361 infected HUVEC, once again indicating that the effects of pUL71 impairment were independent from the cell type.

Table 13. Quantification of envelopment stages of TB71del348-361 virus particles in the AC of HFF (5 dpi) and HUVEC (6 dpi), respectively. The data was assessed from randomly chosen areas of ACs within n cells from at least two independent experiments per cell type.

				mean % particles ± SD		
virus	cell type	n	# particles	enveloped	budding	naked
TB71del348-361	HFF	25	980	26.4 ± 12.4	72.1 ± 10.9	1.5 ± 2.8
TB71del348-361	HUVEC	20	999	33.5 ± 9.7	65.7 ± 9.3	0.7 ± 1.7

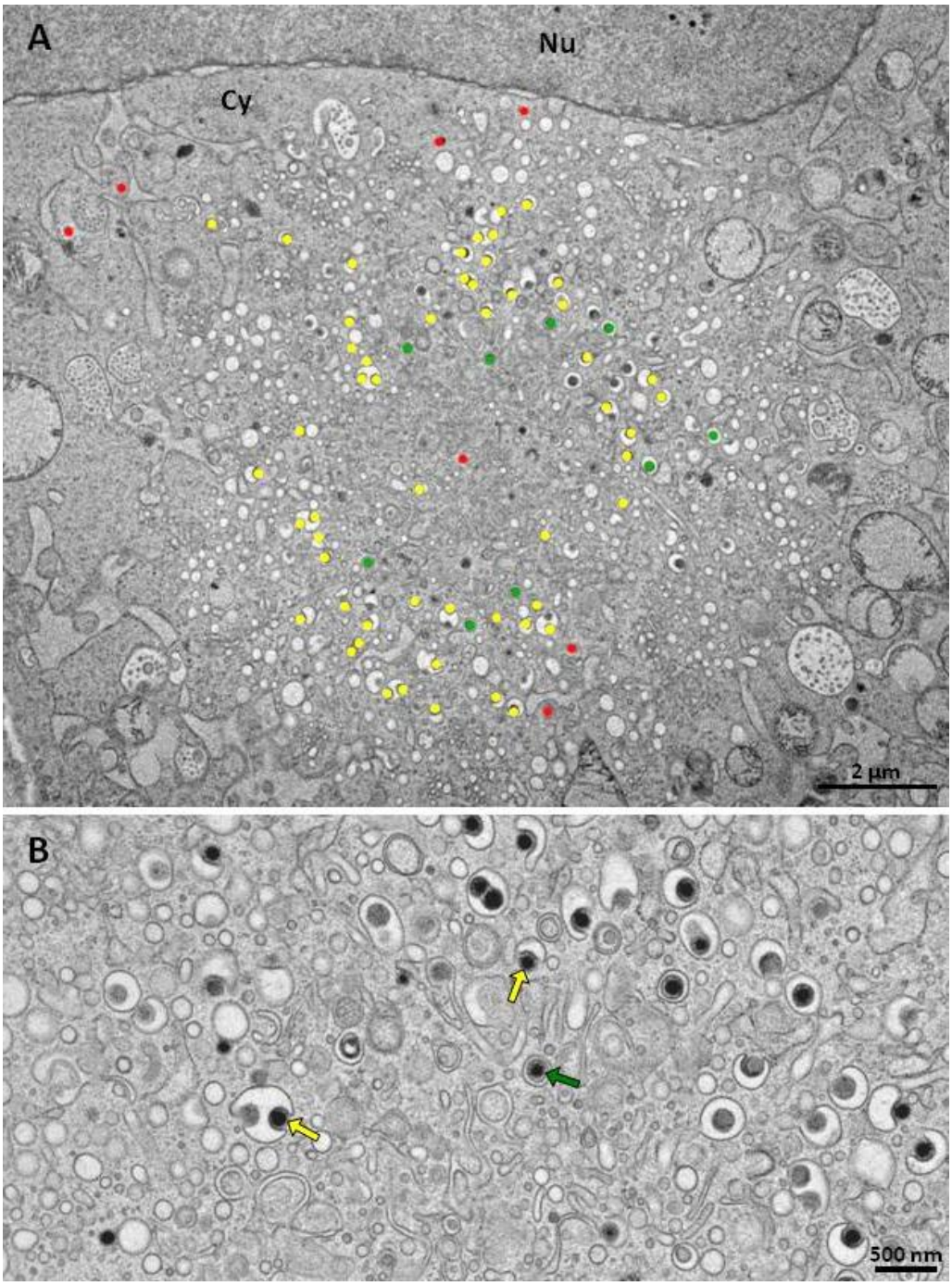


FIG. 38. TB71del348-361 infected HFF at 5 dpi. **(A)** Overview of a viral AC showing the distribution of fully enveloped particles (labeled green), budding particles (labeled yellow) and naked capsids (labeled red). **(B)** A greater magnification of the AC area reveals particles which are fully enveloped (green arrows) or budding (yellow arrows). Nu nucleus, Cy cytoplasm.

Since no enlarged MVBs were seen in the previous analyses of the pUL71 C-terminal deletion viruses, we hypothesized that the observed AC phenotypes of TB71del348-361 virus infected cells were primarily wild-type like. Fluorescence studies confirmed this, as

the vast majority of TB71del348-361 infected cells showed type I ACs, along with a minority of type II ACs, while no type III ACs could be observed (FIG. 39).

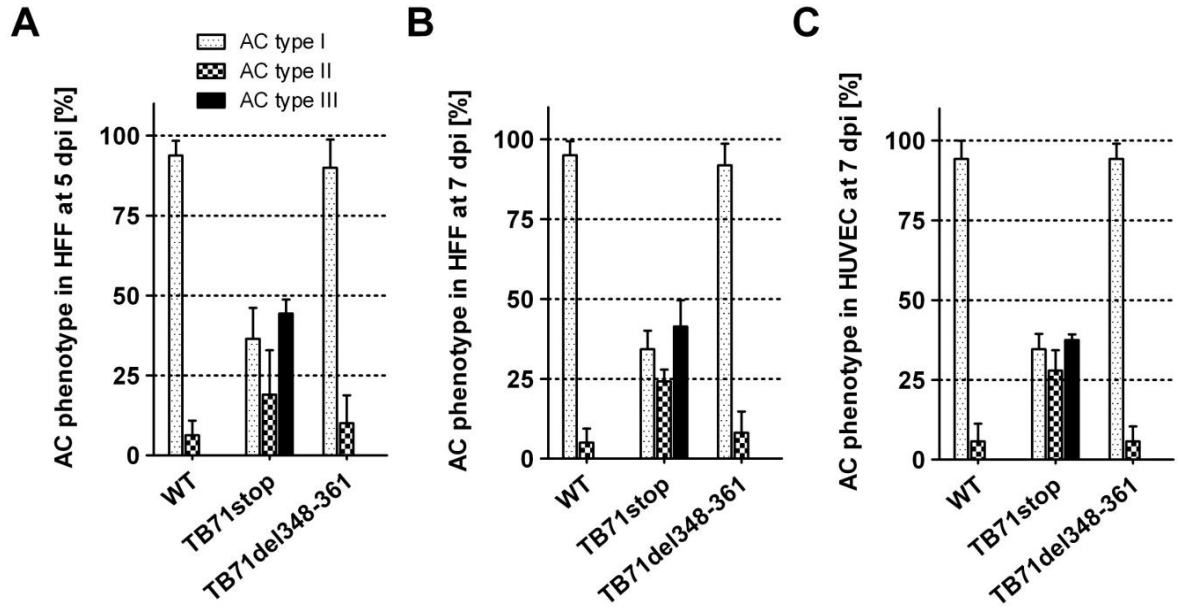


FIG. 39. Frequencies of AC type I (dotted), type II (checkered) and type III (black) were assessed for wild-type, TB71stop and TB71del348-361 infected cells, respectively. **(A)** HFF at 5 dpi, **(B)** HFF at 7 dpi, **(C)** HUVEC at 7 dpi. A MOI of 0.1 to 0.5 was used to infect HFF, and a MOI of 1 to 5 was used to infect HUVEC. To visualize the ACs, the cells were stained against the viral protein pp150 with the respective antibodies and DNA was visualized with DAPI. Three independent experiments were performed for each time point and the AC types were assessed in pictures randomly taken from infected cells. The columns show the mean relative ratio of AC phenotypes and the bars give the SD.

Through the generation of the recombinant virus TB71del348-361 it was possible to narrow down the C-terminal pUL71 motif which is involved in efficient secondary HCMV envelopment. This motif was obviously contained within the endmost 14 C-terminal amino acids.

3.8 Identification of a pUL71 tetra-lysine motif

The deletion of the 14 endmost C-terminal amino acids $_{348}$KKKKPTAAALLSSA$_{361}$ was sufficient to impair secondary envelopment of HCMV. To determine the amino acid motif causative for efficient secondary envelopment, two further recombinant viruses were generated and investigated. The lysines $_{348}$KKKK$_{351}$ were mutated to $_{348}$AAAA$_{351}$ in the TB71K348-351A virus, and the leucines L357 and L358 were changed to alanine in the

virus TB71L357-358A. TEM was applied to assess the number of enveloped, budding and naked virus particles within the AC of TB71K348-351A and TB71L357-358A virus infected cells, respectively. The mutation of two leucines had no effect on viral morphology (data not shown) or envelopment of TB71K348-351A infected cells (Table 14). On the contrary, the mutation of the tetra-lysine region at the pUL71 C-terminus was sufficient to cause a severe envelopment defect and a phenotype comparable to the truncation of the pUL71 C-terminus. Thus we concluded that the tetra-lysine motif was responsible for efficient secondary envelopment of HCMV particles.

Table 14. Quantification of envelopment stages of each TB71L357-358A and TB71K348-351A virus particles in the AC of HFF at 5 dpi. The data was assessed from randomly chosen areas of ACs within n cells from one (TB71L357-358A) or two (TB71K348-351A) independent experiments.

				mean % particles ± SD		
virus	cell type	n	# particles	enveloped	budding	naked
TB71L357-358A	HFF	8	146	83,1 ± 7,7	14,7 ± 6,1	2,2 ± 2,4
TB71K348-351A	HFF	15	514	21,9 ± 14,0	76,5 ± 14,3	1,7 ± 3,1

3.9 Investigation of a pUL103 deficient cytomegalovirus

It has been shown that HCMV pUL103 interacts with pUL71, and furthermore exhibits a similar subcellular localization pattern as pUL71 in infected cells (Jens von Einem, unpublished data). We speculated that both pUL71 and pUL103 could be involved in mediating a common function during HCMV morphogenesis. Since pUL71 plays a role during final particle envelopment, we hypothesized that the absence of pUL103 could lead to a defect in secondary envelopment. Recently a pUL103 deficient virus was used to describe the function of pUL103 as important for maturation and egress of viral particles (Ahlqvist and Mocarski, 2011); however, an effect on secondary envelopment was not clearly mentioned. To investigate the role of pUL103 on an ultrastructural level in the background of the TB40-BAC4, the pUL103 deficient virus TB103stop had been generated in our facility. TB103stop virus infected HFF were analyzed at day 5 post infection after high pressure freezing, freeze-substitution, embedding in plastic and thin sectioning. TEM analyses showed that the amount of enveloped virus particles in the cytoplasm of TB103stop virus infected fibroblasts was significantly reduced compared to wild-type virus infected cells (Table 15). Only about 20 % of the particles were completely enveloped, while the majority of particles in TB103stop virus infected cells were observed in the process of budding. Most of the budding particles were attached to small crescent

shaped vesicles, similar to the budding events observed in wild-type virus infected cells (FIG. 40). No enlarged budding vesicles with many budding events like in TB71stop virus infected cells could be seen.

Table 15. Quantification of envelopment stages of TB103stop virus particles in the AC of HFF at 5 dpi. The data was assessed from randomly chosen areas of ACs within n cells from two independent experiments.

				mean % particles ± SD		
virus	cell type	n	# particles	enveloped	budding	naked
TB103stop	HFF	14	1229	20.9 ± 8.4	76.7 ± 7.0	2.4 ± 2.6

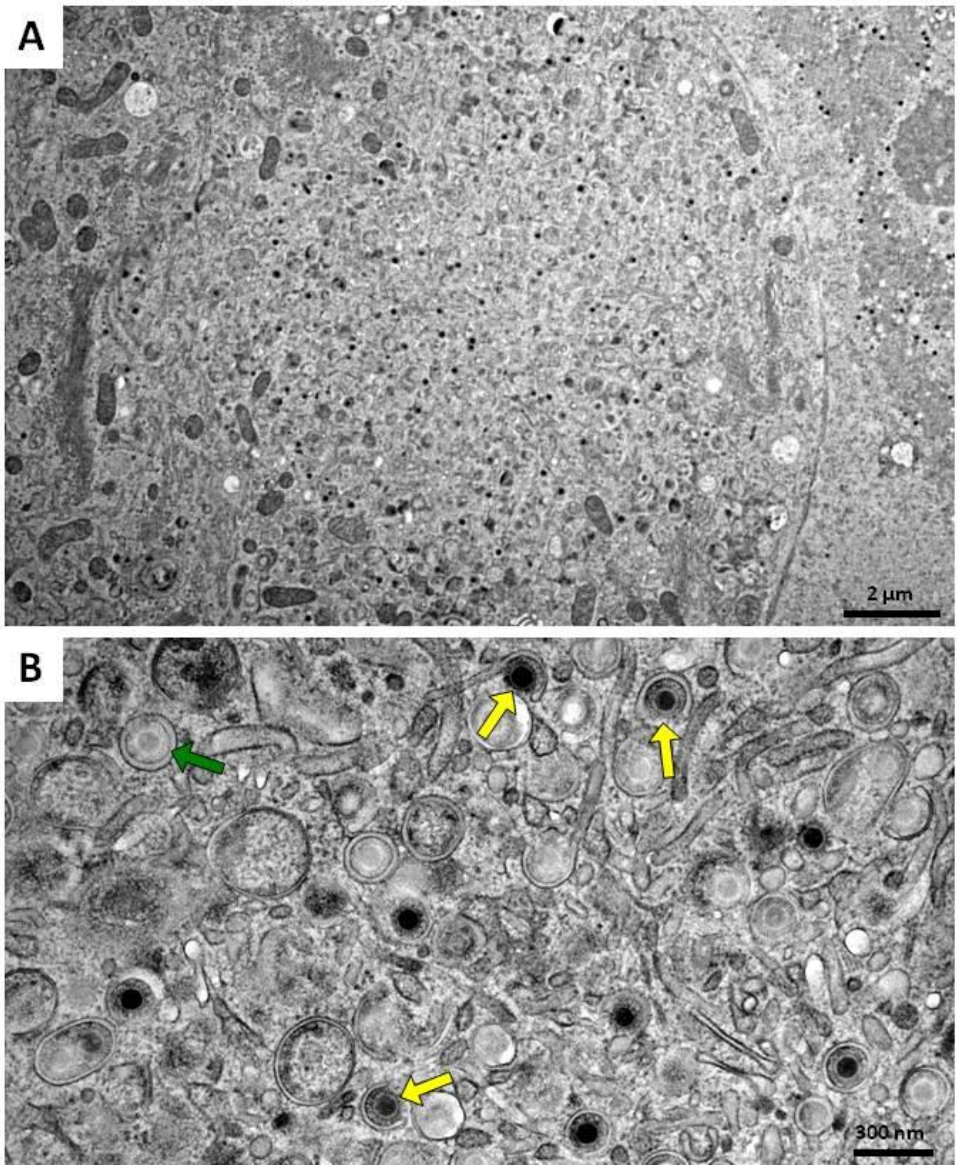


FIG. 40. TB103stop virus infected HFF at 5 days post infection. **(A)** Overview of the AC. **(B)** A greater magnification of the AC area reveals particles which are fully enveloped and contained within a small vesicle (green arrow) or budding (yellow arrows) into small crescent shaped vesicles.

4 Discussion

We could show that HCMV morphogenesis is comparable in fibroblasts, endothelial cells and macrophages and that the absence or the functional impairment of the HCMV tegument protein pUL71 is affecting viral morphogenesis in all investigated cell types in a similar manner. pUL71 is associated with membranes within the AC at late stages of infection, and its absence causes impairment of secondary envelopment, morphological alterations of vesicles within the AC, and influences MVBs in infected fibroblasts, HUVEC, and MDM. Particularly a pUL71 palmitoylation site and a leucine zipper like motif are of great importance for pUL71 function and HCMV morphogenesis, while a C-terminal tetra-lysine motif only augments secondary envelopment. In contrast, a Vps4 interacting motif of pUL71seems to be not important for HCMV morphogenesis.

HCMV is a major opportunistic human pathogen. Since HCMV encodes for more than 200 potential protein products, the contribution of individual proteins to HCMV growth is still unknown in most cases. The characterization of these viral proteins provides a deeper understanding of HCMV morphogenesis and may contribute to the identification of potential targets of antiviral drugs. A valuable tool to provide insights into the function of a given protein is the generation of viral mutants by BAC-mutagenesis in combination with ultrastructural analyses by TEM. This combination allows the investigation of recombinant viruses, where parts or the complete sequence of the protein of interest have been mutated or deleted, and to draw conclusions about the impact of the protein of interest on viral morphogenesis.

4.1 Cytomegalovirus morphogenesis in fibroblasts, endothelial cells and macrophages

To our knowledge, no studies have been undertaken in which the ultrastructural phenotypes of HCMV morphogenesis were compared between different cell types at late stages of infection. The question was whether HCMV morphogenesis as well as HCMV induced morphological changes of host cell structures are comparable in fibroblasts, endothelial cells and macrophages. Our findings showed that in all investigated cell types (fibroblasts, HUVEC, and MDM) HCMV infection caused the establishment of a cytoplasmic compartment in which the virus particles acquired their envelope. The organization of the AC was similar and the majority of virus particles within the AC of wild-type virus infected fibroblasts, HUVEC, and MDM were enveloped at late stages of

infection. This indicated that the process of final particle envelopment is of comparable efficiency in those cell types and suggests a conservation of these late stages of HCMV infection in these cell types. In addition, the absence or functional impairment of the HCMV protein pUL71 caused similar phenotypes in these cell types, regarding both HCMV morphogenesis as well as morphological alterations of the host cells. This could mean that general mechanisms of HCMV morphogenesis are conserved in fibroblasts, endothelial cells and macrophages.

Fibroblasts are commonly used to study cytomegalovirus infection in cell culture, as they are relatively cheap, easy to handle, and high titer replication of HCMV is restricted mainly to primary human fibroblasts (Sinzger et al. 1995). Furthermore, fibroblasts are a predominant target for virus replication *in vivo*, thereby supporting the propagation of the virus. In this study two fibroblast lines - MRC-5 and HFF - were used. HFF are commonly used as a model cell line to study cytomegalovirus infection (e.g. Taylor and Cooper 1989; Jiang et al. 2008; Scrivano et al. 2011) while MRC-5 cells are often used for transfection and transduction experiments (e.g. Spencer 2011; Knoblach 2011). However, HCMV replicates in many different host cells *in vivo* and *in vitro*, including fibroblasts, endothelial cells, epithelial cells, hepatocytes and various leukocyte populations (Sinzger et al. 2008a). Endothelial cells play a central role in the spread of HCMV throughout the host, since they line the entire circulatory system (Adler and Sinzger 2009). The contribution of HUVEC to HCMV persistence and latency is under debate (Kahl et al. 2000; Jarvis and Nelson 2002; Reeves et al. 2004). We used HUVEC in our studies, since they are often used as model endothelial cell line for cytomegalovirus infection (e.g. Ryckman et al. 2006; Scrivano et al. 2011). Macrophages are a very heterogeneous cell population, which contribute to specific and non-specific immune response mechanisms. Monocytes and macrophages are not only susceptible for HCMV infection but also likely reservoirs for HCMV persistence and latency *in vivo* (Taylor-Wiedeman et al. 1991; Jarvis and Nelson 2002). We prepared macrophages from blood of HCMV seronegative donors, by isolation of monocytes and their subsequent differentiation into anti-inflammatory M2 macrophages (Mantovani et al. 2007; Romo et al. 2011). Since macrophages are such a diverse cell population and therefore may behave differently to HCMV infection, it has to be noted that the results of this study might be restricted to M2 macrophages.

Many HCMV strains do not efficiently infect endothelial cells and macrophages (Ryckman et al. 2006), since not all HCMV strains possess the specific glycoprotein

complexes on their envelope, which are required to enter these cell types (Scrivano et al. 2011). For this study, viruses were reconstituted from the TB40-BAC4 (Sinzger et al. 2008b), which is a clone derived from the endotheliotropic and macrophage-tropic TB40/E strain. Due to its broad cell tropism and the usability for the generation of recombinant viruses (Sinzger et al. 2006; Chevillotte 2009; Scrivano et al. 2011), the TB40-BAC4 strain was chosen for this study. Furthermore, viruses derived from the TB40-BAC possess all the same genetic background, i.e. they do not consist of a genetically varying virus population. Therefore, the usage of this virus was consistent with our goal to compare virus morphogenesis between different cell types.

Taken together, given the similarity of morphological changes induced by HCMV infection in fibroblasts, HUVEC and MDM, as well as the similarity of morphogenesis of a mutant virus in all investigated cell types, we conclude that fibroblasts provide a good model to study HCMV morphogenesis. These findings are valuable, since in contrast to fibroblasts both HUVEC and MDM are difficult to cultivate and exhibit a lower infectability than fibroblasts, which complicates the investigation of HCMV morphogenesis in HUVEC and MDM.

4.2 Membrane association of pUL71

At late times post infection pUL71 was located at the AC of wild-type virus infected fibroblasts, endothelial cells and macrophages. Immunofluorescence analyses showed that pUL71 exhibited localization patterns similar but not identical to those of the viral proteins pp28 and glycoprotein B (gB). HCMV pp28 is localized to a compartment related to the endoplasmic reticulum-Golgi-intermediate compartment (ERGIC) (Sanchez et al. 2000), while HCMV gB is proposed to be localized to the *trans*-Golgi network (TGN) in HCMV infected cells (Jarvis et al. 2002). Interestingly, signals for pUL71 were also overlapping with those of the TGN associated cellular protein γ-Adaptin. These data suggested a localization of pUL71 at Golgi-derived membranes. Co-localization of pUL71 with TGN marker Golgin97 and membrane fractionation experiments in HCMV infected fibroblasts further argued in favor of this hypothesis (Daniela Fischer, unpublished data). The application of immuno electron microscopy enabled us to further investigate the localization of pUL71 on an ultrastructural level. Immuno-gold labeling on ultra thin sections of TB71HA virus infected fibroblasts confirmed the localization of pUL71 at membranes. Gold particles were mostly found at the viral envelope or at membranes of

vesicles which originated from the budding process of virus particles, but also at other membranes including Golgi-stacks. The combined data from fluorescence microscopy and immuno-EM strongly supports the hypothesis that pUL71 is attached to cellular membranes of vesicles within the AC, which are also used for virus envelopment, and that these vesicles are Golgi-derived.

4.3 Cytomegalovirus morphogenesis in absence of pUL71

The role of pUL71 for final HCMV particle envelopment has been shown previously for TB71stop virus infected fibroblasts (Schauflinger 2008; Womack and Shenk 2010). However, it was not known whether these defects would also occur in other relevant cell types, like endothelial cells or macrophages. Thus one of the major goals was to compare the effects of pUL71 depletion between those cell types. This study showed that absence of HCMV pUL71 caused various alterations of the morphology of infected fibroblasts, endothelial cells and macrophages, which differed from the morphology of HCMV wild-type infected cells. This included the severe impairment of final particle envelopment as well as a changed morphology of budding vesicles and MVBs. These alterations were surprisingly similar between the various cell types, suggesting an identical function of pUL71 in HCMV morphogenesis in fibroblasts, endothelial cells and macrophages.

Impairment of secondary envelopment. The majority of particles, which accumulated in the cytoplasm of TB71stop virus infected cells were not enveloped, as shown by quantitative EM analyses in fibroblasts, HUVEC and macrophages. This demonstrated that pUL71 supports secondary particle envelopment and that this function is conserved within all investigated cell types. The role of pUL71 seems furthermore to be conserved within the herpesvirus family, since deletion of the homologous α-herpesvirus protein pUL51 led to an impairment of final envelopment of pseudorabies virus (Klupp et al. 2005) and HSV-1 (Nozawa et al. 2005), respectively. Also, both pUL51 deficient viruses exhibited a small plaque phenotype and low extracellular titers, very similar to the HCMV TB71stop virus. Involvement in envelopment processes of HCMV is known for viral envelope proteins, such as glycoprotein O (Jiang et al. 2008), and also tegument proteins, such as pp28 (Silva et al. 2008; Seo and Britt 2008). These proteins are membrane associated and seem to facilitate the contact between membranes that are used for envelopment and the viral particle. This is also the most likely scenario for pUL71, which is associated with

membranes in the AC, and is also contained within the released virions (Varnum et al. 2004). When pUL71 is absent, the process of secondary envelopment is inefficient and thus most particles are stuck in this process. At least a fraction of TB71stop particles become enveloped eventually, since enveloped virions in the cytoplasm and low extracellular titers can be detected. This suggests that either more than one mechanism exists to facilitate the final envelopment of HCMV, or that the role of pUL71 in secondary envelopment is partially complemented by another protein. Taking into account that some α-herpesvirus proteins can partially complement functions of other proteins (Mettenleiter and Spear 1994; Kuhn et al. 2008), it is feasible to assume similar mechanisms for HCMV.

Morphological alteration of budding vesicles. The severe impairment of secondary envelopment in absence of pUL71 went along with a morphological alteration of vesicles which were used for budding. These irregular shaped vesicles were often larger as in wild-type virus infected cells and multiple budding processes occurred simultaneously at their membranes. This phenotype could be observed in TB71stop virus infected fibroblasts, HUVEC and macrophages to a similar extend. It seems very likely that the accumulation of virus particles at these vesicles correspond to the accumulations of pp28 and pp150 signals described for the type II and type III AC. We assume that the longer the replication cycle proceeds the more virus particles accumulate in the cytoplasm of TB71stop virus infected cells. The amount of virions in type II ACs was higher than in type I ACs, and even higher in ACs of type III. Thus, we speculate that accumulations of type II occur first, and that the enlarged MVBs of type III complete the phenotype. Yet there was no shift towards more type III ACs from day 5 to day 7 post infection. However, this might be due to the spread of infection throughout the cell culture, which constantly generates early infected cells that exhibit type I ACs. The reasons for the enlargement of budding vesicles are not yet clear. We hypothesize that they develop by merging of multiple vesicles. Non-enveloped particles are retained within the cytoplasm of TB71stop virus infected cells, along with vesicles into which these particles bud. Membranes of individual budding vesicles might eventually fuse, thereby forming larger vesicular structures. On the contrary, enveloped particles might be rapidly released into the extracellular space, which leaves only short time for budding vesicles to interact with each other.

Enlargement of MVBs. Absence of pUL71 caused a pronounced occurrence of MVBs. Quantitative immunofluorescence assays showed that about one third to one half of

TB71stop virus infected fibroblasts and HUVEC exhibited greatly enlarged MVBs. Ultrastructural analyses suggested that the occurrence of MVBs was enhanced in TB71stop virus infected macrophages as well. MVBs are multivesicular endosomes and their major role is the uptake of proteins, which are destined for degradation or recycling, by their incorporation into intraluminal vesicles that bud from the limiting membrane of the MVB (Piper and Katzmann 2007). The MVBs then fuse with lysosomes, which usually leads to a degradation of the MVB cargo (Piper and Luzio 2001; Katzmann et al. 2002; Hicke and Dunn 2003). It can be hypothesized that the virus infection of a cell goes along with high levels of viral proteins in the cytoplasm and likely stimulates the formation of MVBs. While the enhancement of MVB biogenesis could be a natural response of the host cells to infection, it was not clear why the absence of pUL71 caused the MVBs to become enlarged in size compared to wild-type virus infection.

We considered the possibility that pUL71 functions as a viral inhibitor of MVB biogenesis, which impairs the formation of those endosomes when it is present. MVBs develop with the help of the ESCRT (endosomal sorting complex required for transport) machinery (Nickerson et al. 2007). In short, ESCRT are big protein complexes, which support fission and fusion events at the limiting membrane of MVBs (Hurley and Emr 2006). Various viruses exploit the ESCRT pathway, supposedly for membrane scission events that separate nascent enveloped virions from the host cell membranes, e.g. HIV-1 (Garrus et al. 2001), Ebola (Martin-Serrano et al. 2001), Bluetong Virus (Wirblich et al. 2006) and even the herpesvirus HSV-1 (Calistri et al. 2007; Crump et al. 2007). The only confirmed link of pUL71 to ESCRT is the interaction of pUL71 with Vps4 (Fischer 2008). The cellular AAA+ ATPase Vps4 is required for the disassembling and recycling of ESCRT complexes and thus essential for MVB biogenesis (Shim et al. 2008). pUL71 recruited Vps4 to the AC in HCMV infected cells, while in non infected cells Vps4 was located at endosomal membranes. The pUL71 Vps4 interaction is facilitated by the pUL71 $_{315}$PDVPRE$_{320}$ motif (Suffner 2011). Interestingly, Tandon et al. (2009) reported that ESCRT is involved in the final steps of HCMV replication, since dominant negative forms of Vps4 inhibited viral replication. However, also contradictory data has been published, showing that silencing of Vps4 even enhanced the number of produced HCMV viral particles (Fraile-Ramos et al. 2007). While the deletion or mutation of the pUL71 Vps4 interacting motif led to the disability of pUL71 to recruit Vps4 to the AC, it had no effect on virus growth nor did it change the localization or protein levels of pUL71 (Suffner 2010). Furthermore, ultrastructural investigation of TB71del315-326 virus infected cells

showed that the deletion of the Vps4 interacting motif results in a wild-type like phenotype. These data suggest that the recruitment of Vps4 by pUL71 has no impact on viral morphogenesis and does not support the role of pUL71 as an inhibitor of MVB biogenesis.

Thus, we propose a more likely and simpler explanation as to why MVBs are so dominant in TB71stop virus infected cells. Quantitative EM analyses showed a more than 3-fold increase in the average number of cytoplasmic particles in sections through the ACs of TB71stop virus infected HFF compared to wild-type virus infected cells. This increased amount of viral material within the host cell could simply trigger an enhanced cellular response -such as cargo sorting into MVBs- to get rid of the alien protein load. The fact that the amount of virus particles was five-fold increased in cells with type III AC compared to cells with wild-type like type I AC argues in favor of this hypothesis.

Reduction of cytoplasmic nucleocapsids. The relative amount of cytoplasmic nucleocapsids in TB71stop virus infected fibroblasts was reduced compared to wild-type virus infected cells. Therefore we clarified whether pUL71 influences viral genome packaging in the nucleus, as proposed recently by To et al. (2011) who showed interactions of pUL71 with HCMV tegument proteins pUL51 and pUL89.2 by yeast two hybrid as well as CoIP analyses. Both pUL51 and pUL89 are important for viral DNA genome cleavage and packaging (Dunn et al. 2003; Yu et al. 2003; Evers et al. 2004). However, the fractions of A-, B- and C-capsids in the nuclei of TB71stop virus infected cells did not differ from those in wild-type virus infected cells, suggesting that pUL71 is not involved in viral genome packaging. Furthermore, immunofluorescence analyses of wild-type virus infected cells never showed pUL71 signals in the nuclei. These data suggest that the reduction of nucleocapsids in TB71stop virus infected cells is based on a mechanism within the cytoplasm. For example, a more efficient envelopment process and rapid egress of nucleocapsids would explain an accumulation of non-infectious particles within the cytoplasm. Yet, in TB71stop virus infected cells the relative amount of enveloped nucleocapsids was not significantly higher than the relative amount of non-enveloped nucleocapsids, which does not support the hypothesis that nucleocapsids are more efficiently enveloped. Interestingly, the majority of TB71stop particles at the membranes of MVBs were found to be empty capsids, while the particles in the lumen of MVBs were mainly nucleocapsids. A more efficient degradation of nucleocapsids compared to empty capsids could explain the lower amount of nucleocapsids in the cytoplasm of TB71stop

virus infected cells. Consistently, a reduction of cytoplasmic nucleocapsids was also found in TB71C13A virus infected cells, as well as for the leucine zipper mutants. These viruses are also characterized by the frequent occurrence of large MVBs. However, we are not sure about the underlying mechanism that leads to the reduction of nucleocapsids. Further experiments are required to illuminate this question.

4.4 The pUL71 palmitoylation site

TB71C8A virus infected cells were not distinguishable from wild-type virus infected cells on an ultrastructural level. Therefore, C8 does not seem to be of great importance, if any, for HCMV morphogenesis and growth. Consistently, the mutation of cysteine 8 alone did not affect growth of HCMV (Suffner 2011), nor was the localization of pUL71 impaired in TB71C8A virus infected cells. On the contrary, the ultrastructural phenotypes of both TB71C8/13A and TB71C13A virus infected cells match the characteristics of TB71stop virus infected cells. Consistently, these viruses show reduced plaque sizes and severe growth defects compared to wild-type virus (Böck 2010; Suffner 2011), very similar to the TB71stop virus. Thus, it can be assumed that the integrity of the residue C13 is a prerequisite for the function of pUL71. Recently, palmitoylation of pUL71 cysteines at position 8 and 13 has been confirmed by metabolic labeling experiments (Daniela Fischer, unpublished data). Posttranslational palmitoylation increases membrane association of many proteins, since attachment of palmitate to proteins increases their hydrophobicity (Resh 2006). This has also been demonstrated in a herpesviral context. The membrane association of pUL51, the pUL71 homologue of α-herpesviruses, is mediated by posttranslational palmitoylation (Shen et al. 2009). For example, palmitoylation of the N-terminal cysteine at position 9 of the HSV-1 protein pUL51 is a requirement for its Golgi localization (Nozawa et al. 2003). Furthermore, palmitoylation of HCMV gN is necessary for secondary envelopment of HCMV and virus replication (Mach et al. 2007). Interestingly, immunofluorescence analyses of TB71C8/13A and TB71C13A virus infected HFF revealed only very weak cytoplasmic signals for pUL71. In contrast to the delocalization of the recombinant proteins pUL71C8/13A and pUL71C13A in transfection experiments (Daniela Fischer, unpublished data), the findings for TB71C8/13A and TB71C13A virus infected cells left no sufficient evidence for a delocalization of pUL71. This might be explained by the fact that the situation in infected cells is different compared to transfected cells. First, the cellular levels of the transfected protein are most likely

higher than the pUL71 levels during infection. This might cause a different picture in immunofluorescence stainings. Second, pUL71 might be retained within the area of the AC during infection by the interaction with other AC located viral proteins.

Two possible scenarios might explain the weak pUL71 signals in TB71C8/13A and TB71C13A virus infected cells. First, this could be due to impaired protein expression, or second, due to a rapid posttranslational degradation of pUL71. To clarify whether there is a downregulation of UL71 expression, the UL71 mRNA levels of infected cells would have to be assessed. However, since the UL71 promoter region is not affected by the point mutations, altered UL71 expression seems to be unlikely. A more likely explanation for the low protein levels in TB71C8/13A and TB71C13A virus infected cells is the degradation of the recombinant proteins pUL71C8/13A and pUL71C13A in the cytoplasm of the host cells. Eukaryotic cells are able to rapidly degrade proteins, e.g. when they exhibit structural damage, such as misfolding of the protein (Goldberg 2003). The formation of disulfide bonds by cross-linking of cysteine residues can provide structural and functional properties to a protein, and their disruption may cause instability, non-functionality or mislocation of the protein (Gupta et al. 2004). For example, single mutations of cysteine to alanine in the HSV-1 protein pUL6 led to a loss of pUL6 function due to the disruption of disulfide bonds (Albright et al. 2011); mutation of cysteines to serines in the F protein of the pneumovirus HRSV severely impaired cell surface expression of this protein, suggesting a key role of the cysteines in the proper folding and subsequent transport through the Golgi to the cell surface (Day et al. 2006); mutation of cysteines to alanines in the coronavirus envelope (E) protein increased the rate of degradation compared to wild-type E protein, suggesting that the cysteines and presumably palmitoylation are important for protein stability and for virus production (Lopes et al. 2008). We have no scientific proof for the degradation of pUL71 after impairment of C13 yet. This question could be addressed in further experiments, e.g. by checking the pUL71 levels after drug induced inhibition of proteasomes in TB71C13A virus infected cells.

Independent from the reasons for the low cytoplasmic pUL71 levels in TB71C8/13A and TB71C13A virus infected cells, the observed defects in HCMV morphogenesis are most likely a result of decreased protein levels, which were so low that detection of pUL71 by Western blotting was not possible in lysates f TB71C13A virus infected fibroblasts. This virtually equals the absence of pUL71 during infection, which explains the similarities of the phenotypes of TB71C13A and TB71stop virus infected cells.

4.5 The pUL71 leucine zipper like motif

The ultrastructural phenotype of TB7134-41 and TB71L34/41A virus infected cells suggested a complete loss of pUL71 function. Consistently, both recombinant viruses exhibited reduced titers of infectious viral progeny in the supernatant, as well as reduced plaque sizes compared to wild-type HCMV (Suffner 2011), very similar to the defects observed in TB71stop virus infected cells. Since the deletion or mutation of the pUL71 leucine zipper like motif did not cause a reduction of pUL71 levels in TB71del34-41 and TB71L34/41A virus infected cells (Suffner 2011), the observed defects are most likely based on a functional loss of the pUL71 leucine zipper like motif. A leucine zipper of a protein is a periodic repetition of leucine residues, which may facilitate protein-protein interactions such as dimerization (Landschulz et al. 1988). Previous analyses using non-denaturing gel electrophoresis as well as bimolecular fluorescence complementation (BiFC) showed that pUL71 is able to form oligomers through this N-terminal leucine zipper like motif, and deletion of amino acids 34 to 41 or mutation of L34 and L41 inhibited this oligomerization (Meissner 2012).

Oligomerization of proteins is often required for proper functioning of proteins, e.g. multimerization of the HCMV tegument protein pp28 is a requirement for the correct localization of this protein as well as for the secondary envelopment of HCMV particles (Seo et al. 2008); leucine zipper dependent protein-protein interactions between HCMV proteins pUL84 and IE2, as well as self-interaction of pUL84 are required for pUL84 to function (Colletti et al. 2004). While the impairment of the pUL71 leucine zipper did not alter the localization of pUL71, co-immunoprecipitation (Co-IP) experiments confirmed interactions of pUL71 with itself, but also with the HCMV protein pUL103 (Jens von Einem, unpublished data). A pUL103 deficient recombinant virus has been used to describe pUL103 as an augmenting protein with a small plaque phenotype and low titers (Yu et al. 2003). Furthermore, mutant viruses lacking UL103 exhibited dramatically reduced accumulation of cell-free virus progeny and poor cell-to-cell spread, suggesting a function during the late phase of replication (Ahlqvist and Mocarski 2011). A pUL103 deficient virus which was generated in our facility exhibited a severe envelopment defect. Thus, both pUL71 and pUL103 might have a similar and maybe complementary function for the final envelopment of HCMV particles. However, it is not yet clear whether the interaction of pUL71 and pUL103 is mediated by the pUL71 leucine zipper nor if this interaction is of relevance for HCMV morphogenesis. These questions are addressed currently in our facility, along with the meaning of the self-interaction of pUL71.

Dimerization or oligomerization of pUL71 could be a requirement for the proper function of this protein and explain the severe defects caused by the impairment of the leucine zipper like motif.

4.6 The pUL71 tetra-lysine motif

The investigation of viruses with a C-terminally truncated pUL71 showed that the C-terminus of pUL71 is important for efficient secondary envelopment of HCMV. The mutation of lysines K348-351 was sufficient to cause a phenotype comparable to the one in TB71del315-361 virus infected cells. This demonstrated the importance of this tetra-lysine motif at the very C-terminus of pUL71. Lysines are positively charged amino acids which are frequently found in protein active or binding sites. Many nuclear localization signals (NLS) have been found to contain sequences of the positively charged amino acids lysine (K) and arginine (R) (Makkerh et al. 1996; Nakielny and Dreyfuss 1999). For example, the NLS of the simian virus 40 large T-antigen (SV40 T-ag) consists of a single cluster of amino acids PKKKRKV (Kalderon et al. 1984; Lanford and Butel 1984). However, to our knowledge no reports exist about such a motif being responsible or important for secondary envelopment of viruses. Surprisingly, the knock-out of this C-terminal motif did not affect virus growth, nor was the morphology of TB71K348-351A virus infected cells significantly different from wild-type virus infected cells. The same was true for TB71del315-361 virus infected cells (Daniela Fischer, unpublished data). This demonstrates that there is no severe impact on HCMV growth when the pUL71 C-terminus is truncated or mutated. We currently have no explanation as to why the obvious impairment of secondary envelopment in TB71K348-351A virus infected cells does not result in a reduction of extracellular virus titers or intracellular accumulations of virions. This might be a goal for further research.

4.7 Model of the impact of pUL71 functional domains on virus growth

The investigation of several HCMV pUL71 mutant viruses was performed especially by electron microscopy after cryofixation of infected cells. This method provides the best structural conservation of *in vivo* states, and therefore is the most viable method to directly investigate viral morphogenesis (Roos and Morgan 1990; Buser et al. 2007). Furthermore, the ability to judge about the state of single viral particles is mainly restricted to EM. Yet,

the strength of our investigation is particularly based on the quantification of the EM data. This is a tribute to the diverse and intermediate phenotypes which occur in biological samples. Based on our current knowledge about pUL71, we suggest a model which summarizes the defects that follow impairment of pUL71 functional domains (FIG 41).

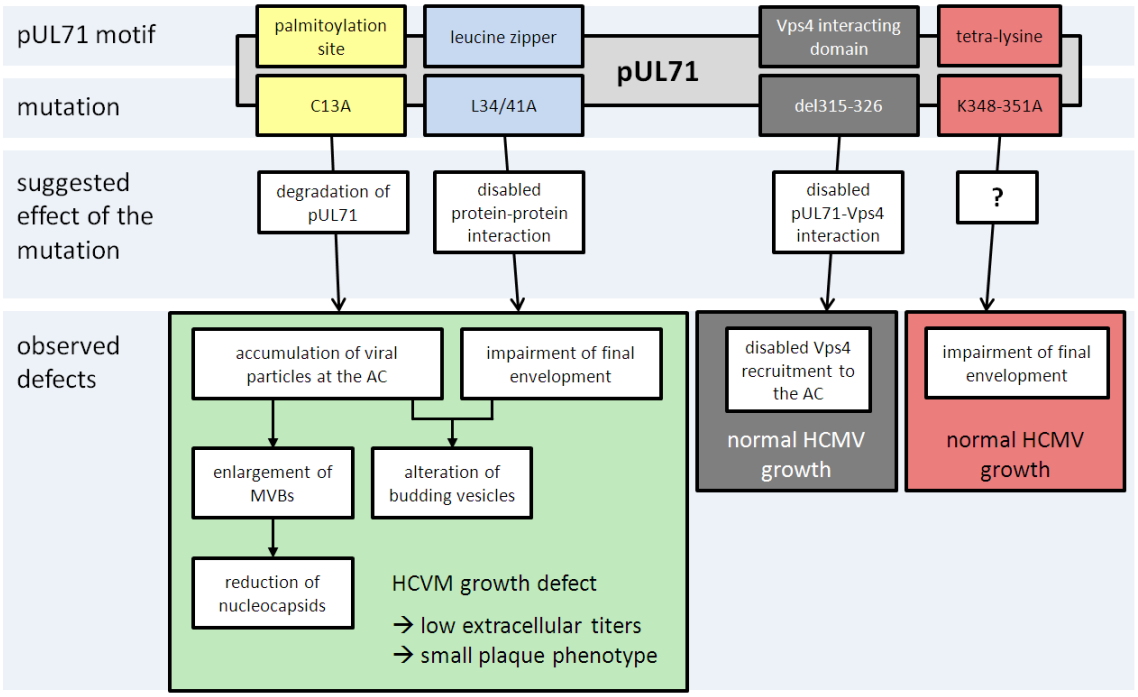


FIG 41. The defects that follow functional impairment of pUL71 and the proposed connections between the individual defects are summarized in this model.

Our investigation of the HCMV tegument protein pUL71 gave us a detailed insight into its function, which is preserved in fibroblasts, endothelial cells, and macrophages. Previous analyses of TB71stop virus infected cells showed that the absence of pUL71 leads to low extracellular titers of infectious viruses and a small plaque phenotype in cell culture (Fischer 2008). In this study we could show that the disabled release of virus particles leads to an accumulation of virus particles within the cytoplasm of the host cell. The major accumulation of virions and viral proteins might trigger an enhancement of the endosomal pathway and thereby explain the pronounced occurrence of MVBs during pUL71 knock-out. This, on the other hand, could entail the reduction of cytoplasmic nucleocapsids.

The key role of pUL71, however, seems to be that it mediates an efficient release of virions from the host cell. Given the impairment of secondary envelopment that follows depletion of pUL71, it seemed sound to assume that the inefficient envelopment of HCMV particles was the major cause for the impaired release of virions. In the light of the findings

that there are no growth defects when the pUL71 C-terminus is truncated despite a defect of secondary envelopment, the explanation for the impaired virus growth is apparently more sophisticated. The loss of pUL71 function after mutation of the N-terminal palmitoylation site is likely due to the degradation of pUL71, which does not allow to interpret the function of this protein in more detail. In contrast, the impairment of the leucine zipper like motif results in a loss of pUL71 function without reduction of pUL71 levels during HCMV infection. This motif facilitates dimerization of pUL71, and might also be responsible for interactions between pUL71 and other proteins. Our findings imply that a leucine zipper mediated protein-protein interaction is a requirement for pUL71 to fulfill its key role, which is to allow for an efficient release and spread of HCMV.

5 Summary

Human cytomegalovirus (HCMV) is an ubiquitous β-herpesvirus causing major morbidity and mortality in immunocompromised hosts. Despite intensive research over many years, the contribution of individual viral proteins to the growth of HCMV is still not clear in most cases. We wanted to extend the knowledge about the function of the HCMV tegument protein pUL71. Light microscopic and electron microscopic methods were used to obtain better insight into the virally induced morphological changes within the cells on subcellular and ultrastructural levels. The subcellular localization of pUL71 at membranes of the viral assembly compartment (AC) of wild-type virus infected cells could be shown by indirect immunofluorescence experiments and immuno-electron microscopy.

An influence of pUL71 on early steps of HCMV morphogenesis was not detectable, however, the ultrastructural investigation of a pUL71 deficient virus (TB71stop) by transmission electron microscopy (TEM) revealed that the absence of pUL71 causes several defects of HCMV morphogenesis. HCMV capsids accumulated in vast numbers within the viral assembly compartment of TB71stop virus infected cells. The capsids were predominantly associated to membranes of enlarged budding vesicles and arrested in the process of secondary envelopment. Furthermore, multivesicular bodies (MVBs) were enlarged in many TB71stop virus infected cells. Interestingly, absence of pUL71 also led to an accumulation of empty capsids within the cytoplasm.

Various recombinant viruses carrying mutations within the sequence of pUL71 were investigated to identify and characterize functional domains of this protein. The mutation of only one cysteine residue at the N-terminus of pUL71 was sufficient to knock-out the pUL71 function. Similarly, the mutation of a N-terminal leucine zipper like motif of pUL71 resulted in a TB71stop virus like phenotype. This suggests that pUL71 homo- or heterodimerization via its leucine zipper like motif is a requirement for efficient HCMV growth. In contrast, a previously identified motif of pUL71 which enables interaction of pUL71 with the cellular ATPase Vps4 seems not to be important for HCMV morphogenesis. Furthermore, we were able to identify a tetra-lysine motif at the C-terminus of pUL71 which augments secondary envelopment, but is not essential for the growth of HCMV.

Another goal of this thesis was to compare HCMV morphogenesis between fibroblasts, endothelial cells and macrophages on an ultrastructural level. We could show that late stage HCMV infected fibroblasts, human umbilical vein endothelial cells (HUVEC), and monocyte derived macrophages (MDM) established a comparable viral

assembly compartment in which the virus particles acquired their envelope. The efficiency of particle envelopment was similar in HCMV infected fibroblasts, HUVEC and MDM. Furthermore, the absence or functional impairment of the HCMV protein pUL71 caused comparable phenotypes in these cell types, regarding both HCMV morphogenesis and morphological alterations of the host cells. This suggests that the general mechanisms of HCMV morphogenesis are conserved between fibroblasts, endothelial cells and macrophages, and also that fibroblasts are a suitable model cell type to study HCMV morphogenesis.

6 Literature

(1) Adler B, Sinzger C (2009): *Endothelial cells in human cytomegalovirus infection: One host cell out of many or a crucial target for virus spread?* Thromb Haemost 102:1057–63.

(2) Ahlqvist J and Mocarski E (2011): *Cytomegalovirus UL103 Controls Virion and Dense Body Egress.* J Virol 85(10):5125–5135

(3) Albright BS, Nellissery J, Szczepaniak R, Weller SK (2011): *Disulfide Bond Formation in the Herpes Simplex Virus 1 UL6 Protein Is Required for Portal Ring Formation and Genome Encapsidation.* J Virol 85(17):8616-24.

(4) Baldick CJ Jr., Shenk T (1996): *Proteins associated with purified human cytomegalovirus particles.* J Virol 70:6097–6105.

(5) Bechtel JT, Shenk T (2002): *Human Cytomegalovirus UL47 Tegument Protein Functions after Entry and before Immediate-Early Gene Expression.* J Virol 76:1043-50.

(6) Becker Y, Darai G, Huang ES (1993): *Molecular aspects of human cytomegalovirus disease.* Springer Verlag.

(7) Böck TC (2010): *Interaktion des Herpesvirus Tegumentproteins pUL71 mit den Proteinen der zellulären ESCRT-Maschinerie.* Diplom thesis, Institute of Virology, Ulm University Hospital.

(8) Bodaghi B, Slobbe-van Drunen ME, Topilko A Perret E, Vossen RC, van Dam-Mieras MC, Zipeto D, Virelizier JL, LeHoang P, Bruggeman CA, Michelson S (1999): *Entry of human cytomegalovirus into retinal pigment epithelial and endothelial cells by endocytosis.* Invest Ophthalmol Vis Sci 40:2598-2607.

(9) Britt WJ, Alford CA (1996): *Cytomegalovirus*. Virology 2(3):2493–2523.

(10) Buser C, Walther P, Mertens T, Michel D (2007): *Cytomegalovirus Primary Envelopment Occurs at Large Infoldings of the Inner Nuclear Membrane.* J Virol 81(6):3042-48.

(11) Calistri A, Sette P, Salata C, Cancellotti E, Forghieri C, Comin A, Göttlinger H, Campadelli-Fiume G, Palu G, Parolin C (2007): *Intracellular trafficking and maturation of herpes simplex virus type 1 gB and virus egress require functional biogenesis of multivesicular bodies.* J Virol, 81(20):11468-78.

(12) Chevillotte M, Landwehr S, Linta L, Frascaroli G, Lüske A, Buser C, Mertens T, von Einem J (2009): *Major Tegument Protein pp65 of Human Cytomegalovirus Is*

Required for the Incorporation of pUL69 and pUL97 into the Virus Particle and for Viral Growth in Macrophages. J Virol 83(6):2480-90

(13) Colletti KS, Xu Y, Cei SA, Tarrant M, Pari GS (2004): *Human Cytomegalovirus UL84 Oligomerization and Heterodimerization Domains Act as Transdominant Inhibitors of oriLyt-Dependent DNA Replication: Evidence that IE2-UL84 and UL84-UL84 Interactions Are Required for Lytic DNA Replication.* J Virol 78(17): 9203–9214.

(14) Compton T, Nepomuceno RR, Nowlin DM (1992): *Human cytomegalovirus penetrates host cells by pH-independent fusion at the cellsurface.* Virology 191:387-395.

(15) Compton T, Nowlin DM, Cooper NR (1993): *Initiation of human cytomegalovirus infection requires initial interaction with cell surface heparan sulfate.* Virology 193:834-841.

(16) Crump CM, Yates C, Minson T (2007): *Herpes Simplex Virus Type 1 Cytoplasmic Envelopment Requires Functional Vps4.* J Virol 81:7380-7387.

(17) Das S, Pellett PE (2011): *Spatial Relationships between Markers for Secretory and Endosomal Machinery in Human Cytomegalovirus-Infected Cells versus Those in Uninfected Cells.* J Virol 85(12):5864–79.

(18) Das S, Vasanji A, Pellett PE (2007): *Three-Dimensional Structure of the Human Cytomegalovirus Cytoplasmic Virion Assembly Complex Includes a Reoriented Secretory Apparatus.* J Virol 81(21):11861-11869.

(19) Day ND, Branigan PJ, Liu C, Gutshall LL, Luo J, Melero JA, Sarisky RT, Del Vecchio AM (2006): *Contribution of cysteine residues in the extracellular domain of the F protein of human respiratory syncytial virus to its function.* Virol J 3: 34.

(20) Dubochet J, Sartori Blanc N (2001): *The cell in absence of aggregation artifacts.* Micron 32:91-92, 99.

(21) Dunn W, Chou C, Li H, Patterson D, Stok V, Zhu H, Liu F (2003): *Functional profiling of human cytomegalovirus genome.* Proc Natl Acad Sci USA 100:14223-14228.

(22) Evers DL, Komazin G, Ptak RG, Shin D, Emmer BT, Townsend LB, Drach JC (2004): *Inhibition of Human Cytomegalovirus Replication by Benzimidazole Nucleosides Involves Three Distinct Mechanisms.* Antimicrob Agents Chemother 48(10):3918–27.

(23) Fischer D (2008): *Die Rolle des viralen Proteins pUL71 bei der Morphogenese des Humanen Zytomegalievirus.* Diplom thesis, Institute of Virology, Ulm University Hospital.

(24) Fraile-Ramos A, Pelchen-Matthews A, Risco c, Rejas MT, Emery VC, Hassan-Walker AF, Esteban M,Marsh M (2007): *The ESCRT machinery is not required for human cytomegalovirus envelopment.* Cell microbial 9(12):2955-67.

(25) Garrus JE, von Schwedler UK, Pornillos OW, Morham SG, Zavitz KH, Wang HE, Wettstein DA, Stray KM, Côté M, Rich RL, Myszka DG, Sundquist WI (2001): *Tsg101 and the Vacuolar Protein Sorting Pathway Are Essential for HIV-1 Budding.* Cell 107:55-65.

(26) Goldberg AL (2003): *Protein degradation and protection against misfolded or damaged proteins.* Nature 426: 895-899.

(27) Gupta A, Van Vlijmen HWT, Singh J (2004): *A classification of disulfide patterns and its relationship to protein structure and function.* Protein Sci 13(8): 2045–58.

(28) Hicke L, Dunn R (2003): *Regulation of membrane protein transport by ubiquitin and ubiquitin-binding proteins.* Annu Rev Cell Dev Biol 19:141–172.

(29) Homman-Loudiyi M, Hultenby K, Britt W, Söderberg-Naucler C (2003): *Envelopment of human cytomegalovirus occurs by budding into Golgi-derived vacuole compartments positive for gB, Rab3, trans-golgi-network 46, and mannosidase II.* J Virol 77: 3191-203.

(30) Hurley JH, Emr SD (2006): *The ESCRT complexes: structure and mechanism of a membrane-trafficking network.* Annu Rev Biophys Biomol Struct, 35:277-98.

(31) Jacobs JP, Jones CM, Baille JP (1970): *Characeristics of a human diploid cell designated MRC-5.* Nature, 227(5254):168-70.

(32) Jahn G, Harthus HP, Bröker M, Borisch B, Platzer B, Plachter B (1990): *Generation and application of a monoclonal antibody raised against a recombinant cytomegalovirus-specific polypeptide.* Klin Wochenschr 68:1003–7.

(33) Jarvis MA, Fish KN, Söderberg-Naucler C, Streblow DN, Meyers HL, Thomas G, Nelson JA (2002): *Retrieval of human cytomegalovirus glycoprotein B from cell surface is not required for virus envelopment in astrocytoma cells.* J Virol 76(10):5147-55.

(34) Jarvis MA, Nelson JA (2002): *Human cytomegalovirus persistence and latency in endothelial cells and macrophages.* Curr Opin Microbiol 5(4):403-7.

(35) Jiang XJ, Adler B, Sampaio KL, Digel M, Jahn G, Ettischer N, Stierhof YD, Scrivano L, Koszinowski U, Mach M, Sinzger C (2008): *UL74 of Human Cytomegalovirus Contributes to Virus Release by Promoting Secondary Envelopment of Virions*. J Virol 82: 2802-2812.

(36) Johannsen E, Luftig M, Chase MR, Weicksel S, Cahir-McFarland E, Illanes D, Sarracino D, Kieff E (2004): *Proteins of purified Epstein-Barr virus.* Proc Natl Acad Sci U S A 101(46):16286–16291.

(37) Johnson RA, Wang X, Ma XL, Huong SM, Huang ES (2001): *Human cytomegalovirus up-regulates the phosphatidylinositol 3-kinase (PI3-K) pathway: inhibition of PI3-K activity inhibits viral replication and virus-induced signaling.* J Virol 75:6022-32.

(38) Kahl M, Siegel-Axel D, Stenglein S, Jahn G, Sinzger C (2000): *Efficient Lytic Infection of Human Arterial Endothelial Cells by Human Cytomegalovirus Strains.* J Virol 74(16):7628–35.

(39) Kalderon D, Richardson WD, Markham AF, Smith AE (1984): *Sequence requirements for nuclear location of simian virus 40 large-T antigen.* Nature 311:33–38.

(40) Kalejta RF (2008): *Tegument proteins of human cytomegalovirus*. Microbiol Mol Biol Rev 72:249–265.

(41) Kaneko Y, Walther P (1995): *Comparison of Ultrastructure of Germinating Pea Leaves Prepared by High-Pressure-freezing, freeze substitution and conventional chemical fixation.* J Electron Microsc (Tokyo) 44:104-109.

(42) Katzmann DJ, Odorizzi G, Emr SD (2002): *Receptor downregulation and multivesicular-body sorting.* Nat Rev Mol Cell Biol 3(12):893-905.

(43) Kinzler ER, Compton T (2005): *Characterization of human cytomegalovirus Glykoprotein-induced cell-cell fusion.* J Virol 79:7827-7837.

(44) Klupp BG, Granzow H, Klopfleisch R, Fuchs W, Kopp M, Lenk M, Mettenleiter TC (2005): *Functional analysis of the pseudorabies virus UL51 protein.* J Virol 79:3831-40.

(45) Knoblach T, Grandel B, Seiler J, Nevels M, Paulus C (2011): *Human Cytomegalovirus IE1 Protein Elicits a Type II Interferon-Like Host Cell Response That Depends on Activated STAT1 but Not Interferon-γ.* PLoS Pathog 7(4):e1002016.

(46) Kremer JR, Mastronarde DN, and McIntosh JR (1996): *Computer visualization of three-dimensional image data using IMOD.* J Struct Biol 116:71–76.

(47) Kuhn J, Leege T, Klupp BG, Granzow H, Fuchs W, Mettenleiter TC (2008): *Partial Functional Complementation of a Pseudorabies Virus UL25 Deletion Mutant by Herpes Simplex Virus Type 1 pUL25 Indicates Overlapping Functions of Alphaherpesvirus pUL25 Proteins.* J Virol 82(12):5725-34.

(48) Landschulz WH, Johnson PF, McKnight SL (1988): *The leucine zipper: a hypothetical structure common to a new class of DNA-binding proteins*. Science 240(4860):1759–64.

(49) Lanford RE, Butel JS (1984): *Construction and characterisation of an SV40 mutant defective in nuclear transport of T antigen.* Cell 37:801–813.

(50) Lopez LA, Riffle AJ, Pike SL, Gardner D, Hogue BG (2008): *Importance of Conserved Cysteine Residues in the Coronavirus Envelope Protein.* J Virol 82(6): 3000–3010.

(51) Mach M, Osinski K, Kropff B, Schloetzer-Schrehardt U, Krzyzaniak M, Britt M (2007): *The Carboxy-Terminal Domain of Glycoprotein N of Human Cytomegalovirus Is Required for Virion Morphogenesis.* J Virol 81(10):5212–24.

(52) Makkerh JPS, Dingwall C, Laskey RA (1996): *Comparative mutagenesis of nuclear localization signals reveals the importance of neutral and acidic amino acids.* Curr Biol 6:1025–27.

(53) Mantovani A, Sica A, Locati M (2007): *New vistas on macrophage differentiation and activation.* Eur J Immunol 37:14-16.

(54) Martin-Serrano J, Zang T, Bieniasz PD (2001): *HIV-1 and Ebola virus encode small peptide motifs that recruit Tsg101 to sites of particle assembly to facilitate egress.* Nat Med 7(12):1313-9.

(55) Meissner CS, Suffner S, Schauflinger M, von Einem J, Bogner E (2012): *A leucine zipper motif of a tegument protein triggers final envelopment of human cytomegalovirus.* J Virol published ahead of print 28 December 2011, doi:10.1128/JVI.06556-11.

(56) Mettenleiter TC (2002): *Herpesvirus assembly and egress.* J Virol 76:1537-47.

(57) Mettenleiter TC (2004): *Budding events in herpesvirus morphogenesis.* Virus Res 106:167-80.

(58) Mettenleiter TC, Spear PG (1994): *Glycoprotein gB (gII) of pseudorabies virus can functionally substitute for glycoprotein gB in herpes simplex virus type 1*. J Virol 68(1):500-504.

(59) Mocarski E, Courcelle CT (2001): *Cytomegalovirus and their replication,* in Fields Virology, D.M. Knipe et al. Editors. Lippincott Williams & Wilkins: Philadelphia, Pa. 2629-2673.

(60) Modrow S, Falke D, Truyen U (2003): *Molekulare Virologie.* Spektrum Akademischer Verlag.

(61) Moor H, Riehle U (1968): *Snap-freezing under high pressure: a new fixation technique for freezeeching.* Proc. 4th European Reg. Conf. of Electron Microscopy 2, 33-34.

(62) Murphy E, Rigoutsos I, Shibuya T, Shenk TE (2003): *Reevaluation of human cytomegalovirus coding potential.* Proc Nat Acad Sci U S A 100:13585-90.

(63) Nakielny S, Dreyfuss G (1999): *Transport of Proteins and RNAs in and out of the Nucleus.* Cell 99:677–690.

(64) Nickerson DP, Russell MRG, Odorizzi G (2007): *A concentric circle model of multivesicular body cargo sorting.* EMBO reports 8, 644-650.

(65) Nozawa N, Daikoku T, Koshizuka T, Yamauchi Y, Yoshikawa T, Nishiyama Y (2003): *Subcellular localization of herpes simplex virus type 1 UL51 protein and role of palmitoylation in Golgi apparatus targeting*. J Virol 77(5):3204-16.

(66) Nozawa N, Kawaguchi Y, Tanaka M, Kato M, Kato A, Kimura H, Nishiyama Y (2005): *Herpes simplex virus type 1 UL51 protein is involved in maturation and egress of virus particles.* J Virol 79:6947-6956.

(67) Pass RF (2001): *Cytomegalovirus,* in Fields Virology, D.M. Knipe et al. Editors. Lippincott Williams & Wilkins: Philadelphia, Pa. 2675-2706.

(68) Piper RC, Katzmann DJ (2007): *Biogenesis and Function of Multivesicular Bodies.* Annu Rev Cell Dev Biol 23: 519-547.

(69) Piper RC, Luzio JP (2001): *Late endosomes: sorting and partitioning in multivesicular bodies.* Traffic 2(9):612-21.

(70) Plattner H, Zingsheim H-P (1987): *Elektronenmikroskopische Methodik in der Zell- und Molekularbiologie.* Gustav Fischer, Stuttgart.

(71) Pols MS, Klumperman J (2009): *Trafficking and function of the tetraspanin CD63.* Exp Cell Res 315:1584–1592.

(72) Reddehase MJ (2006): *Cytomegaloviruses: Molecular Biology and Immunology*. Caister Academic Press.

(73) Reeves MB, Coleman H, Chadderton J, Goddard M, Sissons JGP, Sinclair JH (2004): *Vascular endothelial and smooth muscle cells are unlikely to be major sites of latency of human cytomegalovirus in vivo.* J Gen Virol 85(11):3337–41.

(74) Ren J, Longping W, Xinjiao G, Changjiang J, Yu X, Xuebiao Y, 2008: *CSS-Palm 2.0: an updated software for palmitoylation sites prediction*. Protein Eng Des Sel 21(11):639-644.

(75) Resh MD (1999): *Fatty acylation of proteins: new insights into membrane targeting of myristoylated and palmitoylated proteins.* Biochim Biophys Acta 1451:1-16.

(76) Resh MD (2006): *Use of analogs and inhibitors to study the functional significance of protein palmitoylation.* Methods 40(2):191-197.

(77) Reynolds DW, Stagno S, Hosty TS, Tiller M, Alford CA Jr. (1973): *Maternal cytomegalovirus excretion and perinatal infection.* N Engl J Med 289:1-5.

(78) Roizman B (1996): *Herpesviridae*. *In* B. N. Fields, D. M. Knipe, and P. M. Howley (ed.), Fields virology, 3rd ed. Lippincott-Raven Publishers, Philadelphia, Pa.

(79) Roizman B, Charmichael LE, Deinhardt F, de-The G, Nahmias AJ, Plowright W, Rapp F, Sheldrick P, Takahashi M, Wolf K (1981): *Herpesviridae. Definition, provisional nomenclature, and taxonomy. The Herpesvirus Study Group, the International Committee on Taxonomy of Viruses.* Intervirology 16:201-217.

(80) Romo N, Magri G, Muntasell A, Heredia G, Baia D, Angulo A, Guma M, López-Botet M (2011): *Natural killer cell-mediated response to human cytomegalovirus-infected macrophages is modulated by their functional polarization.* J Leukoc Biol 90(4):717-26.

(81) Roos N, Morgan JA (1990): *Cryopreparation of Thin Biological Specimens for Electron Microscopy: Methods and Applications*. Oxford University Press, Royal Microscopical Society.

(82) Ryckman BJ, Jarvis MA, Drummond DD, Nelson JA, Johnson DC (2006): *Human cytomegalovirus entry into epithelial and endothelial cells depends on genes UL128 to UL150 and occurs by endocytosis and low-pH fusion.* J Virol 80:710-722.

(83) Sambrook and Russel (2001): *Molecular Cloning: A Laboratory Manual.* New York: Cold Spring Harbour Laboratory Press.

(84) Sanchez V, Sztul E, Britt WJ (2000): *Human Cytomegalovirus pp28 (UL99) Localizes to a Cytoplasmic Compartment Which Overlaps the Endoplasmic Reticulum-Golgi-Intermediate Compartment.* J Virol 74(8):3842–3851.

(85) Schauflinger M (2008): *Elektronenmikroskopische Untersuchung zur Beteiligung des viralen Proteins pUL71 an der Morphogenese des Humanen Zytomegalievirus.* Diplom thesis, Electron Microscopy Facility, Ulm University.

(86) Schauflinger M, Fischer D, Schreiber A, Chevillotte M, Walther P, Mertens T, von Einem J (2011): *The Tegument Protein UL71 of Human Cytomegalovirus Is Involved in Late Envelopment and Affects Multivesicular Bodies.* J Virol 85(8):3821–3832.

(87) Schierling K, Buser C, Mertens T, Winkler M (2005): *Human cytomegalovirus tegument protein ppUL35 is important for viral replication and particle formation.* J Virol 79:3084-3096.

(88) Schmolke S, Kern HF, Drescher P, Jahn G, Plachter B (1995): *The dominant phosphoprotein pp65 (UL83) of human cytomegalovirus is dispensable for growth in cell culture.* J Virol 69: 5959-68.

(89) Scrivano L, Sinzger C, Nitschko H, Koszinowski UH, Adler B (2011): *HCMV Spread and Cell Tropism are Determined by Distinct Virus Populations.* PLoS Pathog 7(1):e1001256.

(90) Seo JY, Britt WJ (2008): *Multimerization of Tegument Protein pp28 within the Assembly Compartment is Required for Cytoplasmic Envelopment of Human Cytomegalovirus.* J Virol 82(13):6272-6287.

(91) Shen C, Guo Y, Cheng A, Wang M, Zhou Y, Lin D, Xin H, Zhang N (2009): *Characterization of subcellular localization of duck enteritis virus UL51 protein.* Virol J 6:92.

(92) Shim S, Merrill SA, Hanson PI (2008): *Novel Interactions of ESCRT-III with LIP5 and VPS4 and their Implications for ESCRT-III Disassembly.* Mol Biol Cell, 19:2661-2672.

(93) Shimoni E, Müller M (1998): *On Optimizing high-pressure freezing: from heat transfer theory to a new microbiopsy device.* Journal of Microscopy 192(Pt3):236-47.

(94) Silva MC, Yu QC, Enquist L, Shenk T (2003): *Human Cytomegalovirus UL99-Encoded pp28 Is Required for the Cytoplasmic Envelopment of Tegument-Associated Capsids.* J Virol *77*: 10594-10605.

(95) Sinzger C, Digel M, Jahn G (2008a): *Cytomegalovirus cell tropism.* Curr Top Microbiol Immunol 325:63-83.

(96) Sinzger C, Eberhardt C, Cavignac Y, Weinstock C, Kessler T, Jahn G, Davignon JL (2006): *Macrophage cultures are susceptible to lytic productive infection by endothelial-cell-propagated human cytomegalovirus strains and present viral IE1 protein to CD4+ T cells despite late downregulation of MHC class II molecules.* J Gen Virol 87:1853-62.

(97) Sinzger C, Grefte A, Plachter B, Gouw ASH, Hauw The T, Jahn G (1995): *Fibroblasts, epithelial cells, endothelial cells and smooth muscle cells are major targets of human cytomegalovirus infection in lung and gastrointestinal tissues.* J Gen Virol 76(4):741-750.

(98) Sinzger C, Hahn G, Digel M, Katona R, Sampaio KL, Messerle M, Hengel H, Koszinowski U, Brune W, Adler B (2008b): *Cloning and sequencing of a highly productive, endotheliotropic virus strain derived from human cytomegalovirus TB40/E*. J Gen Virol 89:359-68.

(99) Sinzger C, Kahl M, Laib K, Klingel K, Rieger P, Plachter B, Jahn G (2000): *Tropism of human cytomegalovirus for endothelial cells is determined by a post-entry step dependent on efficient translocation to the nucleus.* J Gen Virol 81:3021-3035.

(100) Sodeik B, Ebersold MW, Helenius A (1997): *Microtubule-mediated transport of incoming herpes simplex virus 1 capsid to the nucleus.* J Cell Biol 136:1007-21.

(101) Spencer CM,Schafer XL, Moorman NJ, Munger J (2011): *Human Cytomegalovirus Induces the Activity and Expression of Acetyl-Coenzyme A Carboxylase, a Fatty Acid Biosynthetic Enzyme Whose Inhibition Attenuates Viral Replication.* J Virol 85(12):5814-24.

(102) Stagno S, Reynolds DW, Pass RF, Alford CA Jr. (1980): *Breast milk and the risk of cytomegalovirus infection.* N Eng J Med 302:1073-1076.

(103) Steinbrecht RA, Müller M (1987): *Freeze substitution and freeze drying.* In Steinbrecht RA, Zierold K(eds): *Cryotechniques in Biological Electron Microscopy*. Springer Verlag, Berlin, 149-172.

(104) Streblow DN, Varnum SM, Smith RD, Nelson JA (2006): *A Proteomics Analysis of Human Cytomegalovirus Particles.* Cytomegaloviruses Molecular Biology and Immunology, M. Reddehase, ed. (Norfolk: Caister Academic Press) pp. 91-110.

(105) Studer D, Michel M, Müller M (1989): *High pressure freezing comes of age.* Scanning Microsc Suppl, 3:253-68; discussion 268-9.

(106) Suffner S (2011): *Charakterisierung funktioneller Domänen des HCMV-Tegumentproteins pUL71*. Diplom thesis, Institute of Virology, Ulm University Hospital.

(107) Szczesny PJ, Walther P, Müller M (1996): *Light damage in rod outer segments: the effects of fixation on ultrastructural alterations.* Current Eye Res., 15:807-814.

(108) Tandon R, AuCoin DP, Mocarski ES (2009): *Human Cytomegalovirus Exploits ESCRT Machinery in the Process of Virion Maturation.* J Virol 83:10797-807.

(109) Taylor HP, Cooper NR (1989): *Human cytomegalovirus binding to fibroblasts is receptor mediated.* J Virol 63(9):3991-98.

(110) Taylor-Wiedeman J, Sissons JG, Borysiewicz LK, Sinclair JH (1991): *Monocytes are a major site of persistence of human cytomegalovirus in peripheral blood mononuclear cells.* J Gen Virol72(9):2059-64.

(111) Tischer BK, von Einem J, Kaufer B, Osterrieder N (2006): *Two-step red-mediated recombination for versatile high-efficiency markerless DNA manipulation in Escherichia coli.* Biotechniques 40(2):191-7.

(112) To A, Bai Y, Shen A, Gong H, Umamoto S, Lu S, Liu F (2011): *Yeast Two Hybrid Analyses Reveal Novel Binary Interactions between Human Cytomegalovirus-Encoded Virion Proteins.* PLoS ONE 6(4):e17796.

(113) Tooze J, Hollinshead M, Reis B, Radsak K, Kern H (1993): *Progeny vaccinia and human cytomegalovirus particles utilize early endosomal cisternae for their envelopes.* Eur J Cell Biol 60:163-78.

(114) Varnum SM, Streblow DN, Monroe ME, Smith P, Auberry KJ, Pasa-Tolic L, Wang D, Camp DG, Rodland K, Wiley S, Britt W, Shenk T, Smith RD, Nelson JA (2004): *Identification of proteins in human cytomegalovirus (HCMV) particles: the HCMV proteome.* J Virol 78:10960-10966.

(115) Walther P, Ziegler A (2002): *Freeze substitution of high-pressure frozen samples: the visibility of biological membranes is improved when the substitution medium contains water.* J Microsc 208:3-10.

(116) Wirblich C, Bhattacharya B, Roy P (2006): *Nonstructural Protein 3 of Bluetongue Virus Assists Virus Release by Recruiting ESCRT-I Protein Tsg101.* J Virol 80:460-73.

(117) Womack A, Shenk T (2010): *Human Cytomegalovirus Tegument Protein pUL71 Is Required for Efficient Virion Egress.* mBio 1(5):e00282-10.

(118) Young MR, Young ME, Wright MA (1990): *Stimulation of immune-suppressive bone marrow cells by colony-stimulating factors.* Esp Hematol 18:806-11.

(119) Yu D, Silva MC, Shenk T (2003): *Functional map of human cytomegalovirus AD169 defined by global mutational analysis.* Proc Natl Acad Sci USA 100:12396–12401.

Acknowledgements

First I want to thank both Thomas Mertens and Paul Walther for welcoming me as a graduate student in the institute of virology and the central electron microscopy facility, respectively. I very much appreciate the freedom and the trust they both granted me in working on this thesis independently. Many thanks go to Jens von Einem for the constructive discussions and his support over the years. I thank Christian Sinzger for generously sharing his expert knowledge about virology. I also want to thank both Christian Sinzger and Wolfgang Weidemann for participating in my final defense committee. I thank all my colleagues in both the virology and the EM labs for their support; special thanks go to Eberhard Schmid for expert technical assistance. I further thank Heinz Schwarz (MPI Tübingen), York Stierhof (Tübingen) and Bruno Humbel (Lausanne) for sharing their broad knowledge about EM methods. To everyone who supported me, encouraged me, enlightened me… thank you!

Curriculum Vitae

Lebenslauf aus Gründen des Datenschutzes entfernt.